

SILL STRATIGRAPHY AND SEDIMENTOLOGY IN  
MARINE INUNDATED BASINS, SACHS HARBOUR,  
NWT, CANADA:  
IMPLICATIONS FOR SEA-LEVEL RECONSTRUCTION

BRYAN G. MARTIN







**Sill stratigraphy and sedimentology in marine inundated basins, Sachs Harbour, NWT,  
Canada: implications for sea-level reconstruction**

**By:**

**Bryan G Martin**

**A thesis submitted to the  
School of Graduate Studies  
in partial fulfillment of the  
requirement for the degree of  
Master of Science**

**Environmental Science Program / Faculty of Science**

**Memorial University of Newfoundland**

**Submitted March 10<sup>th</sup> 2009**

**St John's  
Newfoundland**

## **Abstract**

This study focuses on the seismic interpretation and core-based sedimentology of shallow, coastal marine basins and their sills in the western Arctic to better constrain local relative sea level (RSL) records.

On transgressive coastlines, sea level rise can be measured using the inundation basin approach, which utilizes former coastal freshwater lake basins that have become inundated by marine water as sea level rises. The amount of sea level rise since inundation occurred is measured as the vertical distance between the lowest part of the former lake basin margin - the sill - and the current sea level position. While the approach has been typically applied to basins with rock-cored sills, this study investigates the opportunities and constraints presented by inundation basins with sediment-cored sills, which are more susceptible to post-inundation modification. Specifically, the study examines the processes acting on sediment-cored sills during transgression and their related sedimentary signatures.

The study was carried out at Sachs Harbour, located on Banks Island in the western Canadian Arctic. The regional coastline is submergent with extensive evidence of drowned estuaries and inundated lakes. Sills associated with five basins were investigated using sediment coring techniques, airphoto analysis, and seismic profiling. Air photo analysis and field observations of two basins that have experienced relatively recent marine inundation suggest that initial marine penetration took place through the former lake outlets. It was hypothesized therefore that a similar inundation process took place in the deeper basins of Sachs Harbour.

Two buried channels and an erosion surface were identified on the seismic profiles of two sills and were subsequently targeted for coring. Recovered sediments (80-130 cm thickness) from channels were predominantly mud, which is interpreted to represent post-submergence marine sedimentation by suspension settling. A sediment core from one channel did not penetrate the channel bed, whereas in the other, an erosion surface was encountered at 87 cm core depth above laminated fine sand. Nearby on the same sill, the contact between laminated sand and overlying mud occurs at 22 cm core depth and is also interpreted to represent an erosional surface between in situ deglacial sediment and post-submergence marine deposits. Both erosional surfaces, when adjusted to modern sea level datum, occur at depths between 4.8 and 5 m and are considered to be good estimates of the former RSL position when marine inundation of the basin first took place.

Results of the study have confirmed that outlet channels are the most effective sill depth indicators; however, channel infilling and erosion may obscure the actual inundation elevations and thus provide false apparent depths. A combination of coring and seismic data is required to resolve this issue.

## **Acknowledgements**

I would like to thank both my supervisors, Drs. Trevor Bell and Rod Smith for their assistance in the field, throughout the analysis and writing process, and the entire duration of this Master's project. I would also like to thank my committee member Donald Forbes for giving valuable advice for the completion of this project and his help at BIO. A special thanks to Ruth Plets for her assistance and expertise in seismic interpretation and general assistance. I would also like to thank Warren Esau for his assistance with coring activities, Kate Jarrett, Claire McIntyre, and Caitlin Owens for their assistance with core sub-sampling at the Bedford Institute of Oceanography. I would also like to acknowledge my funding sources NSERC, NSTP, NRCan, and the ArcticNet Network of Centres of Excellence. Logistical support in the field for this project was provided by Polar Continental Shelf Project while the Aurora Research Institute provided logistical support in Inuvik. Finally I would like to thank the members of the physical geography lab for their support, most notably Denise Brushett, Alison Copeland, Dominique St-Hilaire, and Seth Loader, for providing assistance with difficult software, lab equipment, and offering general moral support.

## **Table of contents**

Abstract	ii
Acknowledgements	iv
Table of contents	v
List of tables	viii
List of figures	ix
List of appendices	xi
<b>Chapter 1: Introduction</b>	<b>1</b>
1.1 Introduction	1
1.2 Rational and objectives	2
1.3 Study site	9
1.4 Climate and vegetative cover	14
<b>Chapter 2: Physical setting</b>	<b>16</b>
2.1 Bedrock geology	16
2.2 Glacial History	16
2.3 South-western Banks Island	19
2.4 Sachs Lowland	24
2.5 Records of Holocene warming and initiation of thermokarst activity	26
2.6 Past records of sea level change	27
2.7 Recent records of sea level change	30
2.8 Sediment transport and Sachs Spit	32
2.9 Community impacts and sensitivity to sea level rise	34

<b>Chapter 3: Methods</b>	<b>35</b>
3.1 Introduction	35
3.2 Air photo mapping	35
3.3 Sub-bottom profiling	35
3.4 Vibracoring	36
3.5 Core analysis	37
3.5.1 X-radiography	39
3.5.2 Splitting, description, and sub-sampling	39
3.5.3 Loss-on-ignition	40
3.5.4 Particle size analysis	41
<b>Chapter 4: Results and interpretation</b>	<b>42</b>
4.1 Outline	42
4.2 Landscape change	42
4.3 Sill and basin morphology	45
4.4 Acoustic stratigraphy and sedimentary characteristics	45
4.5 Lithofacies description	46
4.6 Seismic and sedimentary description of sills	64
4.7 Summary of core interpretation	75
4.8 Summary of seismic interpretation	78
<b>Chapter 5: Discussion</b>	<b>79</b>
5.1 Introduction	79
5.2 Sill attributes	79
5.3 Key processes in sill evolution	81

5.4 Sill sediment and basin inundation	87
5.5 Inundation model	88
5.6 Implications of the model on sea level reconstruction	89
5.7 Sill breaching points – index points	92
5.8 Summary of findings and conclusions	96
5.9 Considerations for future research	97
<b>References</b>	<b>100</b>

**List of Tables**

<b>Table 4.1</b> Summary of sill core information	52
<b>Table 4.2</b> Lithofacies present in cores	53
<b>Table 5.1</b> Effective sill depth	93

## **List of Figures**

<b>Figure 1.1</b> Inundation model	4
<b>Figure 1.2</b> Evolutionary scenarios of a sill	6
<b>Figure 1.3</b> Location map of Sachs Harbour, Banks Island	10
<b>Figure 1.4</b> Study site location depicting study basins	12
<b>Figure 1.5</b> Windblown sediment across harbour	13
<b>Figure 2.1</b> Bedrock geology of Banks Island	17
<b>Figure 2.2</b> Extent of Quaternary Glaciations on Banks Island	18
<b>Figure 2.3</b> Maximum extent of ice during last glaciation	20
<b>Figure 2.4</b> Sandhills Moraine	22
<b>Figure 2.5</b> Surficial geology of southwest Banks Island	23
<b>Figure 2.6</b> Exposed coastal section in Sachs Harbour	25
<b>Figure 2.7</b> Beaufort Sea level curve	29
<b>Figure 2.8</b> Zero isobase in western Arctic	31
<b>Figure 2.9</b> Sachs spit progradation	33
<b>Figure 3.1</b> Sediment coring equipment	38
<b>Figure 4.1</b> Aerial photographs from 1950 and 2003	43
<b>Figure 4.2</b> Aeolian deflation at Sachs Harbour	44
<b>Figure 4.3</b> Seismic tracks and core locations	47
<b>Figure 4.4</b> Seismic line 0249	48
<b>Figure 4.5</b> Seismic line 0234	49
<b>Figure 4.6</b> Seismic line 0215	50

<b>Figure 4.7</b> Lithofacies 1	54
<b>Figure 4.8</b> Lithofacies 2	56
<b>Figure 4.9</b> Lithofacies 3	59
<b>Figure 4.10</b> Lithofacies 4	61
<b>Figure 4.11</b> Lithofacies 5	63
<b>Figure 4.12</b> Lithofacies legend for cored sediment	66
<b>Figure 4.13</b> Morphology of sill I	67
<b>Figure 4.14</b> Morphology of sill II	69
<b>Figure 4.15</b> Morphology of sill III	71
<b>Figure 4.16</b> Local unconformity : Core 07-001	72
<b>Figure 4.17</b> Morphology of sill IV	74
<b>Figure 4.18</b> Morphology of sill V	76
<b>Figure 4.19</b> Morphology of Sill VI	77
<b>Figure 5.1</b> Sill evolution	83
<b>Figure 5.2</b> Channel erosion and index points	85
<b>Figure 5.3</b> Sachs Harbour evolution	91

**List of Appendices**

<b>Appendix A: Sediment core section logs</b>	109
<b>Appendix B: Seismic description</b>	122
<b>Appendix C: Loss-on-ignition</b>	129
<b>Appendix D: Particle Size Analysis</b>	139

## **Chapter 1 - Introduction**

### **1.1 – Introduction**

This study focuses on the seismic interpretation and core-based sedimentology of shallow, coastal marine basins and their sills in the western Arctic to better constrain local relative sea level (RSL) records. On transgressive coastlines, sea level rise can be measured using the inundation basin approach, which utilizes former coastal freshwater lake basins that have become inundated by marine water as sea level rises. The amount of sea level rise since inundation occurred is measured as the vertical distance between the lowest part of the former lake basin margin – the sill – and the current sea level position. While the approach has typically been applied to basins with rock-cored sills, this study investigates the opportunities and constraints presented by inundation basins with sediment-cored sills, which are more susceptible to post-inundation modification. Specifically, the study examines the processes acting on sediment-cored sills during transgressions and their related sedimentary signatures.

There is an urgency to understand and accurately model sea level rise in areas surrounding the Beaufort Sea where poorly lithified, ice-rich coastlines (Vincent 1983, French *et al.* 1982) are particularly sensitive to erosion from rising sea levels (Manson *et al.* 2005). In addition, most Arctic communities are predominantly coastal and therefore require accurate sea level predictions to develop impact scenarios and adaptation strategies. Furthermore, around the Beaufort Sea, climate warming is expected to cause thawing of permafrost, reduction of sea ice thickness and extent, as well as increased storm activity (Manson *et al.* 2005), thus increasing the potential for coastal erosion.

This thesis is divided into five chapters. The first chapter focuses on the inundation approach, the goals and defining research question of the project, as well as relevant background information. The second chapter describes the study area, including the study site and physical setting of the surrounding area. The third chapter outlines the methods employed in this project. The fourth chapter focuses on the results, including the morphology and bathymetry of the basins and surrounding sills, the sedimentological and acoustic trends, and their interpretation. The final chapter discusses the implications of the sedimentary and acoustic trends for RSL reconstruction as well as suggestions for further research.

## **1.2 Rationale and objectives**

In order to reconstruct past sea level history, it is necessary to obtain sea level index points that represent the position of past sea levels at specific times. With sufficient index points, a local sea-level curve can be constructed. While emergence curves are common in areas undergoing predominantly glacioisostatic uplift (Dyke 1998), less quantitative information is available on submergent Arctic coastlines due to reworking, truncation, and burial of sediments during transgressions (see however Hill *et al.*, 1985, 1993; Campeau *et al.* 2000).

One method of reconstructing past sea-level changes on submergent coastlines is to document the timing of marine inundation of former coastal freshwater lakes. The “inundation approach” relies on the accurate determination of the former sill height over which marine waters flooded (Sparrenbom *et al.* 2006). Studies by Long *et al.* (1999), Miettinen *et al.* (2007) have examined inundation and isolation basins that had bedrock

sills where the elevation of the former sill is likely to have remained constant through time. However, in areas characterized by unconsolidated material, such as the coastline of Sachs Harbour, complications arise due to erosion and deposition on sills. Therefore this thesis sets out to determine whether it is possible to use inundated basins with unconsolidated sills to help reconstruct palaeo sea levels.

The inundation basin approach is possible on transgressive coastlines where low lying freshwater lakes are present, ideally in relatively low-energy environments. As sea level rises and approaches the lowest section of the lakeshore, storm surges and waves will begin to enter the lake outlet and alter the water chemistry. Through progressive sedimentation, both lakes and marine environments preserve a record of their environmental conditions (Figure 1.1). Diatoms, a class of algae, display a marked association to waters of different salinity and can be used to identify transitions from freshwater to marine conditions within the sedimentary record (Pienitz *et al* 1991, Saulnier-Talbot and Pienitz 2001, Miettinen *et al* 2007). The precise timing of marine incursion is determined by radiocarbon dating the diatom transition using shell or organic fragments found near the salinity transition. From the radiocarbon date and knowledge of the elevation of the submerged sill, the lowest point where marine water flooded the lake is taken to be the position of the sea at the time of marine incursion. In addition to biological factors, additional limitations that may affect the strength of the diatom record in the initial stages of lake breaching relate to the rate and degree of marine incursion.

In the inundation model, the position of the sill is assumed to be the limiting factor influencing marine overtopping of the freshwater basin and the onset of saline conditions. By combining the timing of marine inundation with the original elevation of

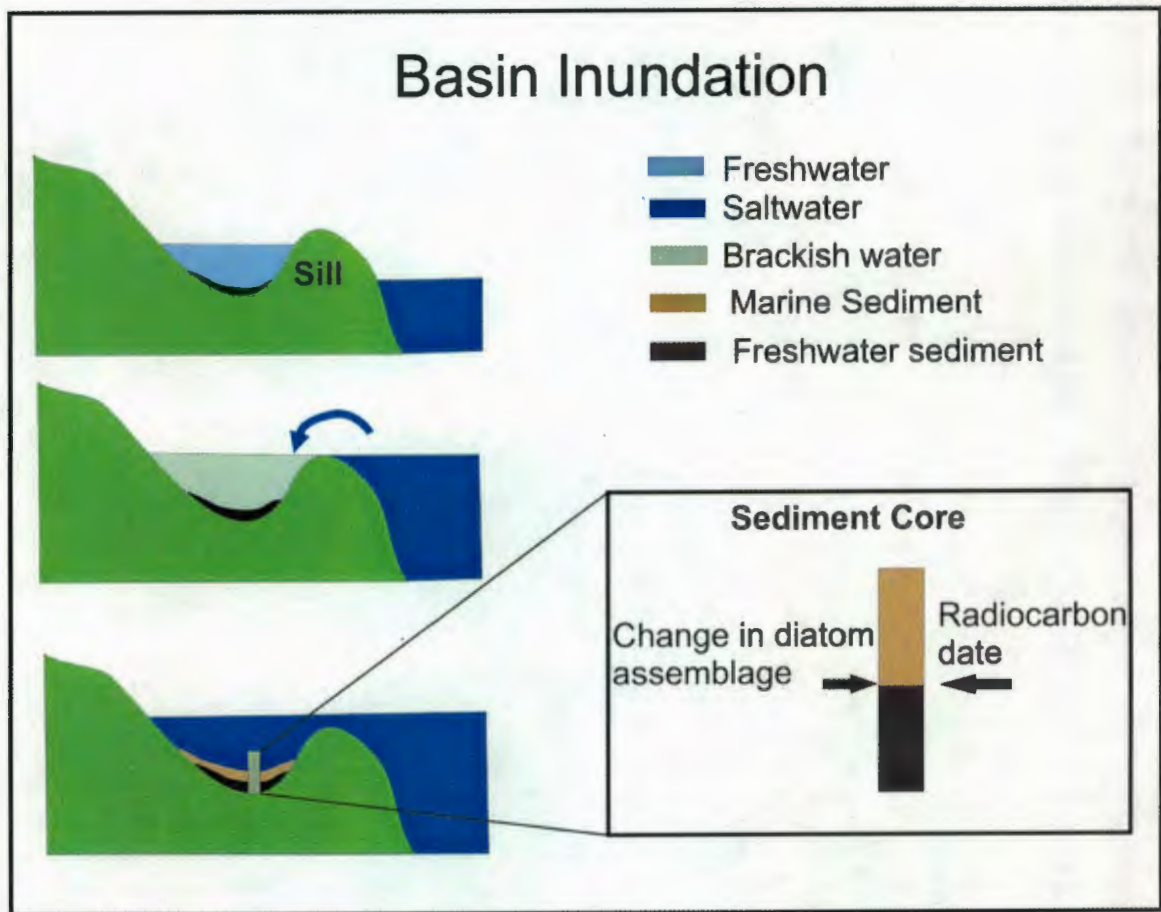


Figure 1.1. Inundation basin model initially showing perched freshwater lake gradually becoming brackish and finally fully marine with sea level rise. Prior to inundation, lake sediment contains freshwater diatoms. Following inundation, the sediments contain marine diatoms. These organisms can taxonomically be classed as freshwater or marine and therefore serve as an indicator of when sedimentation changed from fresh to marine. Radiocarbon dating of the diatom transition can give an approximate age for inundation which occurred when marine water initially flooded over the sill. Accurate determination of the height of the sill and the timing of inundation generates a sea level index point. This is will be further described in the text.

the submerged sill (lowest point of incursion), a precise sea-level index point can be established. The accuracy of the sea-level index point partially relies on the correct identification of the original sill surface and the validity of the assumption that its morphology has remained unchanged since submergence. However, this assumption may be violated for unconsolidated sediments because during submergence, several processes may act singly or together to influence the sill morphology. For instance i) the sill may have remained unchanged during submergence, ii) the sill may have been subject to erosion, iii) the sill may have experienced subsidence, iv) the sill may have been buried by deposition. The lowest breach observed along the margins of the submerged basin cannot therefore be assumed to represent the original sill, nor can its height be considered an accurate measure of the former sea-level position during inundation (see Figure 1.2). The first objective of the thesis therefore is to differentiate key processes in the evolution of sill morphology in this environment during and following its submergence.

Certain processes in the evolution of sill morphology have been documented by Dallimore *et al* (1996), Hill and Solomon (1999), Campeau *et al* (2000). These authors have shown that various erosional mechanisms are at work, either from storm events and marine overwash, ice scour, or tidal currents. Other mechanisms include ground ice melt, either in the form of thaw subsidence or sediment slumping.

Following the melt of ground ice, wave action and currents are likely the most effective way of removing or remobilizing sediment in the nearshore zone (Héquette and Barnes 1990), including the removal of previously slumped material. Likewise, much of the sediment that is removed by waves and currents is often redeposited as spits and bars (Clark *et al* 1984). Sea ice ploughing, ice keel disturbance, and plucking of sediment by

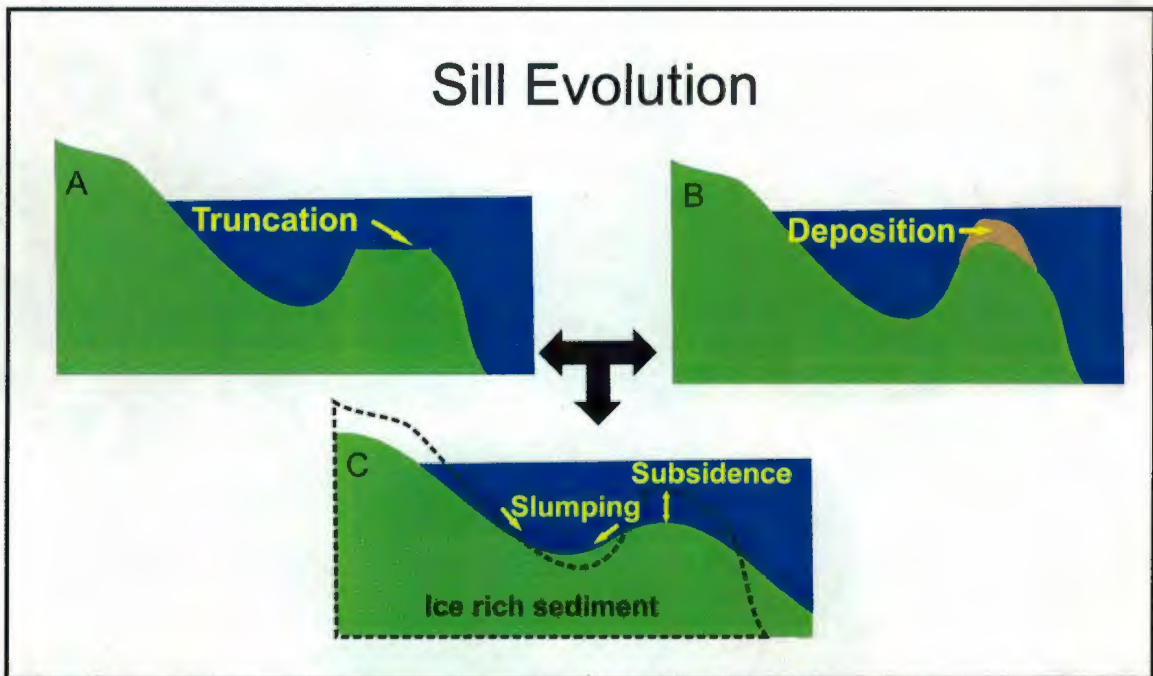


Figure 1.2. Models depicting the evolutionary scenarios of a sill made of unconsolidated sediment following inundation. Diagrams show (A) erosion of the sill, (B) deposition on the sill, and (C) thaw-subsidence of the sill related to melting of ice-rich sediments causing settling and slumping.

landfast ice has also been documented as agents of coastal erosion (Reimnitz and Barnes 1987). However, Héquette and Barnes (1990) found that most ice keel disturbance was seaward of the 12 m isobath and that ice gouges were virtually absent or reworked landward by waves and currents. In addition, grounded ice increased the hydraulic flow under or around the ice keels leading to a winnowing of the sediment (Héquette and Barnes 1990). Conversely, Hill and Solomon (1999) noted constructive processes in the form of resedimentation from nearby eroding bluffs as well as the formation of spits.

A second objective of this research is to define a range of geomorphological and sedimentological attributes that may be used to characterize sill reworking in submergent basins. Sill attributes are based upon scenarios that are either predominantly erosional or depositional and are directly related to the key processes acting upon the sills during inundation.

In predominantly depositional low energy environments, sediment dominated by marine or estuarine mud will exist (Benn and Evans 1998), especially in areas of deeper water away from shorelines exposed to longshore drift. This can also include coarser grains made up of ice rafted and aeolian sediment. Deep troughs are likely to accumulate much of the muddy sediment (Boggs 2006). However, these low energy environments may periodically be affected by storms washing in coarser than average sediment.

In higher energy depositional environments, growth of spits and longshore progradation would be expected (Benn and Evans 1998). Spits and well sorted sands may occur in some cases either above or below the water surface (shallow bars) in the initial stages of development. Spit overwash or distal platform deposits may also occur as laminated entities displaying flaser bedding in areas with a constant supply of fine

sediment and where constantly shifting depositional energies exist (Solomon and Hill 1999).

Described by Belliveau (2007), coastal erosion of unconsolidated bluffs is occurring at a rapid rate in Sachs Harbour, which is supplying a large amount of sediment for nearby beach and spit nourishment. In other studies, some of the sediment was observed to be moving across basin sills (Harry *et al* 1983). Depending on current strength and source material, sediment sorting would be expected. Such an example was observed on spits near Tuktoyaktuk consisting of medium sand with varying amounts of interbedded cross-laminated sand and mud (Hill and Solomon 1999).

In predominantly erosional systems, erosion would involve the removal of sill sediment deposited prior to basin formation. Therefore the former basin margins, following subsidence and headwall retreat, would continue to erode after submergence. Similar structures were described on Richards Island where spit-like features between thermokarst lakes were shown to be clearly erosional and part of the underlying Kittigazuit Formation (Hill and Solomon 1999). Predominantly erosional systems are also expected to be impacted by wave action, ice scouring, ice ploughing, and current winnowing. Diagnostic indications of such erosional processes would include unconformities and deflation lags overlying the finer outwash material (Hill and Solomon 1999). However, lag deposits would not easily be discernable if coarse grained material was not part of the original sill. Likewise, where high energy currents or wave action were capable of removing large grains from the sill surface, including ice ploughing and plucking, lag surfaces would be destroyed. These surfaces would normally occur as ravinement surfaces directly exposing the original sill sediment. Certain areas prone to

unconformities include channels cross-cutting sills, especially within those hypothesized to be outlet channels prior to submergence. Knowledge of the pre-inundation sediment is therefore crucial in order to better recognize sedimentary interfaces.

Additionally, near-surface ice-bonded sediments thaw annually to form an active layer and subsequently refreeze when in contact with winter bottomfast ice (Hill and Solomon 1999) and therefore permafrost remains in the sediment below the active layer until sea ice is no longer in contact with the sea floor (Dyke 1991). Ice-bonded sediment below sea level is more resistant and less likely to erode than thawed sediment (Dallimore *et al* 1996).

Certain areas likely begin as predominantly erosional systems and subsequently change to depositional environments. This would include areas within deep channels or the deeper sections along sill tops. Abandonment of river channels following a transgression would likely result in burial of palaeo-channels, which are subsequently only seen in seismic profiles or in cores.

### **1.3 Study site**

Sachs Harbour (71°58.15'N; 125°12.84'W) is located on the southwest coast of Banks Island, NWT (Figure 1.3). Banks Island is situated at the southwestern edge of the Canadian Arctic Archipelago. The community of Sachs Harbour, with a population of 123 (NWT Bureau of statistics 2007), is the only permanent settlement on Banks Island, and was established in 1929 (INAC 2005). The community is situated along a large end moraine (described in subsequent section). The study area is located to the south of the community, in the harbour where a number of inundated basins and sills are located.



Figure 1.3. Study site location (Banks Island image from Herbert (2002)), inset image modified from NRCan Atlas of Canada.

Sachs Harbour was chosen as a study site for two main reasons; first, it is situated along a submergent coastline with an array of inundated basins. Second, the basins are relatively sheltered from the sea and therefore are more likely to preserve original sedimentary characteristics and stratigraphy.

The focus of this study was along the sills of five inundated basins in the harbour (Figure 1.4). The basins varied in width between 400 m and 2 km and had maximum recorded depths between 16 and 45 m. The basins are presently under full marine influence. Of the five basins, there are two (Mirabilite Basins 1 and 2) that are seasonally cut off from marine influence when winter sea ice thickness exceeds the depth of their sills (c.f. Smith *et al* 2006).

The Sachs River drains a catchment of approximately 1100 km<sup>2</sup> (Good and Bryant 1985). The braided channel above the estuary has an average summer discharge of 5.7 m<sup>3</sup>/s and is characterized by a low suspended load owing to various sediment traps at its mouth (Good and Bryant 1985). During the spring of 2007, large amounts of windblown coarse and fine sand were found mantling the snow cover along many sections of the Sachs River, upper estuary, and harbour (Figure 1.5).

Sea cliffs rarely exceeding 6 to 8 m are developed around the basins in poorly consolidated and often ice rich sediments (Harry *et al* 1983, Belliveau 2007). These cliffs were shown to be retreating up to 4 m/a depending on the location (Harry *et al* 1983, Belliveau 2007).

Previous work in the harbour by Brown (2007), and Siferd (2001) have shown that shallow sand sheets with low biological diversity dominate the nearshore Sachs Harbour



Figure 1.4. Study site depicting the five study basins and there surrounding sills and shorelines. The community of Sachs Harbour is north of the Sachs Channel and the airstrip is located top center of the photo. Modified Ikonos and Quickbird images 2003.



Figure 1.5. Windblown granules and coarse sand forming small immature dunes atop snowcover on Sachs Estuary, approximately 10 km east of Sachs Harbour. Photo taken towards the south.

area, likely due to highly mobile sand along the sill tops. Black anoxic mud was found in up-harbour basins, which in places periodically released gas.

#### **1.4 Climate and vegetative cover**

Sachs Harbour lies within the zone of continuous permafrost and is considered to be in the mid-Arctic climate zone (French 2007). Mean annual temperature (1971-2000) is  $-13.3^{\circ}\text{C}$  with mean January temperatures of  $-29.3^{\circ}\text{C}$ , and mean July temperature of  $6.8^{\circ}\text{C}$  (Environment Canada 2004). Sachs Harbour is considered a polar desert with a mean annual precipitation of 149 mm, with an average of 52.2 mm falling as rain (Environment Canada 2004).

Sachs Harbour is normally ice free for less than 4 months of the year, breaking up in early July and refreezing in late October (Canadian Ice Service 2003) with ice thicknesses reaching approximately 2.2 m within the harbour. The average number of storms occurring during the open water season since initial data records has increased from 15% in June to over 25% in October (storms are considered as having wind speeds of over 10 m/s for a 12 h period) (Manson *et al* 2005). Storm impacts remain largely undocumented at Sachs Harbour (Manson *et al* 2005), but, Harry *et al* (1983) noted large thermo-erosional niches, undercutting, and the removal of debris talus at the base of cliffs (leading to cliff failure by block detachment).

Vegetation in the area is relatively sparse due to a short growing season (Pielou 1994) and the shallow (70-90 cm) active layer (French 1974). As the plant roots do not penetrate into the underlying permafrost (Canadell *et al.* 1996) they likely do not play much of a role in stabilizing large scale erosion and block failure. However, plants on the

outwash plain, namely *Salix alaxensis* and *niphoclada*, were found growing in small sand dunes (West and Pettit 2000) and were thought to be stabilizing the sediment.

## **Chapter 2 - Physical setting**

### **2.1 Bedrock Geology**

Banks Island lies within the Arctic Platform geological province (Wheeler *et al* 1997) and is underlain predominantly by Mesozoic and Tertiary rocks (Miall 1979). The southwest corner of the island is underlain by pre-Quaternary units including the Glenelg, Christopher, Isachsen, Kanguk, Eureka Sound, Beaufort, and Worth Point formations (Vincent 1983) (Figure 2.1). Quaternary sediment exposed in coastal bluffs are likely derived from these formations. The Beaufort Formation, composed of bedded fluvial sands, sandstones, dolomites, and silstones underly the large outwash plain south and southeast of the community (Vincent 1990). Situated between the Beaufort Formation and the overlying Quaternary sediments is the Worth Point Formation which includes organic peat mats. These old organic materials pose problems for radiocarbon dating of Holocene organic samples.

### **2.2 Glacial history**

Three major glaciations have been described on Banks Island based upon the spatial distribution of till sheets, marginal glacial landforms, and glacial stratigraphy (Vincent 1983). Pertinent to this study is the Amundsen glaciation, the last of the three known glaciations on Banks Island (Figure 2.2) (Vincent 1982, 1983).

The Amundsen glaciation involved part of the Late Wisconsinan (Marine Isotope Stage 2) Laurentide Ice Sheet (Dyke 1987, 2004). It covered most of the northern, eastern, and southern coasts of the island as it wrapped around the island in M'Clure Strait, Prince-of-Wales Strait, and Amundsen Gulf. The western coast of Banks Island is

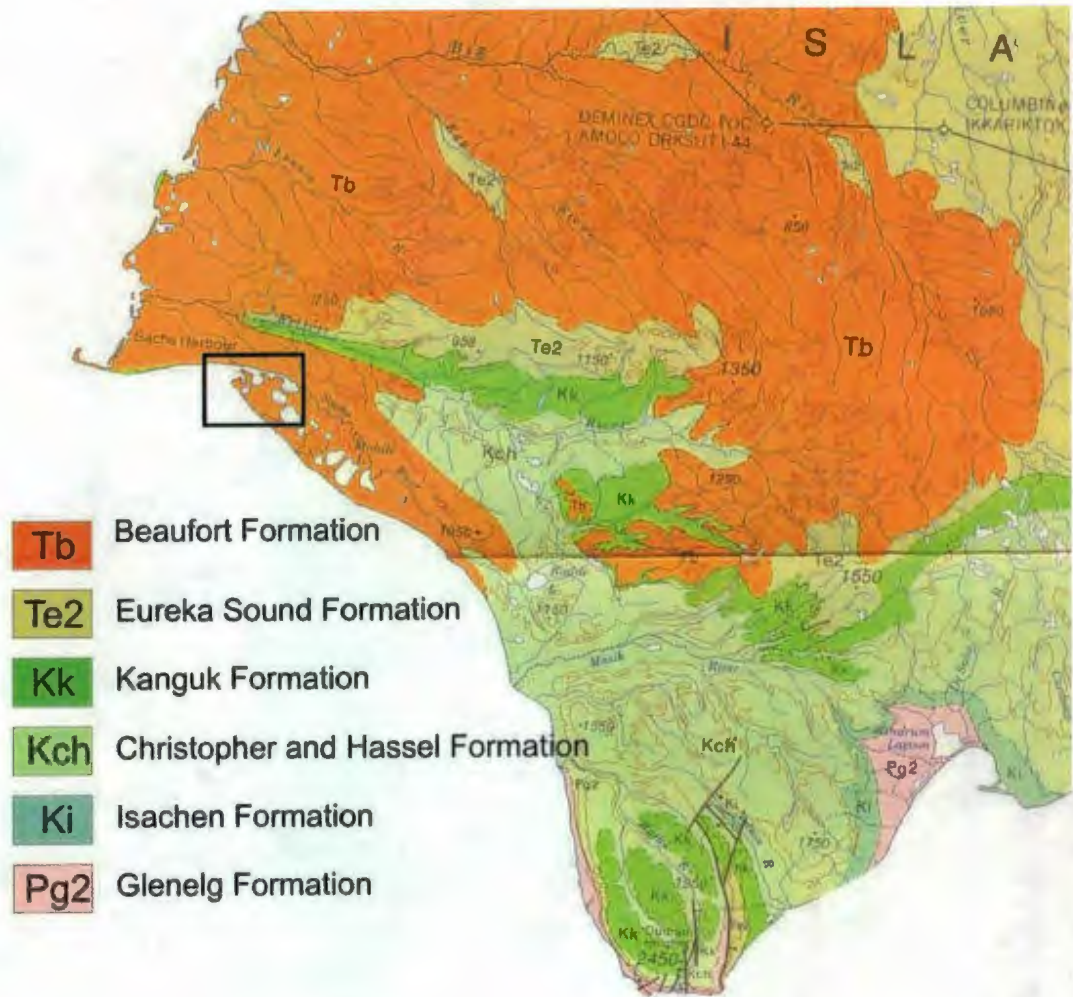
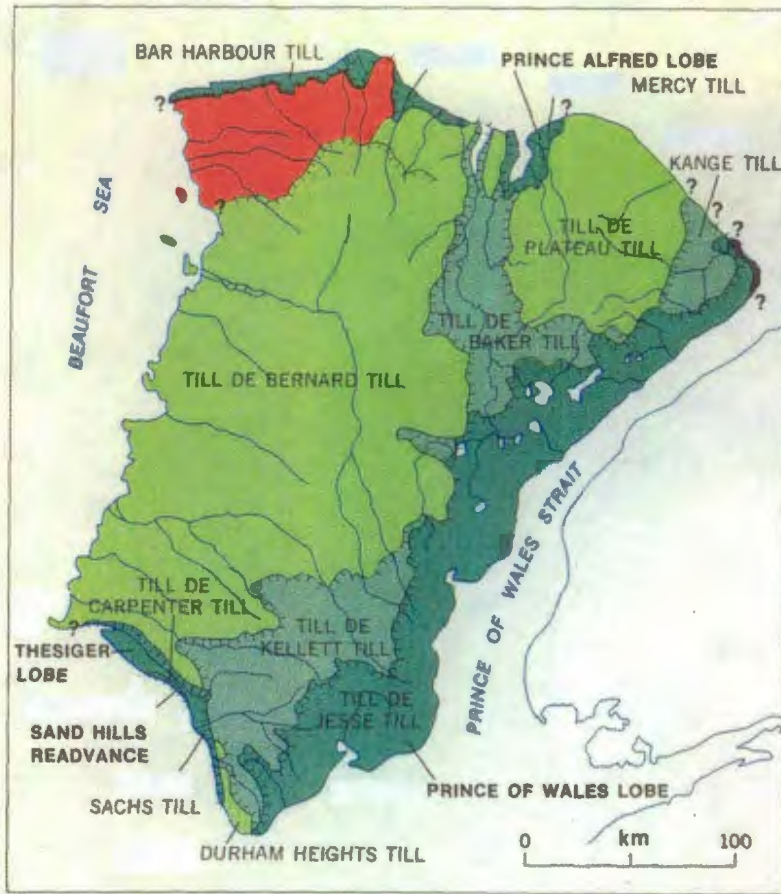


Figure 2.1. Bedrock geology of Banks Island. Study area highlighted within box. Modified from Miall's 1979 map.



**Quaternary Glaciations of Banks Island**

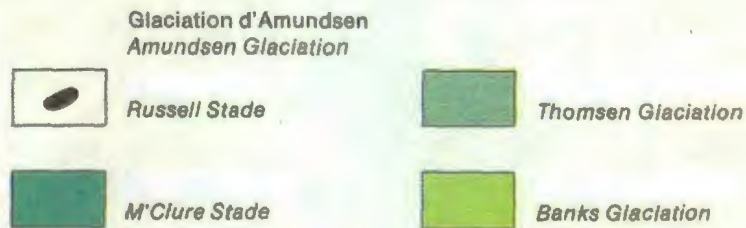


Figure 2.2. Extent of three Quaternary glaciations on Banks Island. Modified from Vincent (1983).

thought to have been ice free during the Amundsen Glaciation (Vincent 1982, Dyke 1987, 2004), although recent work by England has questioned this (England, pers. com 2008). The northwestern limit of the Thesiger Lobe in Amundsen Gulf is delimited by the Sachs Till, the presence of terminal moraines, and proglacial outwash channels (Vincent 1978). The height of the glacier is thought to have been less than 100 m near Sachs Harbour, decreasing rapidly to the west where it was likely buttressed by the cliffed coastline (Vincent 1983). More recently, Stokes *et al* (2006) have mapped seabed evidence for a large ice stream reaching the shelf edge in the Beaufort Sea (Figure 2.3). Although its age remains unconstrained, it supports England's assertion that Banks Island was completely ice-covered during the Late Wisconsinan (Marine Isotope Stage 2 – (MIS)). Following ice retreat, the Meek Point Sea flooded glacio-isostatically depressed lowlands (Vincent 1983).

The current consensus suggests a late Wisconsinan (MIS 2) age for ice retreat although a quasi stable ice cover was present throughout most of the Late Wisconsinan (MIS 2) and part of the Mid Wisconsinan (MIS 3) (Dyke 2004, 1987, Dyke *et al.* 2002, Dyke and Prest 1987, Prest *et al* 1968). Dyke and Prest (1987) assigned an age of 25 ka BP or "early" Late Wisconsinan (MIS 2) to the Amundsen Glaciation on Banks Island with deglaciation of southwest Banks Island between 13.5 and 12.5 ka BP (14.4-15.6 cal ka BP) (Dyke 2004).

### **2.3 South-western Banks Island**

As the Thesiger Lobe retreated towards Thesiger Bay, it left a series of end moraines which dammed large palaeo glacial lakes, and discharged considerable volumes of

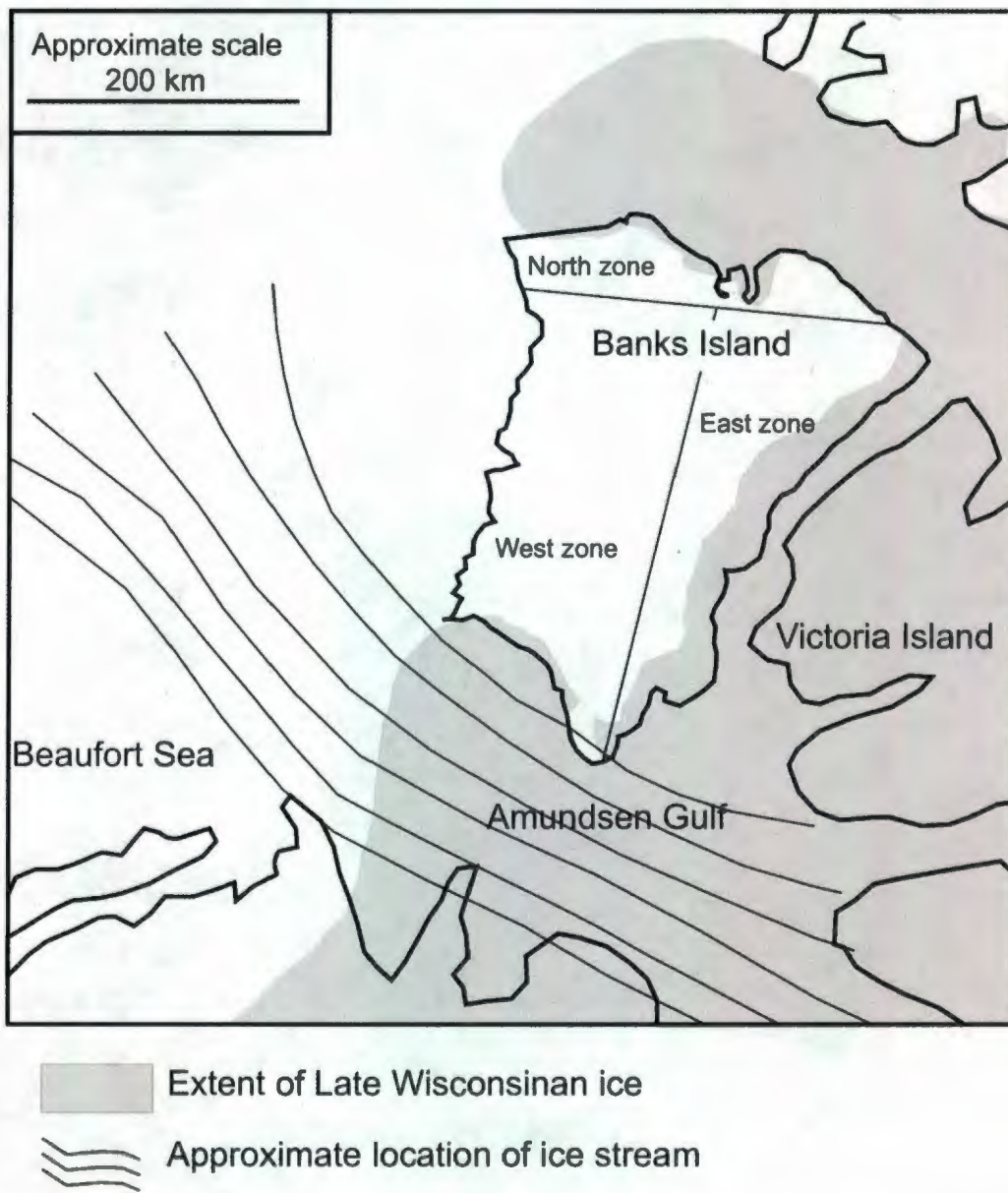


Figure 2.3. Maximum extent of ice during the last Glaciation on Banks Island as depicted by Dyke *et al* 2002. Note postulated ice stream from Stokes *et al* 2006.

sediment westward (Vincent 1982, 1983, 1992). These sediments were deposited as an extensive delta in a shallow marine embayment that extends to the southeast of Sachs Harbour (Vincent 1983). These sediments, which now form the Sachs Harbour lowlands (discussed in more detail below) are graded to a former sea level at *ca.* 20 m above sea level (a.s.l.) (Vincent 1983, Dyke *et al* 2005). The marine embayment is believed to have been part of the Meek Point Sea (Vincent 1982). Craig and Fyles (1960) were the first to record a marine transgression on the west coast of Banks Island, the limit of which is most often marked by a low wave cut cliff into the Sachs Till and other sediments. The Meek Point Sea is considered to be part of the same transgression as the East Coast Sea, which drowned most of the eastern part of Banks Island (Vincent 1983). Although part of the same transgression, submergence in the eastern part of the island was thought to have been up to 120 m, and thus a full 100 m higher than in the west and southwest (Vincent 1983).

Southeast of Sachs Harbour, the Sandhills Moraine (Figure 2.4), which extends approximately 25 km on a southeast-northwest trajectory, overlies the Sachs Till and is made up of the bouldery Carpenter Till (Figures 2.4 and 2.5) (Vincent 1982, French and Harry 1988). The Sandhills Moraine, in contrast to other moraine systems on Banks Island, possesses a distinctive hummocky topography, which according to French and Harry (1988) gives it a younger appearance than the Sachs Moraine. Vincent (1983, 1992) suggested that the Sandhills Moraine is associated with a local readvance of the Thesiger Lobe near the end of the the M'Clure stade of the Amundsen Glaciation; however, Gurney and Worseley (1997) have suggested that the moraine may simply be a retreat feature. Harry (1982) proposed that outwash associated with the Sandhills

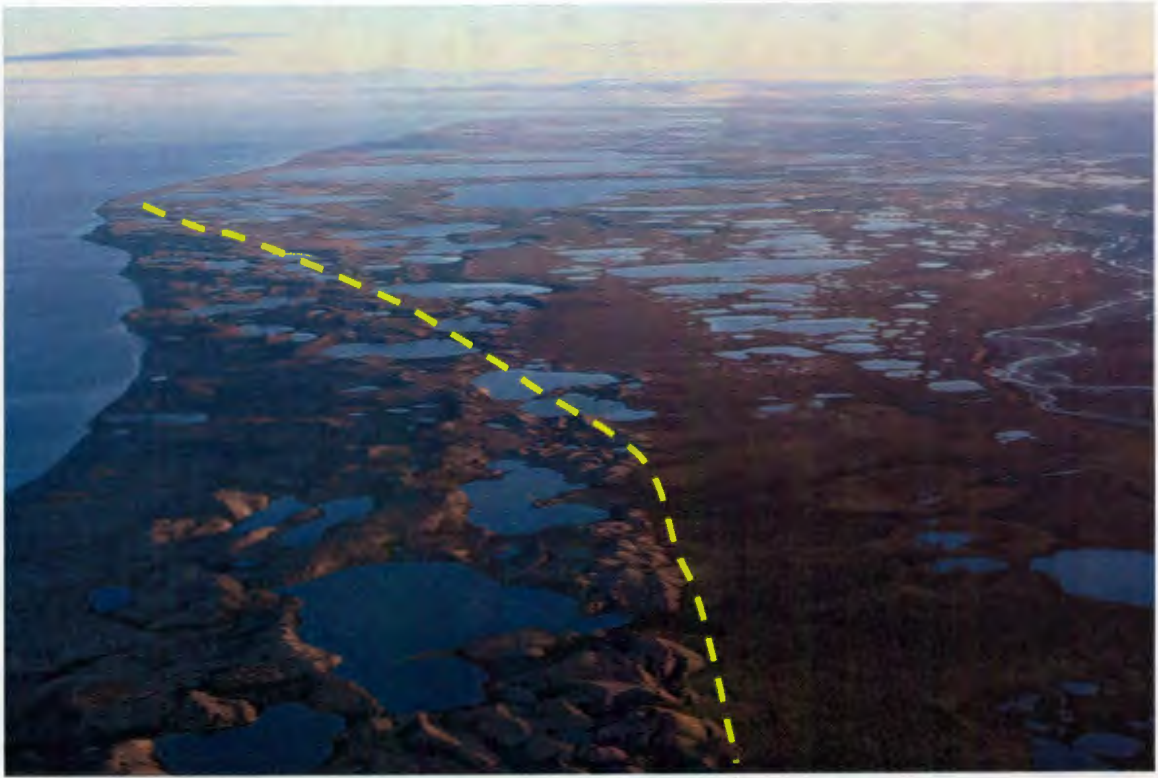


Figure 2.4. Photograph depicting the Sandhills Moraine to the left of the yellow line overlapping the Sachs Lowlands: View is towards the Northwest, photo by D. St Hillaire.

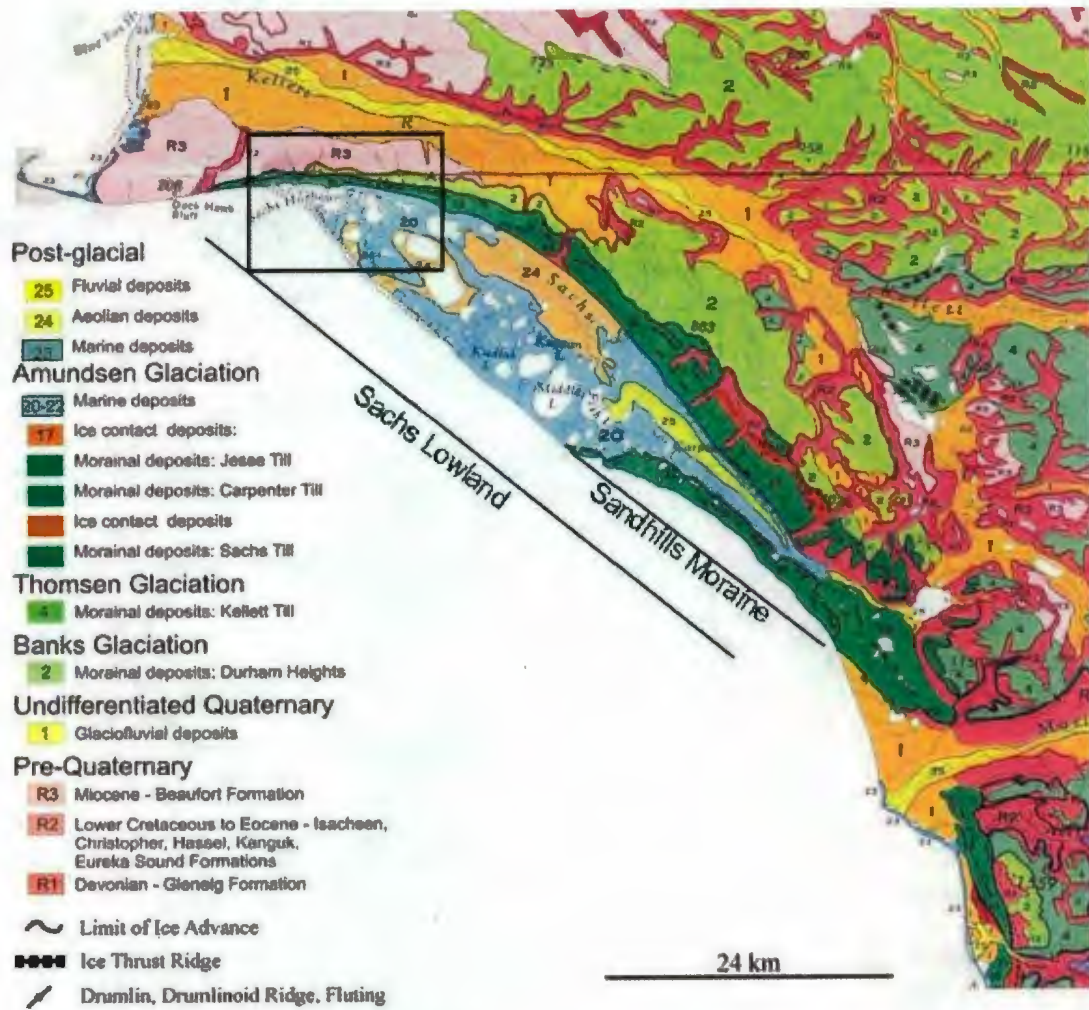


Figure 2.5. Surficial geology of the southwest coast of Banks Island, including limits of glacial advance. Note the location of the Sandhills moraine and the extent of the Sachs Lowland positioned between the two moraines in green. Study area outline within box. Modified from Vincent (1983).

Moraine is distinct from and overlies outwash deposited during the retreat of the Thesiger lobe and together form part of the Sachs Lowland.

#### **2.4 Sachs Lowland**

The Sachs Lowland (Figure 2.5) was described by French *et al.* (1982) as a pitted outwash plain bounded by the Thesiger Bay to the south and the Sachs Harbour moraine to the north. Harry (1982) argued that the outwash was initially deposited on a subaqueous delta front prograding to the northwest, but shallow marine conditions were replaced by a subaerial fluvial depositional environment. Manson *et al.* (2005) describe the coastal plain as glacimarine.

The lowlands contain numerous thaw lakes of either glacial ice origin (kettle lakes) or melt of ice rich permafrost, depending on depth (Harry 1982). The lowland reaches a maximum width of approximately 10 km and extends 35 km to the southeast from Sachs Harbour. The stratigraphy of the outwash plain was mapped from a coastal section 2.5 km southeast of Sachs Harbour by French and Harry (1983) and Harry (1982). At this coastal section, six sedimentary units were recognized (Figure 2.6).

The stratigraphy of the outwash plain was also described in a second coastal section approximately 4 km southeast of Sachs Harbour within exposed sediments beneath a drained thermokarst lake (French and Harry 1983). The lake, with a width of 420 m and a depth of 5 m, showed a similar stratigraphic sequence on either side of the basin as noted in Figure 2.6. The sand and silty sand underlying the lacustrine sediments were shown to be compressed and to contain 40-50% less excess ice than the equivalent materials outside the margins of the lake basin. Sediment compression was further shown

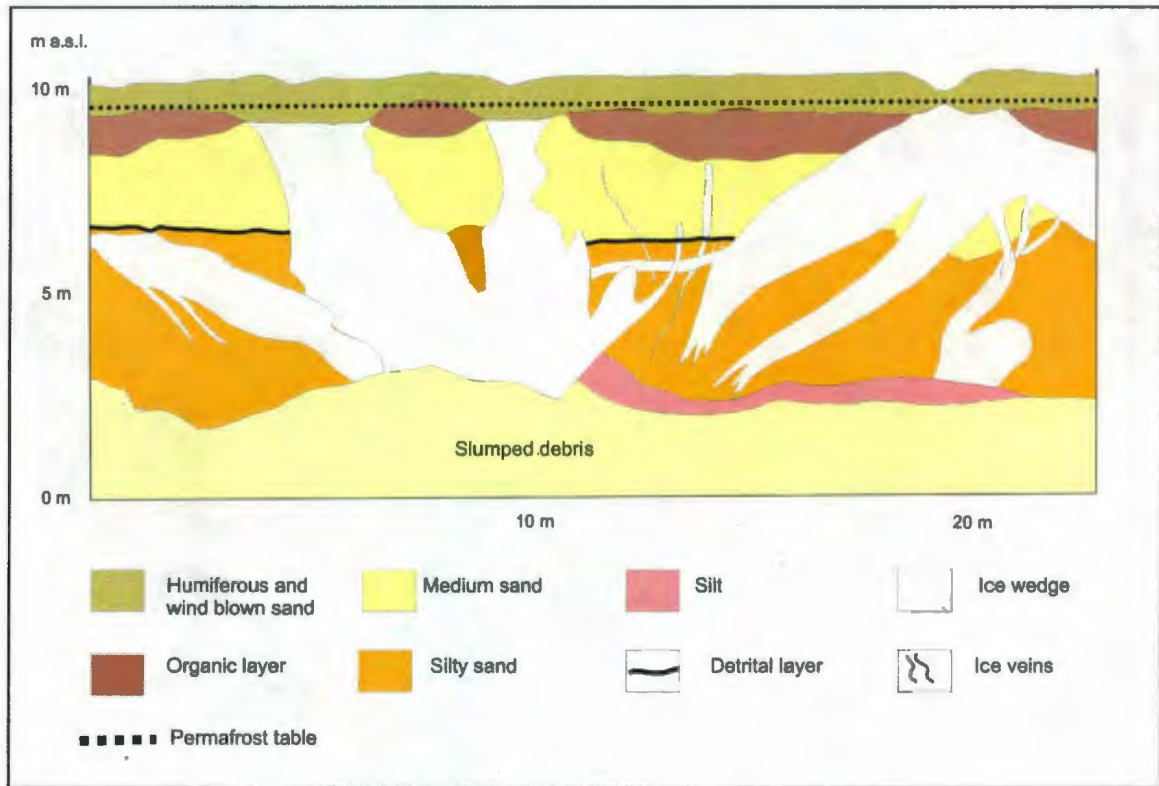


Figure 2.6. Coastal section in exposed bluff illustrating sediment and permafrost stratigraphy South of Sachs Harbour. Modified from French *et al* 1982. Units are described as the following:

- The basal unit, rarely exposed above sea-level, is a blue grey till likely deposited by the Thesiger ice lobe. This can be observed at several localities near the townsite at the base of cliffs. Its presence elsewhere is frequently indicated by a beach armouring of exhumed erratics. Its depth was unknown at many stratigraphic locations.
- The till is overlain by a minimum of 1 to 5 m of laminated grey silt and silty sand which is often poorly and irregularly cross-bedded. This unit had between 20 and 75% excess ice by volume and was interpreted as deltaic in origin.
- A thin 1 to 6 cm thick horizon of detrital willow roots and stems overlies the silt and silty sand and yielded a date of  $10,600 \pm 130$  years BP (GSC-3229).
- The overlying unit varies between 1 and 4 m thick and is composed of yellow-brown well sorted medium sand. It was said to have a gradational contact with the underlying silty sand within which the organic horizon was found. It was described as glacialfluvial outwash.
- The yellow brown sand is overlain by peaty, organic material commonly exceeding 1 m in thickness and yielded a date of  $6490 \pm 60$  years BP (GSC-3216).
- The peaty organic material graded upwards into approximately 0.25 m of humiferous wind blown sand.

by the detrital organic horizon, which normally occurred at an elevation of approximately 6 m a.s.l., but dipped to 0.5 m a.s.l. beneath the basin flank and was said to likely be beneath sea level in the central part of the basin (French and Harry 1983). This suggests a thaw subsidence of at least 5-6 m, a feasible value given the high initial ice content of the silty sand (French and Harry 1983). These findings were consistent with field observations that many thermokarst lakes in the area range between 1 and 5 m in depth (Harry 1982).

Organic material was collected by French and Harry (1983) from the basal horizon of the lacustrine sediment described above. These yielded a radiocarbon date of  $8560 \pm 210$  years BP (GSC-3292) (discussed further in the next section). From the three radiocarbon dates originating from the outwash plain and lacustrine sediments, it can be hypothesized that the first outwash episode, which deposited laminated fine silty sand, had a minimum age of  $10,600 \pm 130$  years BP while the medium sand was deposited between  $10,600 \pm 130$  years BP and  $6490 \pm 60$  years BP.

### **2.5 Records of Holocene warming and initiation of thermokarst activity**

Many of the lakes in and around the Sachs Lowland were interpreted to be of either thermokarst or kettle origin (Harry 1982). Glacial ice is thought to still exist within the Sandhills Moraine (French and Harry 1988). Harry (1982) proposes that the initiation of thermokarst activity and initial formation of thermokarst and kettle lakes took place during a warming period in the early Holocene between 8000 and 9000 years BP based on organic material collected from the basal horizon of lacustrine sediments. The organic material yielded radiocarbon dates of  $8560 \pm 210$  years BP (GSC-3292) and  $8280 \pm 140$

years BP (GSC-2246) and were considered minimum ages for the initiation of lake sedimentation at these sites (French and Harry 1983). These dates are consistent with that of Rampton and Bouchard (1975), and Rampton (1988) with respect to the origin of thaw lakes on the Tuktoyaktuk Peninsula, where thermokarst activity would have begun as early as 12.9 ka BP and was widespread between 10-9 ka BP. More recently, Kaufman *et al* (2004) indicated that the period of maximum Holocene warmth in the western Arctic was between 11.5 and 9 ka during which warmer air would have triggered the melt of ground-ice. This is consistent with Ritchie (1984) who indicates that a slow warming had commenced *ca* 15 ka BP followed by a rapid warming between 12 and 10 ka BP. Thermokarst processes appears to have remained active in Tuktoyaktuk between 8.5 and 4 ka BP but with limited development of new thermokarst depressions (Héquette *et al* 1995). The warm period ended between 7.8 and 2 ka BP (Kaufman *et al* 2004) which coincides with the period of increased aeolian activity on Banks Island *ca* 4 ka BP (Pissart *et al* 1977) as well as an increase in pingo growth around the same period (French *et al* 1982).

## **2.6 Past records of sea level change**

Eustatic sea-levels have fluctuated by up to 140 m along the Beaufort Sea shelf throughout the Quaternary (Hill *et al* 1985). Based upon seismic evidence along the Beaufort Sea shelf and radiocarbon dating, Hill *et al.* (1985, 1993) found that relative sea level rose from -140 m at 27 ka BP to a relative highstand of -40 m which was then lowered to the Late Wisconsinan (MIS 2) lowstand of -70 m at a poorly constrained time between 21,000 and 8000 BP. A sea level curve for the Beaufort Sea region has been

reconstructed for a large geographical area and indicates that sea level has been rising throughout most of the Holocene (Hill *et al* 1993) (Figure 2.7). The sea level curve shows sea level rising at rates of 4 to 5 mm/a in the early Holocene (*ca.* 9 ka yrs BP), a rapid rise of between 7 and 14 mm/a during the middle Holocene (*ca.* 5 ka yrs BP) and a slower rise of less than 3 mm/a for the past 3000 yrs (Hill *et al.* 1993). The lowstand for the Beaufort Sea was thought to be due in part from subsidence and sediment loading (35 m) but mostly from glacioeustatic effects (remaining 105 m) (Hill *et al* 1985). Kerr (1996), on the other hand, argued that the late Wisconsinan lowstand was solely from glacioeustatic effects because the region was located beyond the peripheral forebulge of the ice sheet.

No detailed sea level curve has been completed for southwestern Banks Island, however, relative sea level was affected by glacio-isostatic depression and rebound since the last glaciation. This is evident from the marine transgression that affected the southwestern coast of Banks Island up to approximately 20 m a.s.l. creating wave cut notches in exposed sediment (Vincent 1983, Dyke *et al* 2005). The eastern portion of the island was thought to have been depressed further, up to 120 m (Vincent 1983).

In contrast to the sea level curve for the Beaufort Sea from Hill *et al* (1985, 1993), relative sea level near Sachs Harbour was likely higher than at present prior to 10,600±130 years BP. This is shown from the grey silty sand found within the Sachs lowlands which was interpreted to be deposited in a shallow marine deltaic environment (Meek Point Sea) (French *et al* 1982). However, relative sea level was likely lower than the contact between the grey silty sand and medium yellow sand (6 m a.s.l.) following 10,600±130 years BP as the sand is interpreted to have been deposited subaerially. This

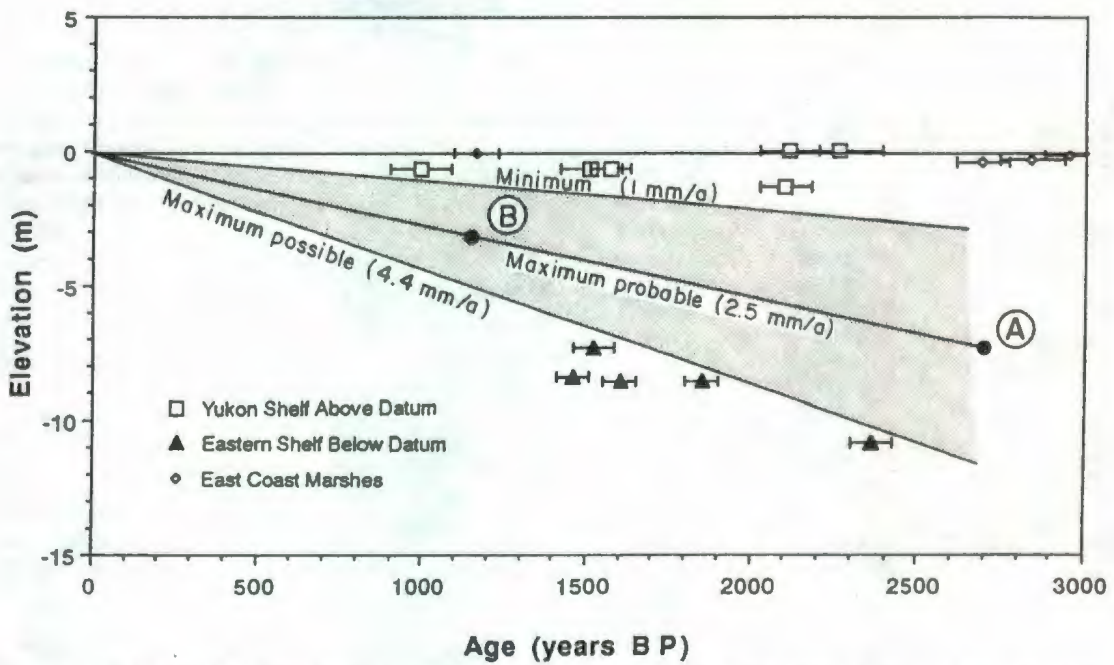
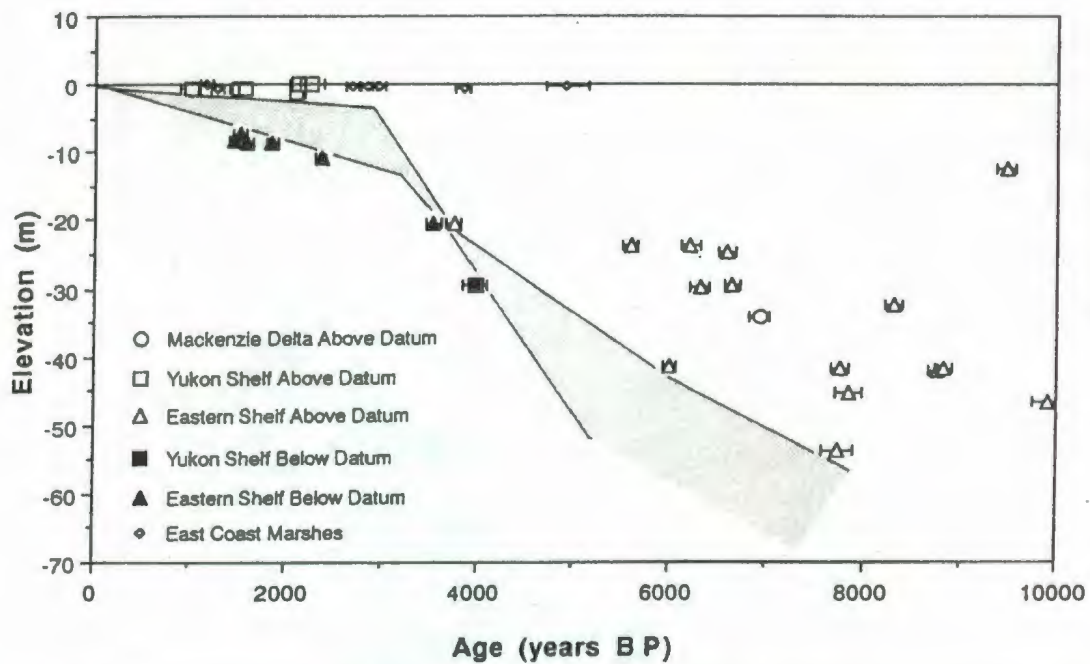


Figure 2.7. Beaufort Sea level curve and estimated rate of sea level rise during the late Holocene. Modified from Hill *et al* 1993. In the first diagram, the upper line constrains samples that were deposited above sea level, while the lower line constrains samples deposited below sea level. The actual sea level position therefore lies at some point between the two lines.

contact may represent the emergence of the delta. Due to the detrital nature of the dated organics, these positions must be considered limiting points. Kerr (1996) similarly suggests a sea level position at approximately 5 m a.s.l. by 9600 BP.

Kerr (1996) produced a map displaying marine limit elevations from Cape Parry to Bathurst Inlet. It showed a marine limit increasing from 10 to 225 m a.s.l. from west to east resulting from the differential rates of uplift. Kerr (1996) suggests that the West Bernard Harbour area, (Figure 2.8) with a marine limit of 135 m, is the approximate location of the zero isobase separating areas of present submergence to the west and emergence to the east.

## **2.7 Recent records of sea level change**

Global eustatic sea levels have risen at an average rate of approximately 1.3-2.3 mm/a between 1961 and 2003 and an average rate of 2.4-3.8 mm/a from 1993 to 2003 (IPCC 2007, Church *et al* 2004). Unfortunately, in the Canadian Beaufort Sea, there has been only one long-term tide gauge record (Shaw *et al* 1998). Manson *et al.* (2007) have shown that relative sea level at Tuktoyaktuk has been rising at  $3.5 \pm 1.1$  mm/a since 1961 as a consequence of both isostatic subsidence and eustatic sea level rise. Evidence of submergence in the western Arctic can be seen in flooded river mouths, flooded ice-wedge polygons, the widespread erosion of unlithified deposits (Forbes *et al* 2004A), as well as the inundation of coastal lakes. Rates of submergence throughout the Canadian Arctic, including Sachs Harbour, are measured using continuous GPS monitoring stations. Preliminary results over the space of one year for Sachs Harbour showed a subsidence rate of  $-9.8 \pm 2.7$  mm/a (Forbes *et al* 2004B). Models on the other hand show

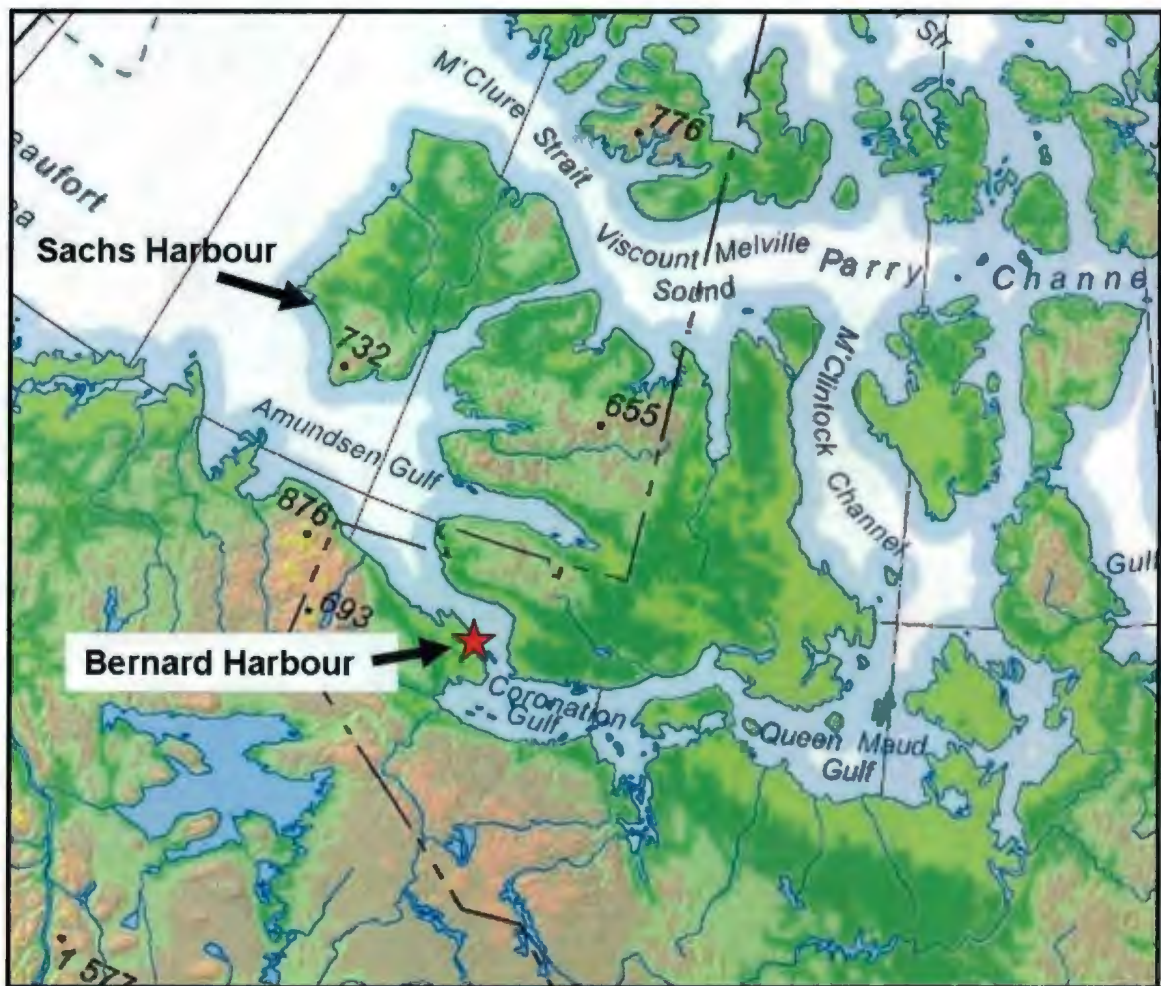


Figure 2.8. Location of West Bernard Harbour, with a marine limit of 135 m, is the approximate location of the zero isobase separating submergence to the west and emergence to the east. Numbers on image represent elevation. From Kerr (1996).

a submergence of 2.5 mm/a in both Sachs Harbour and Tuktoyaktuk (Manson *et al* 2005), which, in the case of Tuktoyaktuk, seems to be reasonably similar to tide gauge measurements.

## **2.8 Sediment transport and Sachs Spit**

The Sachs spit (Figure 1.4), a prominent feature in the Sachs Harbour estuary, has a 1.6 km-long trunk and a 0.7 km-long hook at its end. The spit has a maximum crest elevation of 0.7 m a.s.l. (Belliveau 2007). The trunk is oriented parallel to the coastline of the outwash plain. Its growth is a result of sediment transport from eroding cliffs southeast of the harbour along the outwash plain (Harry *et al* 1983). Belliveau (2007) has shown that the spit has undergone considerable progradation and backstepping (Figure 2.9). Harry *et al* (1983) have also shown evidence that the size of the spit has increased both in terms of trunk, and more significantly, in the hook. The spit is vulnerable to overtopping from storm surges, as seen in aerial photographs from 1950 where a complete breach of the spit 30-40 m wide was present. The breach was completely infilled by 1958 suggesting that approximately  $4.6 \times 10^5 \text{ m}^3$  of sediment was emplaced during the 8 years (Harry *et al* 1983). Nearshore current circulation experiments were carried out by Harry *et al* (1983) to develop a sediment transport model. The model suggested that the sand cliffs of the Sachs Lowland form the main source of sediment while the Sachs Spit acts as the main sink through normal littoral drift. They suggested that sediment may also be moving south from the shoreline across the shallow "water bridge" (sill II – Figure 1.4) originating from the receding cliffs west of the community.

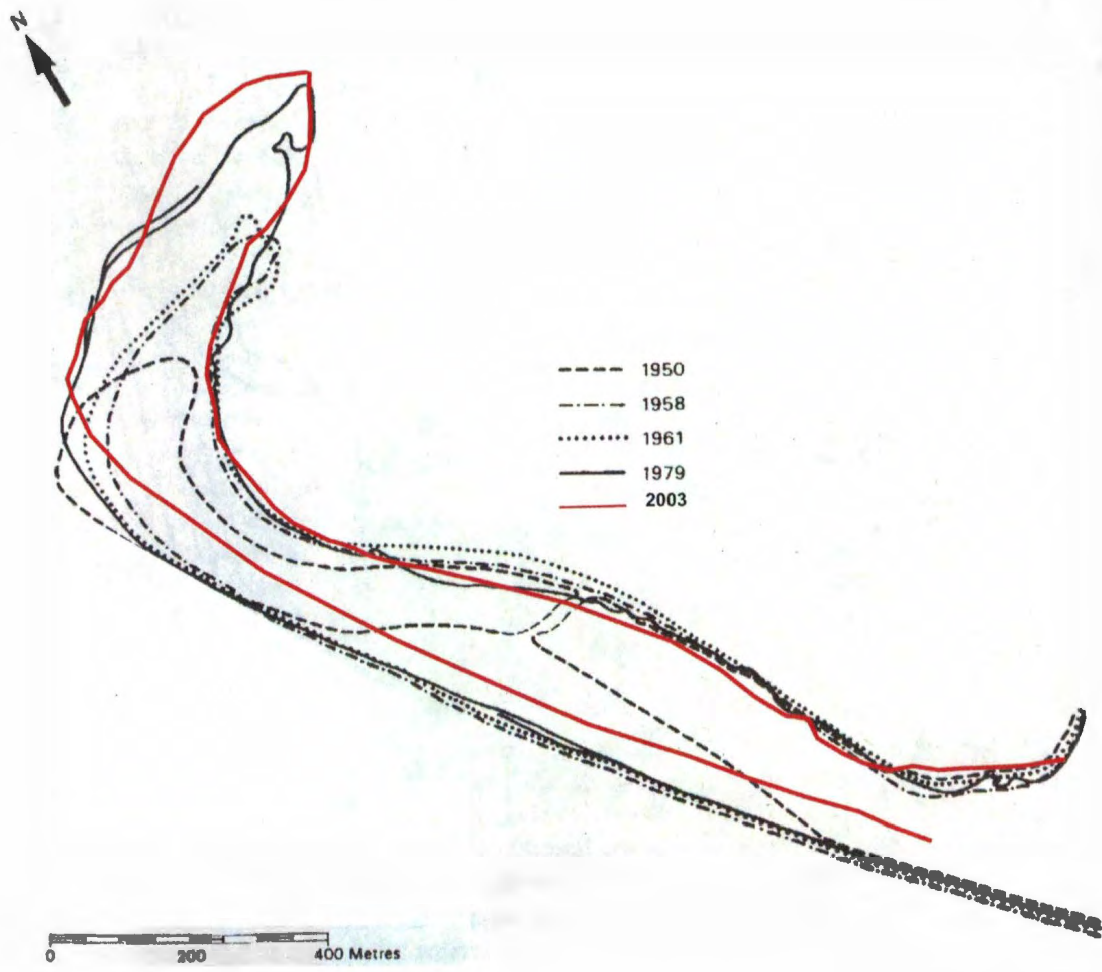


Figure 2.9. Sachs spit showing progradation over the last 50 years, modified from Harry *et al* (1983) and Belliveau (2007).

## **2.9 Community impacts and sensitivity to sea level rise**

With climate change the Polar regions have experienced the greatest regional warming on earth in recent decades due largely to various feedback processes (Huntington *et al.* 2005). Some of these changes have been interpreted to be due in part to anthropogenic intensification of the global greenhouse effect (Huntington *et al.* 2005). With an increase in greenhouse gases and a changing climate, global sea levels are rising from thermal expansion of the oceans as well as from increased input from melting glaciers and ice caps (IPCC 2007, Proshutinsky *et al.* 2001). Sea level rise increases the risk of flooding and erosion on Arctic coasts and may exacerbate other coastal hazards such as ice ride-up and pile-up (Furgal and Prowse 2008, Walsh 2005).

With increasing sea levels, storm waves are able to reach higher up the shoreline and are capable of removing more sediment. With warmer air temperatures, higher ground temperatures are expected to lead to an increase in retrogressive thaw slumps (Forbes 2005). With warmer temperatures, freeze-up is predicted to occur later in the fall, contributing to increased periods when the coast will be exposed to storm waves and a longer period for waves to form. These combined factors suggest that rates of coastal erosion may increase significantly in the coming decades. Furthermore, increased temperatures, leading to increased thaw subsidence, as well as an increase in erosion may increase the rate at which coastal lakes in the area are inundated.

## **Chapter 3 – Methods**

### **3.1 - Introduction**

The methods used in this study examine the geomorphic, stratigraphic, and sedimentary characteristics of recently inundated basins on Banks Island in order to better understand the processes involved during inundation and their effects on both the height of the sill and its evolution. The stratigraphy was observed remotely using marine acoustic techniques and ground-truthed through core retrieval. Sedimentary characteristics were analyzed in the cores to decipher possible origins of sedimentary structure and depositional environments.

### **3.2 Air photo mapping**

Air photo mapping was used to detect landscape and morphological changes on the outwash plain over the span of the available airphoto set (~50 years). Both high resolution satellite images from 2003 and 2002, as well as multiple sets of air photos, were utilized to give a sense of the landscape change. Particular characteristics observed were coastal bluff retreat, sediment transport and spit development. With the aid of ArcGIS, satellite images, and Quaternary maps, suitable sampling areas were located.

### **3.3 Sub-bottom profiling**

Information on sediment type, sediment thickness, distribution and water depth were gathered from a detailed sonar profile. The acoustic stratigraphy from the upper portion of the sill was targeted. For this project, high resolution imagery was preferred in order to clearly visualize the small scale stratigraphy within the upper section of each sill.

Sub-bottom profiling was done using a Knudsen K320B/R 3.5 kHz sub-bottom profiler aboard the CSL *Heron* launched from the CCGS *Amundsen* in October 2006. Seven profiles were obtained within the harbour. The acquisition of multibeam bathymetry aboard the CSL *Heron* was planned but not carried out due to technical difficulties.

### **3.4 Vibracoring**

Sediment cores were retrieved for the purpose of ground-truthing seismic sections and to interpret sill stratigraphy. The coring locations specifically targeted the deepest and shallowest parts of the sills and channels or areas along seismic lines. The deepest parts of the sill were targeted for they likely represent remnants of the basin outlet prior to submergence and during the initial stages of inundation. The shallowest parts were targeted with the intention of penetrating into pre-inundation sill material, and to be used as a reference when comparing the sedimentology of the different units with those encountered in coastal sections (i.e., French and Harry 1982; Harry 1983).

A percussion coring system was used from the sea ice in the spring of 2006 while a vibracoring system was used in 2007 with the intention of obtaining a greater penetration. The vibracoring system, originally developed in the 1960s, has the main advantages of simplicity and portability. Vibracoring has also been shown to penetrate sand in river beds and deltas with much more ease than with other coring systems (Glew *et al.* 2001). However, well sorted, compacted, quartz sand (i.e., beach deposits) may be very difficult to penetrate using the vibracoring system (Smith 1984). Vibracoring also results in sediment compaction by as much as 60% but normally varies between 10 and 40% (Glew *et al.* 2001, Smith 1984). When using the inundation model, compaction can

be a source of error in determining an index point and must therefore be taken into account. Compaction was determined by subtracting the final core length from the penetration measured in the field.

The core tubing consisted of a 5 m-long aluminium irrigation pipe with a diameter of 76 mm (Figure 3.1). A sheet metal core catcher prevented the sediment from escaping upon retrieval and was firmly attached to the bottom of the core barrel with rivets.

Following augering through the sea ice and depth measurements, the core barrels were inserted through the ice and coupled until the required length was attained. The vibracore head was then attached and the engine subsequently turned on. The core barrels were vibrated into the sediment until penetration had ceased and subsequently removed from the sea floor using a winch attached to a tripod. The cores were quickly lifted to the surface where very fine quartz sandblasting sand was added to the top of the core (to reduce sediment loss or mixing) and then subsequently capped. Cores were marked for direction and location, stored at temperatures above 0°C, and shipped to the core laboratory in Dartmouth, NS (Bedford Institute of Oceanography).

### **3.5 Core analysis**

Core processing was carried out at Bedford Institute of Oceanography while sediment analysis was performed at Memorial University of Newfoundland. Although a multi sensor track was available for use at BIO to measure properties such as discrete velocity and magnetic susceptibility, data were not utilized due to the large errors that occur when measuring through or near aluminum core barrels.

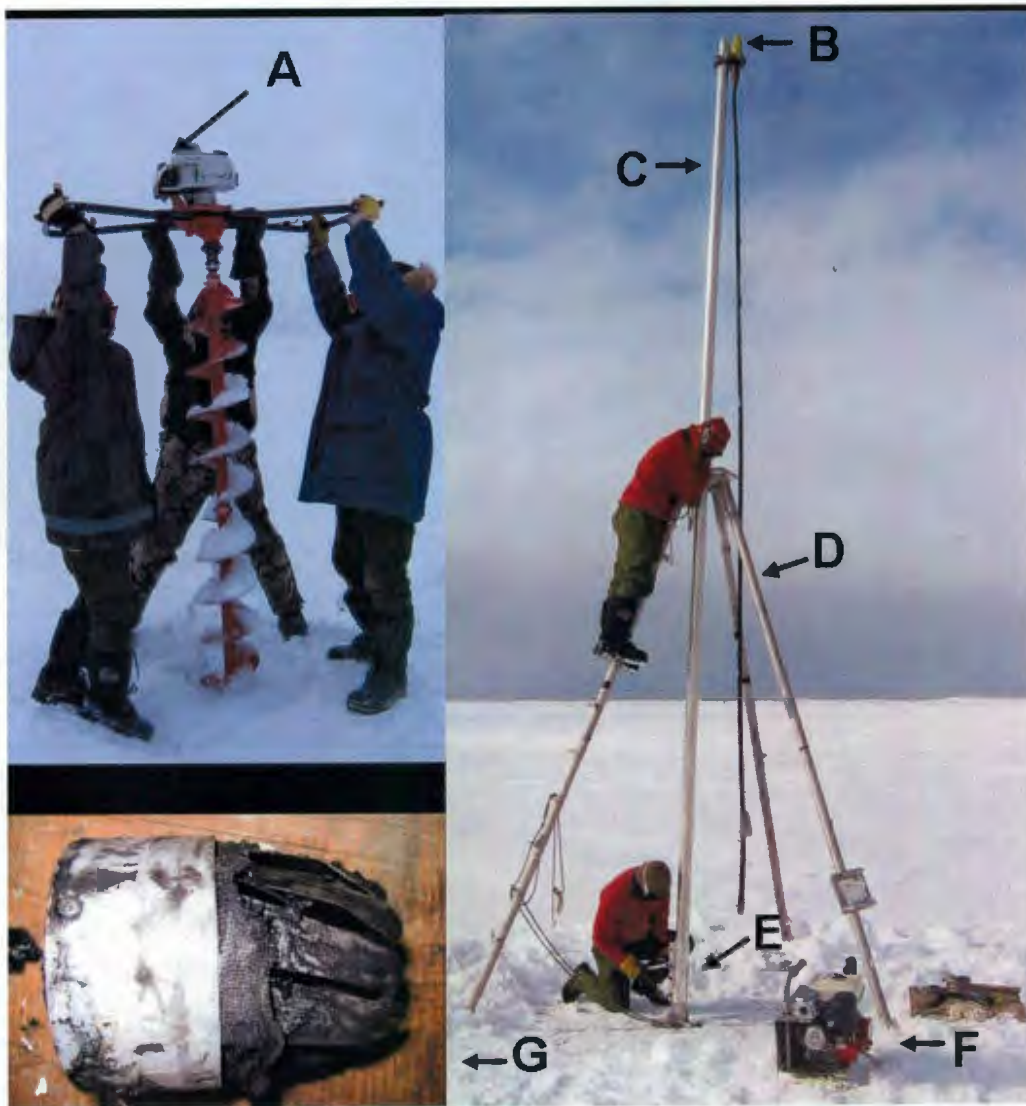


Figure 3.1. Image depicting ice auger(A) and coring apparatus above a sea ice platform: vibracore head (B), core barrel (C), tripod (D), coupler (E), vibracore engine (F), and subsequently removed core catcher (G).

### **3.5.1 X-radiography**

At the laboratory in Dartmouth, whole sediment cores were X-rayed in real time to determine core quality (presence/absence of gaps and disturbances), to assess the sediment structure for best splitting angle, for the presence/absence of laminations, and to determine the location of potentially dateable shell material.

### **3.5.2 Splitting, description, and sub-sampling**

Cores were described and subsampled in order to visually characterize the core, determine the particle size and carbon content, and to interpret the stratigraphy. Initially, core catchers were removed and placed in bags for subsequent analysis. The aluminum core barrels were then cut longitudinally using a table saw set at a low height so as not to cut into the sediment. The sediment cores were then split longitudinally by pulling a piece of fine wire through the sediment along the cuts in the core barrels. The two halves, "archive" and "working", were then labeled with metre tape to indicate down-core depth.

The archive half was photographed using a digital camera where overlapping photos were taken at two scales; a close up image covering 30 cm intervals and a long shot covering 90 cm intervals. The cores were then described visually for the condition of the sample (cracks and disturbance), consistency (soft, firm, hard), colour (Munsell soil colour), and visual core descriptions consisting of colour, texture, grain size, bedding, contacts, bioturbation, and other visible features.

The working half of the cores were then sub-sampled for organic and inorganic carbon (loss-on-ignition method) using modified 10 cc syringes. Approximately 2 cc of sediment was taken at a 5 cm sampling interval or wherever sediment transitions (grain

size, colour, sedimentary structure) occurred. Sub-samples for particle size analysis were taken using a stainless steel spatula retrieving approximately 10 cc. The particle size sub-samples were taken at 10 cm intervals or wherever distinct changes in grain size occurred. Shells and organic matter were removed for radiocarbon dating.

### **3.5.3 Loss-on-ignition**

Sequential loss-on-ignition (LOI) is a common and widely used method to estimate organic and inorganic carbon content of sediments (Dean 1974, Heiri 2000). Loss-on-ignition was used to help distinguish between sediments containing higher carbon contents and clastic sediments with lower carbon contents. Carbon content can help in determining sedimentary origin.

Loss-on-ignition analysis was performed along the entire length of the cores at a 5 cm interval or higher along sedimentary boundaries and processed as described in Dean (1974) and Heiri *et al* (2000). The dried and weighed samples were placed a muffle furnace six at a time and heated to 550°C for 4 hours. After 4 hours, the crucibles were removed, cooled in a desiccator, and re-weighed to determine the dry weight. The crucibles were then placed back into the muffle furnace for a further 2 hours at 950°C to determine the inorganic carbon content. Samples were then re-weighed.

The percentage of the dry weight lost upon ignition was recorded as the loss-on-ignition value for each sample. An increase in the percent loss on ignition can either be interpreted as an increase in organic matter in the sediment or conversely to a decrease in the amount of clastic material (i.e., reduced clastic sedimentation rates). The results were then tabulated and graphed to determine if trends were present. Inorganic carbon was

deemed not likely to be indicative of marine conditions as originally postulated due to the carbonate rich source material (22% - Vincent 1983) and a low number of foraminifera found in sediment cores.

#### **3.5.4 Particle size analysis**

Grain size is a fundamental physical property of sediment and is a useful descriptive property (Boggs 2006). Also, because the size and sorting of sediment grains may reflect sedimentation mechanisms and depositional conditions (Boggs 2006), grain size data were used to help interpret the depositional environment of sediments.

Grain size analysis was performed on cores at 10 cm intervals or where transitions were evident. As many samples were high in mud (silt and clay) content, the samples were wet-sieved to remove as much of this fraction as possible using standard wet sieving techniques on sieves between 63 and 4000  $\mu\text{m}$ .

## **Chapter 4 – Results**

### **4.1 Outline**

This chapter begins with the landscape change and morphology of the study area. Next the acoustic stratigraphy and sedimentary characteristics are presented followed by an in-depth look at the lithofacies descriptions. The acoustic and sedimentary descriptions of the sills are then presented followed by a summary of the interpretations.

### **4.2 Landscape change**

Landscape changes within the harbour were initially investigated by Harry (1982) and later by Belliveau (2007). Air photo interpretation has shown that Sachs Harbour, on a large scale, has experienced only minor changes within the past 50 years. Most notably, the Sachs Spit has grown in size and volume and Sill II has widened (Figures 4.1 and 2.9). Furthermore, coastal erosion has caused minor headwall retreat along many of the cliffs within the harbour, particularly in areas directly exposed to Thesiger Bay (Harry *et al* 1983, Belliveau 2007). Within the harbour, significant change is not easily discernable, especially for many of the channels and basin sills. The outlet channels for the Mirabilite Basins do not appear to have increased in depth nor have they migrated significantly. West of the town site, the disappearance of a small island surrounding what appears to be a small basin has occurred (Figure 4.1). Areas experiencing aeolian deflation can be seen on the coastal bluffs by the large deflation lags (Figures 4.2 and 2.5).

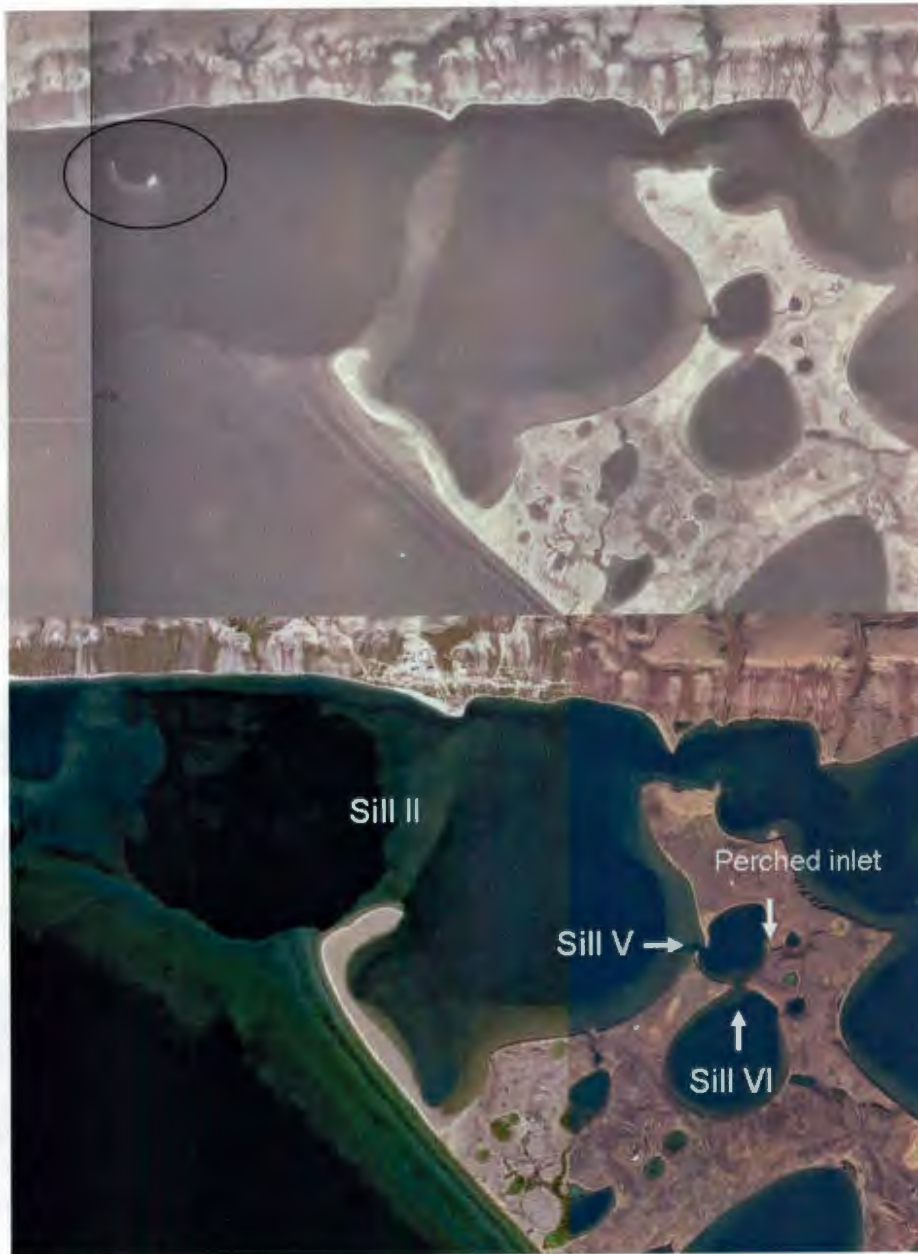


Figure 4.1. Aerial photograph from 1950 (top) compared to satellite images from 2003 (bottom). Progradation has occurred on the spit at sill V, and much more noticeably along the Sachs Spit accompanied by noticeable retreat along the outer Sachs Lowland shoreface. The spit has likely had an effect on sill II as it appears to have widened significantly, however it is unknown for certain whether the widened appearance is simply due to better resolution at depth. The channel cutting sill II near the community appears to have narrowed, likely from the apparent beach progradation. Erosion on the western portion of the photograph is evident near a small basin where the edges, appearing as a small island in the 1950 airphoto, are no longer exposed above the surface.



Figure 4.2. Aeolian deflation along coastal bluffs of Sachs Harbour. Photo taken adjacent to the Inner Basin near sills V and VI.

### **4.3 Sill and basin morphology**

Sachs Harbour has previously been shown to have a complex bathymetry (Siferd 2001). Inner and Outer basins have irregular bottoms in excess of 46 and 37 m water depth, respectively, whereas Shore Basin and Mirabilite Basin I and II have depths of at least 14 m, 12 m, and 19 m, respectively. The irregular bottoms and great depths are consistent with the interpretation of kettle lakes (Benn and Evans 1998). Headwall retreat and thermokarst erosion may have widened the unusually large Inner and Outer basins to a point where multiple basins originally surrounding the larger basins may have amalgamated to form the two larger basins. This is further suggested by the unusual shape of these two large basins.

The sills have relatively steep slopes on their inner basin margins and much gentler slopes next to the palaeo Sachs River channel (Figure 1.4) or where exposed to Thesiger Bay. Sills were as shallow as 1.2 m, such as the section separating the Inner and Outer Basins (sill II), or as deep as 4.5 m along sections of the Inner Basin sill (sill III). The sill tops were generally flat and measured approximately 300 to 600 m across. Many of the sill slopes exhibit slumping near their bases. The palaeo Sachs River channel, which sits north of the Inner Basin, had water depths between 4 and 7 m with an average of approximately 5 m. Smaller channels that cross cut the sills were shown to have water depths varying between 1.5 and 5 m. Sills will be discussed further in section 4.6.

### **4.4 Acoustic stratigraphy and sedimentary characteristics**

Seismic profiles taken during the Amundsen 2006 ArcticNet Expedition (Leg 2) were intended to address questions of sea-level rise and associated coastal change in the

western Canadian Arctic. Surveys were carried out in Sachs Harbour on October 3<sup>rd</sup> and 4<sup>th</sup>, 2006. Four seismic lines were obtained within the Inner basin, two across the northern sill (sill III) and two across the sill separating the Inner and Outer basins (sill II), as well as a line across the Outer Basin sill (Sill I) (figure 4.3). These seismic lines, although occurring largely over acoustically impenetrable sediment, proved to be invaluable for the sill and sediment interpretation. Water depths were determined by multiplying half of the two way travel time (displayed in seconds) by the assumed velocity through water (1500 m/s).

The sill tops are characterized by an acoustically impenetrable unit (Figure 4.4) that in places underlies a thin acoustically transparent to semi-transparent stratified unit draping the uneven hummocky surface. In places there appear to be thin reflectors within a faintly stratified unit (Figure B5 – appendix). Cut and fill channels were encountered within sill III (Figures 4.5 and 4.6). These were thought to either represent outlet channels or part of a migrating palaeo Sachs River. These cut and fill channels were characterized by U-shaped depressions ponded with faintly stratified sediment situated within an acoustically impenetrable unit. Sill slopes commonly showed slumping and were draped by acoustically transparent to well stratified sediment which continued into the basins. Further seismic descriptions can be seen under section (4.6) while a line by line description can be found in appendix B.

#### **4.5 Lithofacies description**

A total of 11 sill cores (Figure 4.3) were obtained in the spring of 2007 in addition to 2 sill cores from the spring of 2006. Cores ranged between 48 and 176 cm in length and

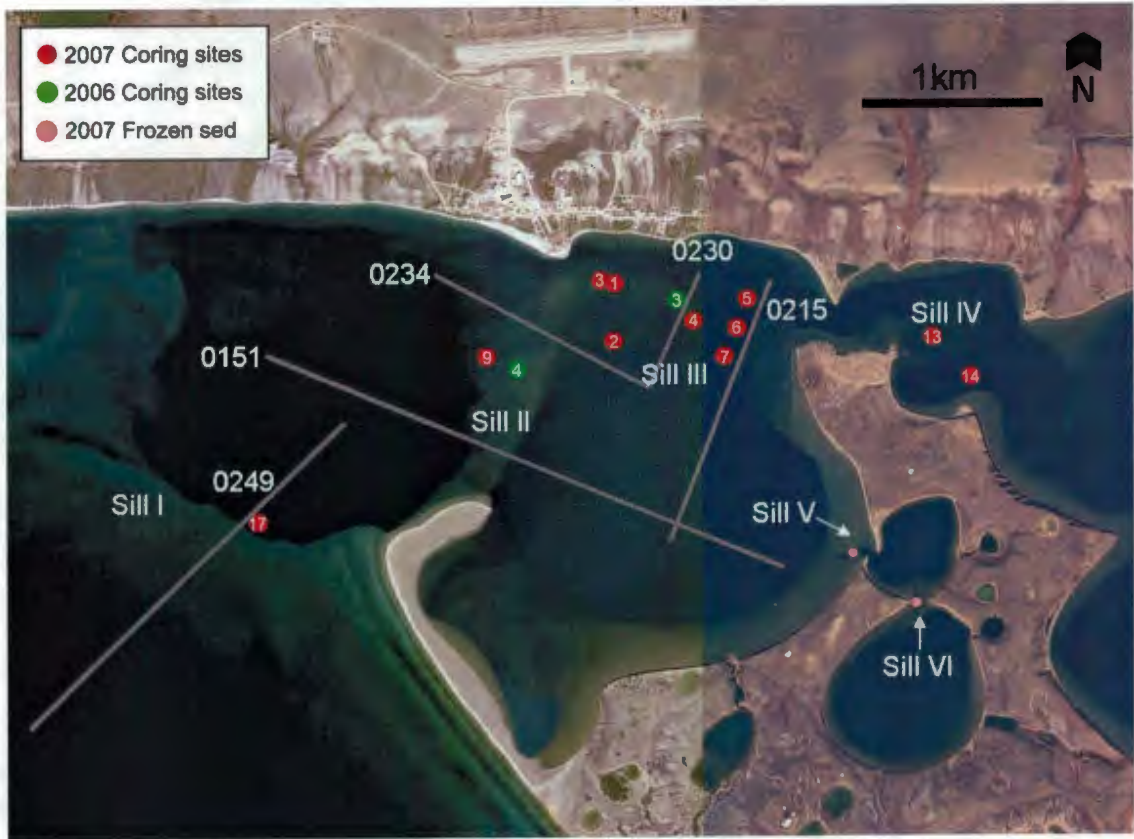


Figure 4.3. Seismic tracks and core locations within Sachs Harbour.

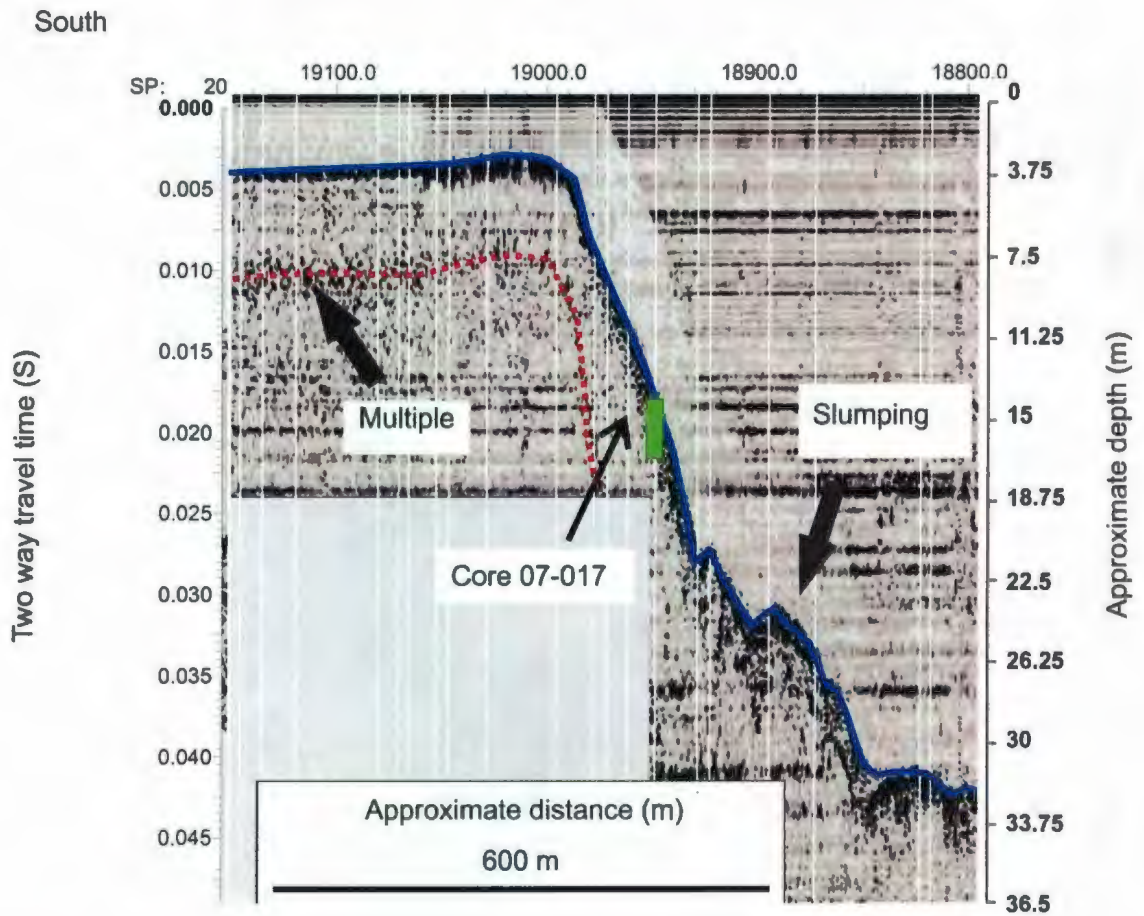


Figure 4.4. Portion of seismic line 0249 depicting impenetrable sill top along with weakly stratified area towards Thesiger Bay (left). Note the sea bed multiple highlighted in red. Location of core 07-017 is indicated by green line.

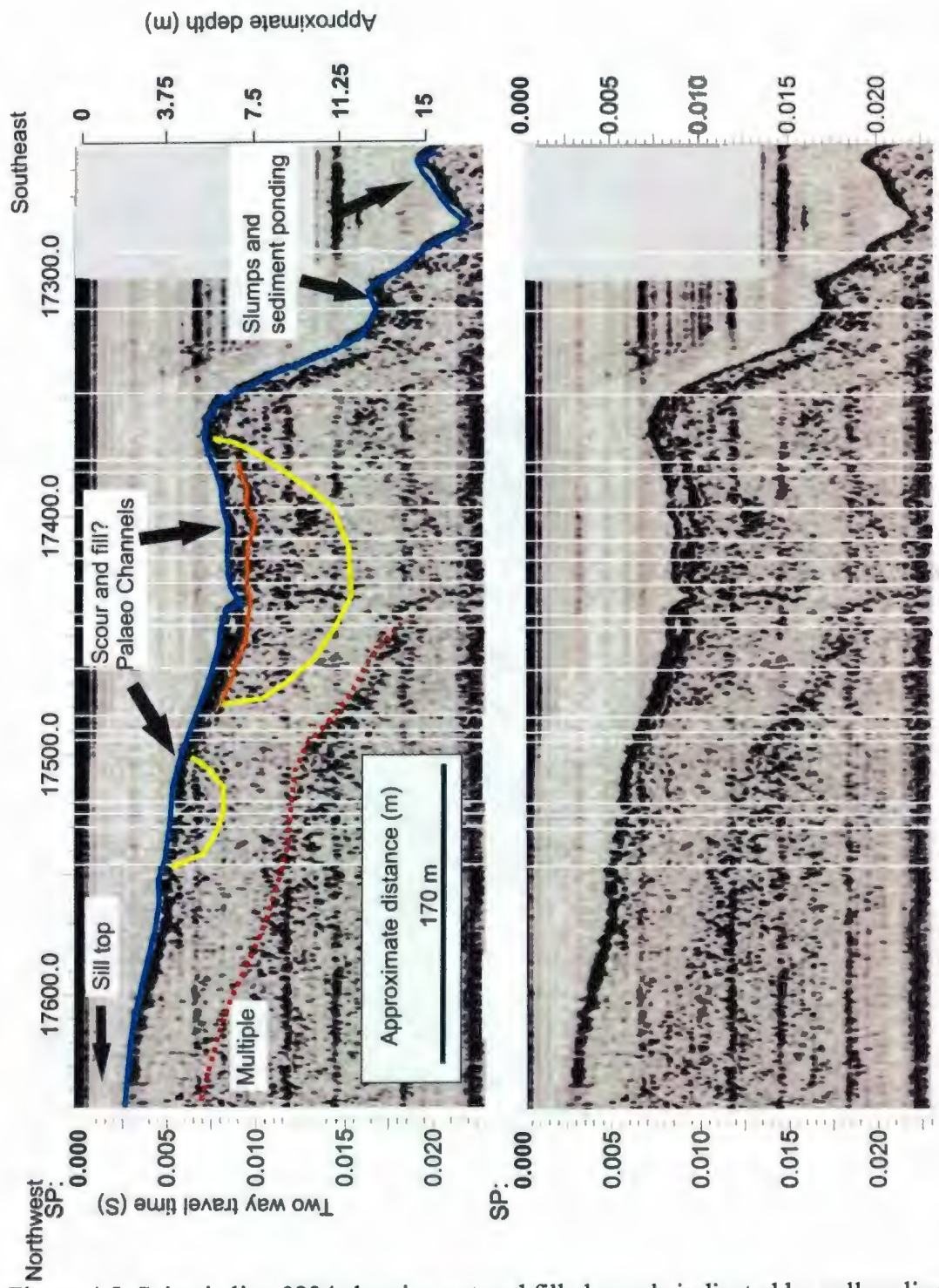


Figure 4.5. Seismic line 0234 showing cut and fill channels indicated by yellow lines. Note the acoustic reflector (orange) within the channel that is thought to be associated with a sand layer from core 07-002.

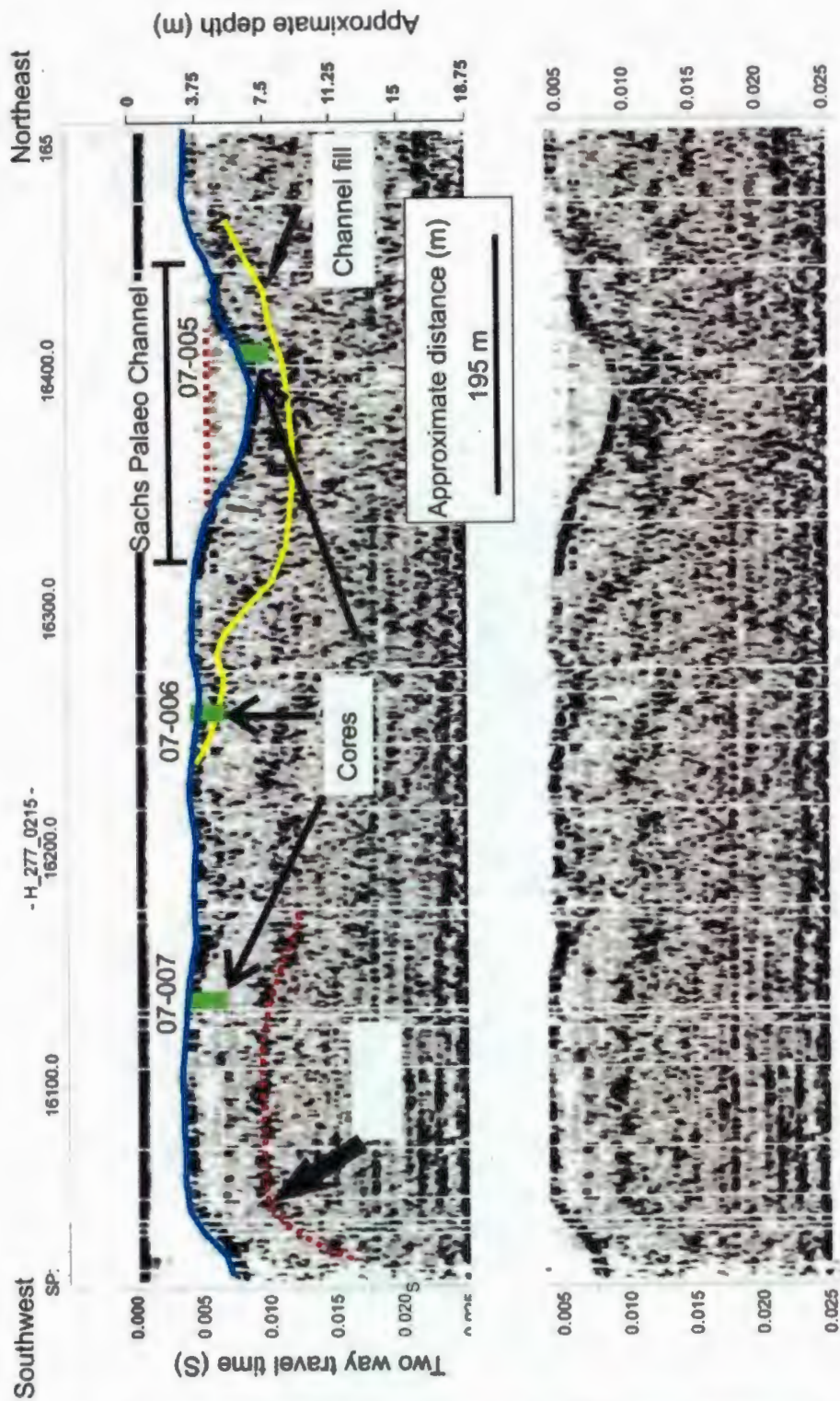


Figure 4.6. Seismic line 0215 showing cut and fill channel associated with migration of the palaeo Sachs River channel indicated by yellow line. Note the location of cores 07-007, 07-006, and 07-005 from left to right shown by green lines.

were taken in depths ranging between 1.8 and 9.2 m. Two other cores were attempted on the sills of Mirabilite Basins 1 and 2. A summary of core depths and lengths are listed in Table 4.1 while core stratigraphy can be seen within figures under section 4.6.

Sediment types varied throughout the harbour but were dominated by certain characteristics depending on the depositional or erosional environment. The main sediment types encountered included mud, fine sand, and medium to coarse sand. Within the collected cores, five lithofacies were described while two distinct depositional environments have been suggested; i) post-inundation estuarine or reworked sediment, including fluviably derived sediment (lithofacies 3, 4, and 5) and, ii) pre-inundation sediment likely associated with deglaciation (lithofacies 1 and 2). A description of each lithofacies is shown in Table 4.2.

### **Lithofacies 1**

The sediment from lithofacies 1 was generally found within the sill sediments on the western section of sill III and interpreted as a pre-inundation sediment. The sediment (e.g., Figure 4.7) was described as beige (2.5Y 4/3 – 3/2) coarse to very coarse sand with pebbly laminations and occurring with or without black fine to medium sand laminations (see lithofacies 3 for black sand) (core 07-001, 07-003, 06-003 – with 3-5mm mud laminations (5Y 4/2)). This lithofacies was most commonly but not exclusively found at the base of cores and had thicknesses varying between 20 and 40 cm. Grain size varied between 1-52% mud, 5-83% fine sand, 2-91% medium/coarse sand, and 1-6% granule. Organic carbon varied between 2 and 7%. A similar more consistently massive beige medium sand (2.5Y 5/4) was also found in cores 07-004, 07-003, 06-004 with a more

Table 4.1. Summary of core information from sills. Tides were corrected to low tide using charts and time of water depth measurement.

Core number	Retrieval date	Water depth (m)	Tide corrected depth (m)	Core Penetration (cm)	Core length (cm)	% compression
07-001	26/04/07	4.2	4.05	n/a	130	n/a
07-002	26/04/07	4.2	4.05	188	120	36
07-003	26/04/07	2.9	2.75	n/a	104	n/a
07-004	28/04/07	4.95	4.8	255	176	30
07-005	27/04/07	4.9	4.75	111	74	33
07-006	27/04/07	3.35	3.20	92	86	7
07-007	27/04/07	4.9	4.75	99	66	33
07-009	29/04/07	3.9	3.8	55	48	12
07-013	01/05/07	2.0	1.9	140	129	8
07-014	01/05/07	4.7	4.6	83	73	12
07-017	03/05/07	9.4	9.2	78	66	15
06-003	21/04/06	3.2	3.0	n/a	118	n/a
06-004	21/04/06	2.0	1.8	n/a	146	n/a

Table 4.2. Lithofacies present in cores. All lithofacies are not necessarily in each core nor in this particular order

<b>Lithofacies</b>	<b>Description</b>	<b>Interpretation</b>
<b>1</b>	Coarse sand with pebbles or mud laminations	Glacifluvial / glacimarine
<b>2</b>	Fine to very fine cross laminated sand	Glacimarine sediment
<b>3</b>	Black fine massive to laminated sand	Cut and fill deposit
<b>4</b>	Fine massive sand	Mobile sand sheet
<b>5</b>	Mottled shell bearing mud	Estuarine or marine mud

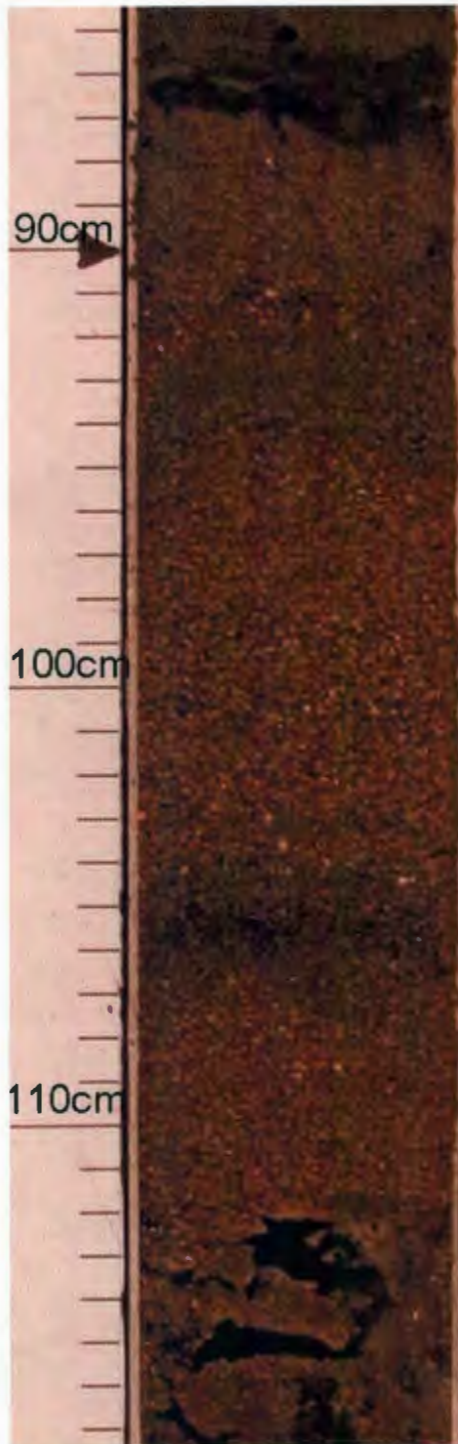


Figure 4.7. Example of lithofacies 1. Note the coarse grained sand with small gravel lags and thin black layers. Photo from base of core 07-001. Disruption at base caused by core catcher.

consistent grain size varying between 1-7% mud, 36-45% fine sand, 32-62% medium/coarse sand, and 3-5% granules. Organic carbon was between 3 and 5%.

Coarse grained sand of this nature is typically found associated with coarse grained bed-load, from delta fronts, directly from ice contact sediment as gravity flows, or from glacialfluvial derived sediment (Lonne 1995, Benn and Evans 1998). Thin laminations of coarser sediment are commonly associated with current reworking and lag deposits (Powell 1984, Benn and Evans 1998, Hill and Solomon 1999) or episodes of ice rafted sediment (Lonne 1995, Benn and Evans 1998). The varied sediment types suggest a dynamic environment. Massive bedding may be due to multiple processes including highly concentrated sediment dispersions during gravity flows (Lonne 1997, Boggs 2006), as a function of secondary disturbances such as liquefaction whereby original stratification is destroyed (Boggs 2006), or from the reworking of sediment (Lonne 1995). Within core 07-001, an unconformity was particularly evident, suggested from the core location within a deep channel. Coarse sediment associated with lithofacies 1 from core 07-001 was characterized by a thin (<2 cm) lag deposits and may represent an erosional surface which was subsequently buried with finer sediment.

### **Lithofacies 2**

The most prominent unit associated with lithofacies 2 is seen in cores 07-004, 07-007, 07-013, 07-017, 06-004 and is interpreted as pre-inundation sediment. It was found within various portions of the sill top cores and is composed of a beige (2.5Y 5/4 to 4/2) fine sand with faint 2-8 mm planar to cross laminated brown muddy fine sand (Figure 4.8).

Laminations, composed of a finer sand/silt, have contacts with normal grading near their



Figure 4.8. Example of lithofacies 2. Note the fine laminated sand which is commonly interbedded with laminated muddy fine sand seen in the lower section of the photograph. Photo from core 07-004.

base and abrupt and/or erosive contacts at the top. The thickness of this lithofacies typically encompassed the entire core with the exception of 5 to 20 cm of sediment from lithofacies 4 or 5 in the uppermost sections. Unit thicknesses varied from 50 to 140 cm. Grain size varied between 2-42% mud, 37-94% fine sand, and 1-12% medium/coarse sand. Organic carbon varied between 6 and 10%. This sediment is found associated or interbedded with a finer brown (5Y 4/2 to 5/1) fine sand with similar planar or cross laminations 1 to 3 mm thick. Grain size varied between 10-66 % mud, 32-87% fine sand, 0-8% medium/coarse sand. Organic carbon varied between 8 and 12%.

This lithofacies resembles the subaerial sediment cover described by French and Harry (1983; Figure 2.6) on the Sachs Lowland. The sediment from this lithofacies showed a rhythmic sedimentation similar to those described as cyclopsams (Stewart 1988). Fine sand containing planar to crossbedded laminations has multiple possible origins; glacial marine sediment deposited from suspension relatively proximal to a retreating glacier (Cowan and Powell 1990), glacial fluvial sediment deposited relatively distal to the glacier terminus (Lonne 1995), or as a subaqueous delta front relatively distal to a retreating glacier, which in certain cases was found to extend over 10 km (Boggs 2006). Other possibilities include overbank deposits in flooded streams or, as Hill and Solomon (1999) discovered, sediment deposited in a regularly changing environment such as a tidal or fluvial dominated embayment displaying flaser bedding. Sediment displaying flaser bedding could have been deposited over a large portion of the lowland prior to emergence.

Given a proposed 20 m a.s.l sea level highstand on the lowlands (Dyke *et al* 2005, Vincent 1983), which occurred shortly after deglaciation (Dyke *et al* 2005), this sediment

was not likely deposited sub-aerially as a sandur plain in the earliest stages. This unit is therefore interpreted to be deposited in a marine environment. The gradational to erosive contacts suggest possible deposition by a combination of current flow, underflow, and overflow as described by Powell (1991) and Lonne (1995) during the retreat of the glacier terminus showing similarities to cyclopsams deposited by proximal turbid plumes (Stewart 1988). Similarly, sediment displaying flaser bedding may have been deposited shortly after deglaciation while in a shallower marine environment prior to basin formation and emergence (Hill and Solomon 1999).

### **Lithofacies 3**

The sediment from lithofacies 3 was found within cut and fill channels observed on the seismic profiles. It was described as black fine sand (Gley 1 2.5N) usually containing 0.2-2cm thick grey (Gley 1 4/N – 3/N) fine sand laminations with abrupt or irregular contacts (07-001, 07-003, 07-006, 06-003)(e.g., Figure 4.9). Cores containing lithofacies 3 were extracted exclusively along the Inner Basin sill III, positioned adjacent to the southern bank of the palaeo Sachs Channel. The thickness of this facies varied from thin 3 to 4 cm laminations to entire core lengths of over 80 cm. Grain size varied between 7-45% mud, 52-87% fine sand, and 1-20% medium/coarse sand. Organic carbon varied between 6 and 10%.

The relatively low number of laminations and lack of structure suggests that this unit was either deposited relatively rapidly, in a stable environment, or periodically homogenized. This sediment likely occurred as a scour and fill deposit, such as those described by Boggs (2006). In most cases, the black colour appears to be due to chemical



- Figure 4.9. Example of lithofacies 3. Note the fine black sand and thick beige laminations. With the exception of colour, sedimentary properties are near identical within the core. Photo from core 06-003.

reduction as the sediment from the aforementioned cores had subsequently oxidized to lighter beige after splitting.

As shown in seismic line 0215 (Figure 4.6), the sediment near the edge of the palaeo channel appears to have been eroded and subsequently infilled. The scour and fill or channel fill of abandoned channels was likely related to cutbanks in the palaeo Sachs River channel prior to inundation either when sea level was lower than present and was still flowing into a lower sea, or prior to complete emergence in the earliest stages of the Sachs River. A second possibility for the origin of lithofacies 3 is sub-marine channel scour from density flows prior to basin formation. However, the former is more likely due to its presence solely adjacent to the palaeo Sachs River. Periodic flooding of abandoned channels into quiet anoxic embayments would also explain the sediment reduction.

#### **Lithofacies 4**

The sediment from lithofacies 4 is described as beige (10YR 10/3 – 5/6) massive fine sand with or without large pebbles resembling dropstones (up to 8 mm in diameter) (Figure 4.10). This lithofacies occurred at the uppermost section of cores where lithofacies 5 was not present (Cores 07-003, 07-009, 07-013, 06-003 and 06-004). Cores containing lithofacies 4 were taken in the upper sections of sills within 1.8 to 3.8 m water depth, in areas generally dominated by longshore sediment movement. The sediment varied between 6 and 17 cm in thickness. Grain size varied between 4-11% mud, 61-87% fine sand, 2-22% medium/coarse sand, and 0-4% granule. Organic carbon varied between 6 and 9%.



Figure 4.10. Example of lithofacies 4. Massive beige sand occurs at the uppermost section of cores in areas proximal to spit. Photo from uppermost section of core 06-003. Note sandblasting sand above the 0 cm mark added following core retrieval to minimize sediment mixing.

Massive bedding of this type and in this sedimentary sequence was thought to be from the reworking of sediment above wave base or by ice keels (Lonne 1995), further shown by the abrupt and irregular lower contacts. It has previously been shown that the sedimentary nature in shallow sea beds similar to the present setting, are generally erosive with thin and patchy veneers of mobile sand (Hill and Solomon 1999). Due to the relatively thin facies and the position in the uppermost portion of the cores, lithofacies 4 was interpreted to be a secondary feature from the reworking of sediment. Reworked sediment likely originated in situ from the underlying sediment or was deposited as a semi-mobile sand sheet transported along the sill tops (Harry *et al* 1983).

#### **Lithofacies 5**

The sediment from lithofacies 5 was generally found within channels or in the deepest sections of the sills. It was described as shell bearing black to dark brown (Gley 1 2.5N – Gley 1 2.5/10Y) mud and fine sand with varying amounts of mottling (Figure 4.11). It was found only in the uppermost section of cores with the exception of those capped by lithofacies 4, both of which were thought to represent recent sedimentation. It comprises all of cores 07-005, 07-014, and the top sections of cores 07-001 and 07-004, and varied between 24 and 87 cm in thickness. These cores were all taken from deep channels or in the deepest sections of the sills between 4 and 4.8 m water depth and likely represented sheltered localities. Grain size varied between 47-82% mud, 16-51% fine sand, and 0-8% medium/coarse sand. Mud was usually mottled, suggesting the presence of organisms and bioturbation. Organic carbon varied between 8 and 14%. Sediment with similar

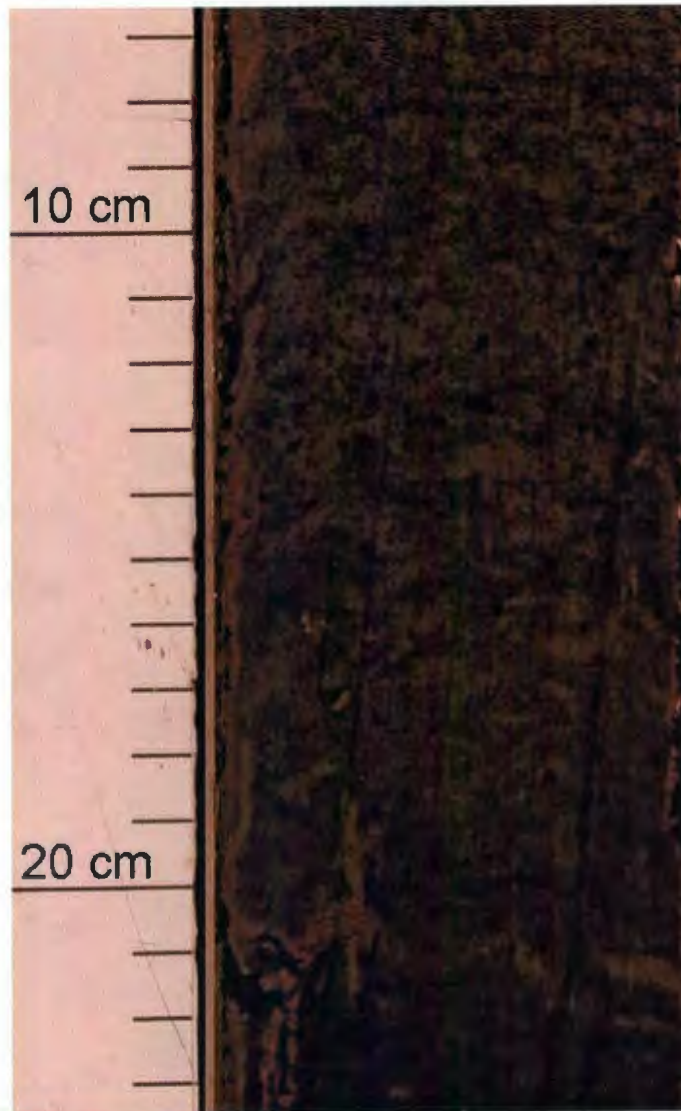


Figure 4.11. Example of lithofacies 5. Note the extensive mottling within the dark coloured mud. Photo from uppermost section of core 07-005.

appearance and grain sizes were found in cores from marine dominated transgressed basins on Richards Island (Solomon *et al* 2000).

This lithofacies was not found in bluffs along the Sachs Lowland. Sills only showed mud accumulation when submerged below 4 m and did not appear to be accumulating in areas near spit development. Mud was interpreted to be deposited from suspension in a low energy environment such as marine settings, estuaries, lagoons, or lakes (Boggs 2006). The presence of shells and bioturbation attests to a relatively low sedimentation rate (Boggs 2006). The slow deposition rate is further shown by the rather extensive mottling and the relatively low biota abundance (Brown 2007). Solomon *et al* (2000) suggest that sediments within marine embayments are sourced from a combination of suspension settled sediment from river plumes, marine sediments advected into bays during storms, and minor input from nearby bluff erosion. Lithofacies 5 was shown to have the highest organic carbon content, which is consistent with the ranges found in other transgressive basins (Solomon *et al* 2000, Sparrenbom *et al* 2006). The presence of *Pectinaria* casings within the cores further attests to a brackish to marine sediment (Sparrenbom *et al* 2006).

#### **4.6 Seismic and sedimentary description of sills**

Sills have been identified by numbers I to VI (Figure 1.4) and described with available seismic and core data. Sill III is the most extensively sampled with multiple cores and seismic profiles. Diagrams constructed using available seismic and depth data were used to display approximate morphology of core and channel locations. Depth measurements were acquired using the lead line method and, where available, single beam sonar from

Belliveau (2007). Core diagrams are shown in their approximate position within the sill and can be further seen in a larger format within appendix A. A legend of the lithofacies is displayed in figure 4.12.

### **Sill I**

Sill I, the outer and most exposed sill along the southern part of the Outer Basin, was described from seismic line 0249 (Figure 4.4) and core 07-017. The sill is over 1.8 km long while the sill top was flat and relatively narrow (150 m) and approached 2.2 m in depth. The basin floor rises abruptly along the steep slope of the sill where slumping occurs slightly downslope from core 07-017. The Thesiger Bay side of the sill had a long (>1 km) slope (shallow gradient) and deepens to over 5 m. Its morphology is shown in Figure 4.13. The sediment on the sill top (< 2 m water depth) was acoustically impenetrable and incoherent, likely due in part to the sandy nature of lithofacies 2. The sediment core was taken downslope from the sill top in 9.2 m water depth. The core did not show any major features nor did it have mud accumulating over top of the sand. This site suggests a depositional setting from spillover and sediment migration from eroding bluffs interspersed with erosional events owing to its exposure to Thesiger Bay. In deeper water south of the sill and along the margins of Thesiger Bay, there is a discernable acoustic stratigraphy suggesting draping of the underlying units and may represent sediment that has been washed alongshore from the eroding bluffs to the east.

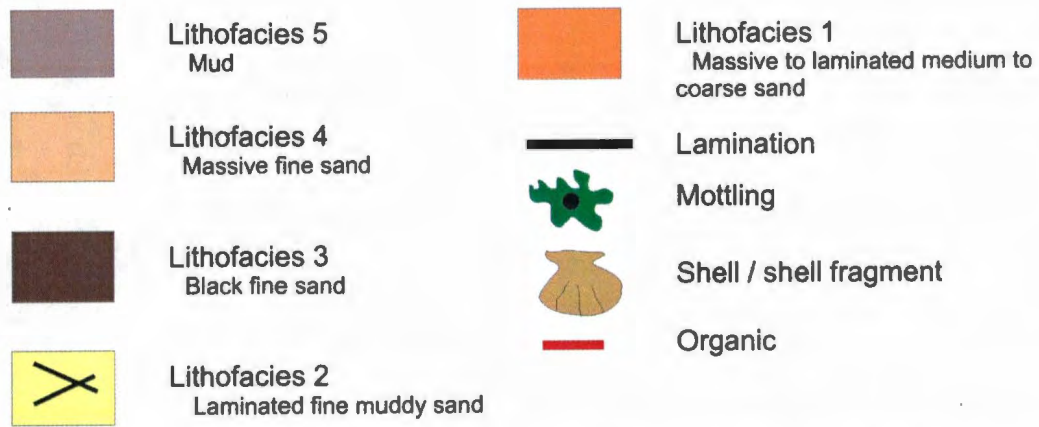


Figure 4.12. Legend of lithofacies from cored sediments and structures found within.

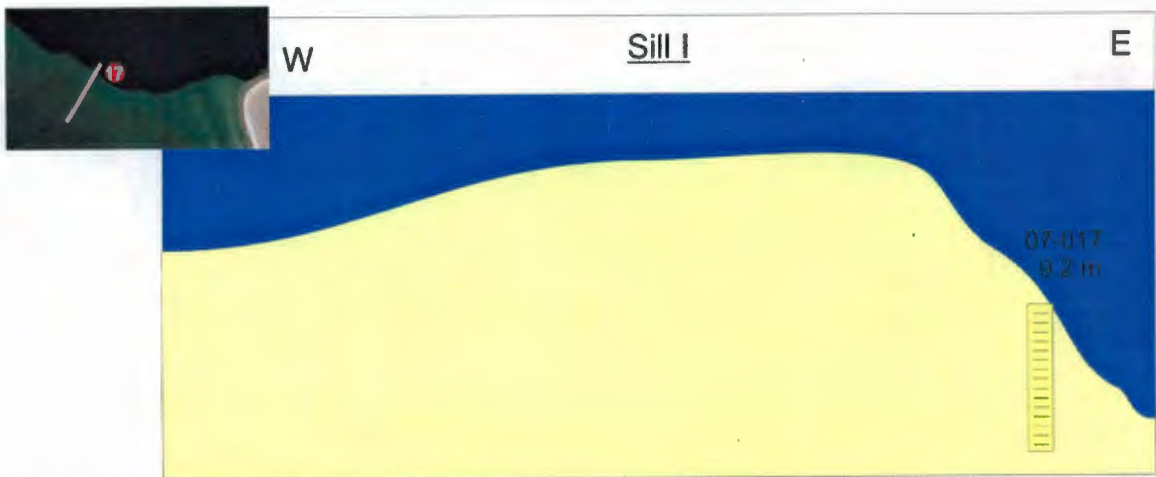


Figure 4.13. Illustration depicting morphology of sill I and sedimentology of core 07-017.

## **Sill II**

Sill II, situated between the Inner and Outer Basins, was described from seismic lines 0234 (Figure 4.5) and 0151 along with cores 07-009 and 06-004. The sill was approximately 1.2 km in length between the tip of the spit and the shoreline and over 700 m in width, much wider than the other sills. Much of the sediment appears to have been deposited following inundation as the sill seems to have increased in width since 1950, possibly causing the much rounder appearance to the sill top. Due to the shallow depth (< 2 m in certain areas) and attenuated seismic signal, the sill top reveals very little structure, appearing acoustically impenetrable. The cores 07-009 and 06-004, taken in 3.8 and 1.8 m of water, respectively, displayed characteristics of a mobile sand sheet in the upper portion associated with lithofacies 4. This is consistent with the interpretation that sand is traveling between the hook of the spit and the shoreline along sill II (Harry *et al* 1983). The lower section of core 06-004 showed similarities to other cores associated with lithofacies 2, and thus resembling cyclopsams. Acoustically stratified sediment appears to be accumulating lower down the sill face and ponding within the troughs of slump deposits. The sill morphology and sedimentology from cores is shown in Figure 4.14.

## **Sill III**

Sill III, situated between the Inner Basin and the Palaeo Sachs River, has a length of approximately 1.2 km and is over 400 m wide. The sill was crossed perpendicularly by both seismic lines 0215 and 0230, and is sub-parallel to seismic line 0234. Sill III was also sampled by core 06-003 and by cores 07-001 through 07-007. It was shown to have

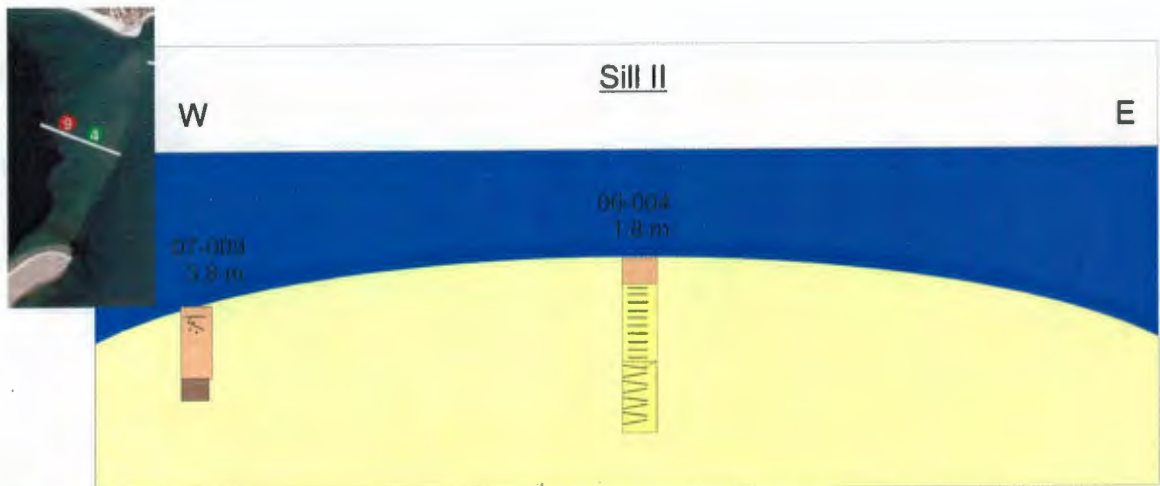


Figure 4.14. Illustration depicting sedimentology and morphology of sill II from cores 07-009 and 06-004.

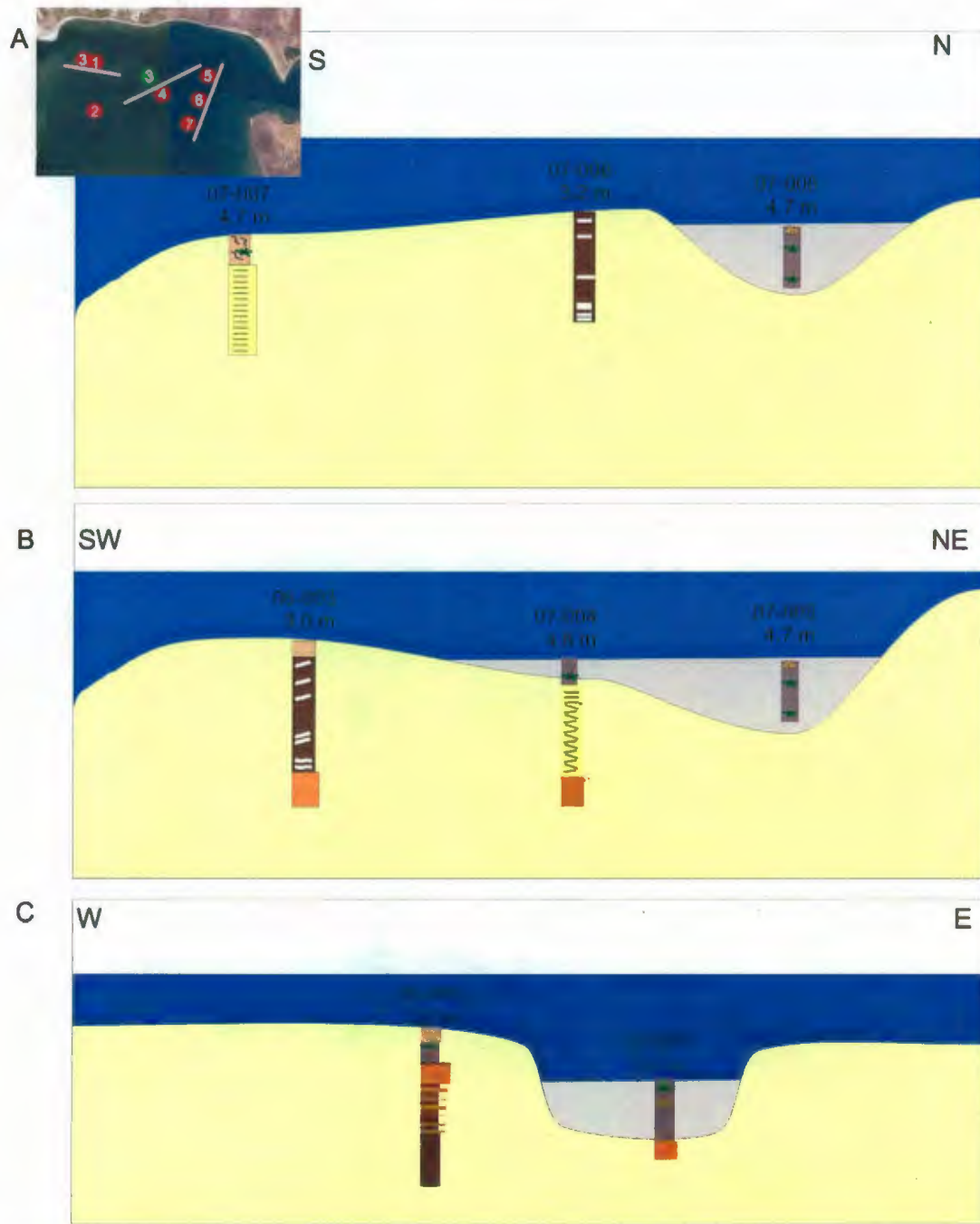
a flat top with small depressions in certain areas. Sedimentary characteristics were represented by all five lithofacies along the length of the sill. Its morphology and sedimentology from cores is shown in Figure 4.15.

Both seismic lines 0234 and 0215 showed evidence of cut and fill channels (Figures 4.5 and 4.6) associated with both the Palaeo Sachs Channel as well as the possible inlet/outlet to the Inner Basin. Core 07-006 was taken within one of the cut and fill channels and contained fine black sand associated with lithofacies 3, while a second core, 07-007, taken just outside of the cut and fill channel resembles the dominant sediment type from the sills associated with lithofacies 2 (laminated fine sand). Core 06-003, which is situated directly adjacent to the Sachs Palaeo Channel, also appears to have been affected by a cut and fill channel.

Although no cores were taken directly along seismic line 0234, the apparent cut and fill channels appear to be on a submarine slope below the outlet channel within which cores 07-001 through 07-003 were taken. The channels are acoustically stratified where sediment appears to drape the channel base. The cores consisted of lithofacies 1, 3, 4, and 5. The lower section of core 07-001 is thought to contain a local unconformity (Figure 4.16) at the boundary between coarse sand and marine mud possibly representing an erosional surface formed during a lower sea level. Within the cut and fill channel there appears to be a thin acoustic reflector that may be associated with sand found within core 07-002, separating two muddier deposits (Figure 4.5).

From seismic line 0230, the sediment within the sill top is acoustically impenetrable, but also exhibits a slight thickening of an acoustically semi-transparent unit in the troughs, likely associated with mud from lithofacies 5. This is seen within core 07-

Sill III



Figures 4.15 Illustration depicting sedimentology and morphology of sill III from cores 07-001, 07-003, 07-004, 07-005, 07-006, 07-007, and 06-003. Depth labels from lead line measurements prior to coring while general morphology extrapolated from single beam depth measurements.

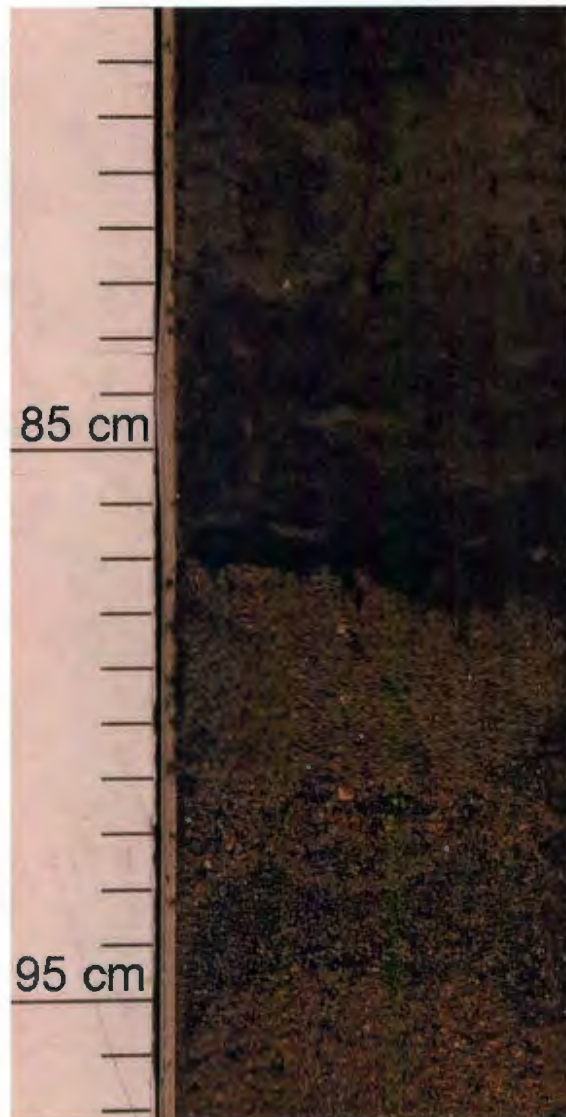


Figure 4.16. Local unconformity within core 07-001 at 87 cm depth. Note the change from medium to coarse sand (below) into an estuarine mud (above).

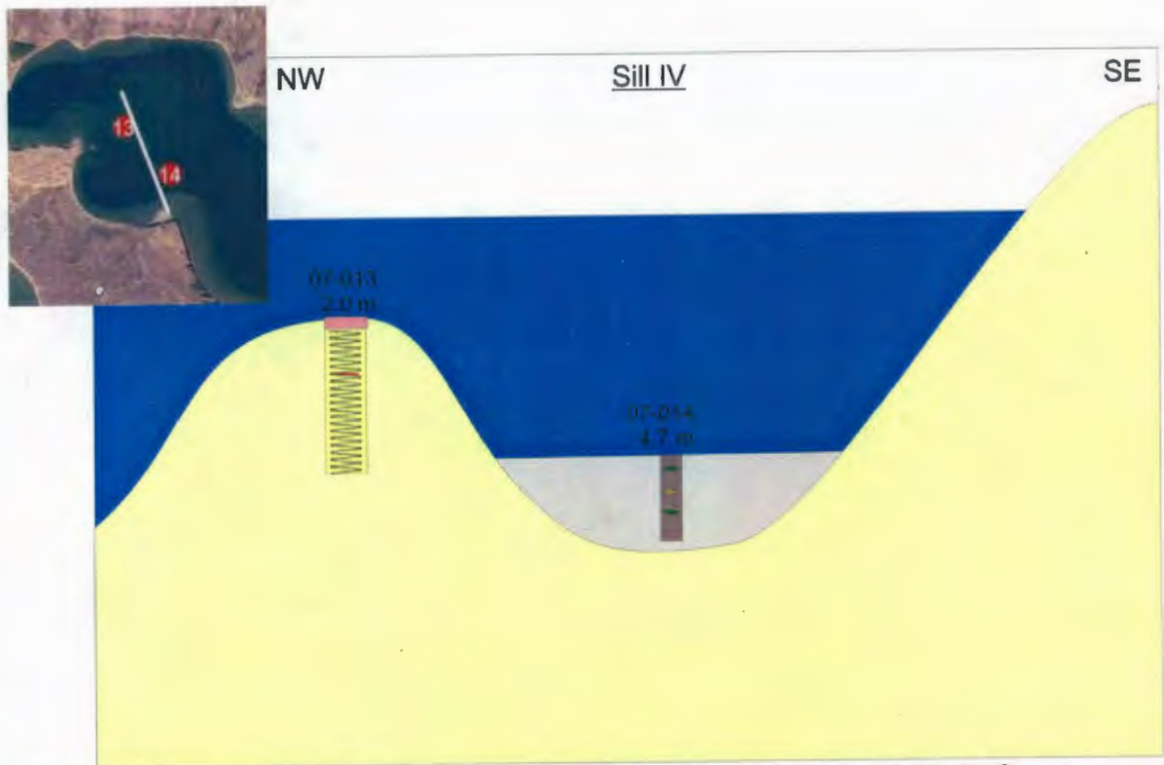
005 taken from the palaeo channel which was composed entirely of marine mud. The draping is further shown from core 07-004 which had a thin, 20 cm thick layer of mud overlying the acoustically impenetrable sands associated with lithofacies 2.

#### **Sill IV**

Sill IV situated between the Shore Basin and the Palaeo Sachs River Channel was not investigated by seismic techniques but was cored in a shallow area along the upper sill as well as within the deepest section of its channel. Unlike the other sills investigated, sill IV has a slight semi-circular shape with a shallow section in just over 2 m water depth and a deeper section across a channel in over 5 m water depth. Its morphology and sedimentology from cores is shown in Figure 4.17. The upper sill was composed almost entirely of laminated sands from lithofacies 2, with the exception of the uppermost 5 cm composed of reworked sand. The upper sill was thought to represent a predominantly erosional system. The channel cross cutting the sill was composed entirely of shell bearing mud associated with lithofacies 5. Core 07-014 only penetrated mud and did not expose an erosional surface.

#### **Sills V and VI**

Sills V and VI were the shortest sills studied, at less than 100 m each, and approximately 150 m wide. These sills differed from the other sills studied in the fact that they were much narrower and that either side of each channel was subaerial. Cores were attempted on each sill, unfortunately sea ice was frozen to the surface of Sill V while no penetration was obtained on sill VI where the sill was less than 20 cm from the base of the ice. The



Figures 4.17 Illustration depicting sedimentology and morphology of sill IV from cores 07-013 and 07-014.

deepest sections of the sills measured were 1.15 and 2.5 m, respectively. Examples of the morphology from depth measurements are shown in Figure 4.18 and 4.19. These coring attempts will be further discussed in the following section.

#### **4.7 Summary of core interpretation**

Cores from the sills can be grouped into similar sediment type and depositional environment, whether from channels, proximal to spits, or predominantly erosional areas. Cores 07-005, 07-014, and the tops of others containing mud are interpreted to be marine sediment and have been deposited following inundation of the surrounding area.

The uppermost sections of many of the cores taken near the Inner Basin/Outer Basin (06-004, 07-009, 07-003) are thought to be composed largely of reworked sand occurring as a mobile sand sheet originating both from the Sachs Spit and the Sachs Harbour beach.

The unusual black sand is due to a reduction of either organic material or manganese and is not from dark coloured (mafic) minerals. Its presence as massive sand and interbedded with beige sand may indicate either seasonality or surges in sediment deposition. Due to its presence in cores found only adjacent to palaeo channels and the observation from seismic lines, the sediment was thought to be associated with channel fill deposited prior to inundation in an anoxic environment when the Sachs River would have been flowing into a shallower sea or lake.

Cores containing laminated fine sand and mud were most common and were located within all of the cored sills. Sediment occurred as rhythmic couplets interpreted as cyclopsams/cyclopels deposited subaqueously as glacial outwash (Cowan and Powell

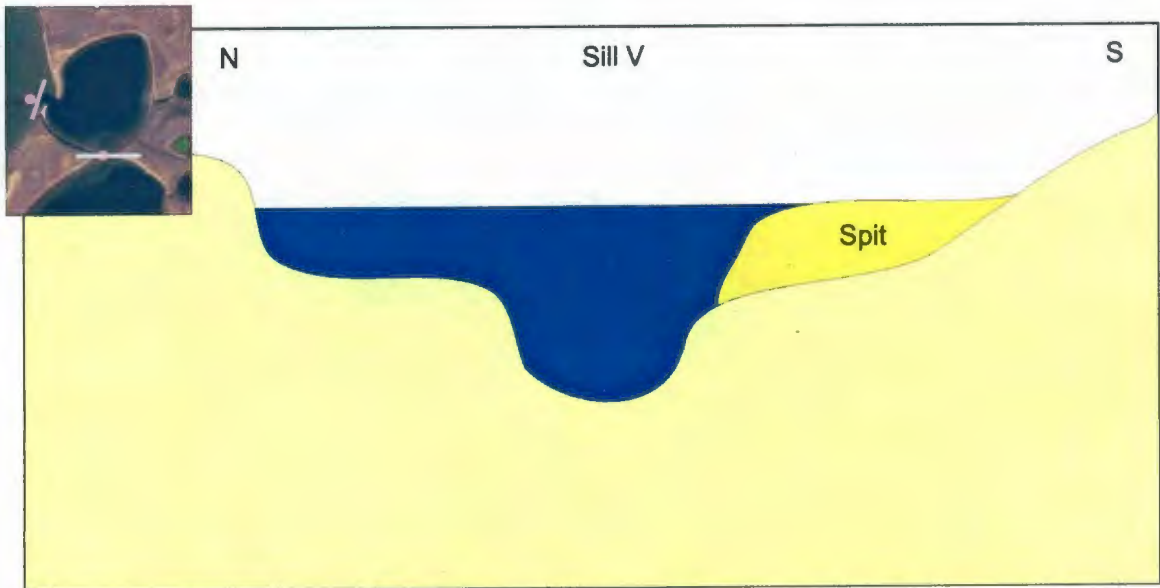


Figure 4.18. Illustration depicting the morphology and erosional sill surface above the frozen sill V along with prograding spit.

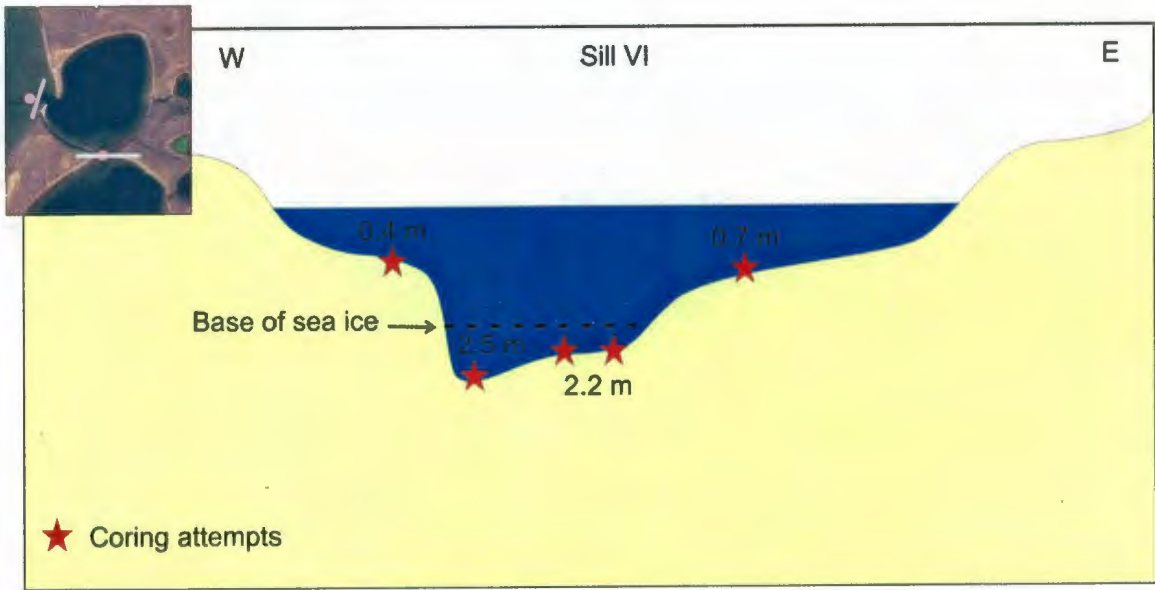


Figure 4.19. Illustration depicting the morphology and coring attempts of the frozen sill VI.

1990, Hill and Solomon 1999, Mackiewicz *et al* 1984), or as a secondary deposition with flaser-type bedding such as seen within certain spits in the Mackenzie Delta (Hill and Solomon 1999).

The medium to coarse sediment, whether laminated or massive and typically found at the base of cores, was thought to represent bed load, gravity flows, alluvial sediment, or sediment that had been reworked by ice and currents. Depending on its position with respect to other lithofacies, the sediment may be interpreted as glacial or of postglacial origin. With the exception of the estuarine sediment, a particular genesis is difficult to invoke without dating control. Particular cases where local erosional surfaces were thought to be observed will be further discussed in the following section.

#### **4.8 Summary of seismic interpretation**

Most of the sediment from the sill tops was acoustically impenetrable with the exception of thin drapings and accumulations in troughs. The draping unit, interpreted as mud, was acoustically transparent to semi-transparent and faintly laminated in places. Acoustically impenetrable sediment, found in sill tops or underlying acoustically transparent sediment was interpreted as sand. On line 0215, the cut and fill channel was interpreted as a palaeo channel of the Sachs River. Cores from within and outside of the boundary of the cut and fill showed a distinct difference in the sediment type. Cut and fill channels from line 0230 were interpreted as fill from a palaeo outlet channel downslope from core 07-001.

## **Chapter 5 – Discussion**

### **5.1 Introduction**

The coastal changes encountered in Sachs Harbour are similar to observations on other transgressive coastlines in the western Arctic where combinations of depositional and erosional environments are found (Hill and Solomon 1999). Although poor seismic returns were recorded along the shallowest sections of the sills, due to shallow water depth and abundant sand, much information was attained in reference to channels, cut and fill palaeo channels, areas with draped sediment, and the general sill morphology. Core data were an invaluable tool in interpreting seismic profiles. The seismic and core data have shown that the harbour has been a dynamic area that has been affected by erosion and deposition to varying degrees both spatially and temporally.

In this chapter the results from the previous section are used to address the following research goals: i) differentiate key processes in the evolution of sill morphology during and following its submergence, ii) define a range of geomorphological and sedimentological attributes that may be used to characterize sill reworking in submergent basins. The outcome of these research questions will attempt to provide baseline information on index points to help constrain sea level curves.

### **5.2 Sill attributes**

Most of the sediment from within the sills was composed of fine laminated sand and was capped by a thin layer of reworked sediment. One exception occurred within buried channels where sediment is muddier. Exceptions also occurred at the base of certain cores where coarser massive sand was present. This suggests that much of the sediment

within the sills has a similar composition to the nearby bluffs which French and Harry (1983) described.

As known from previous studies, the deepest channels in the sills separating inundated basins are usually used as index points (Sparenbom *et al* 2006). Missing such deep channels or outlet features could result in erroneously choosing index points above the actual palaeo sea level. However, along dynamic transgressive coastlines, sedimentary structure can often be destroyed or buried as the coastline changes. This will be further discussed in the following section.

In depositional environments, deep channels situated below wave base often become buried and appear undifferentiated from the surrounding sills without subbottom profile data. However, channels that cut into the sills are easily discernable using acoustic profiling techniques provided that the sedimentary characteristics and structures between units are sufficiently different. This was the case for channels found within Sill III on seismic line 0234 (Figure 4.5) and can be seen in cores 07-001 and 07-014. In other cases where nearby sediment is simply remobilized and redeposited, the acoustic response may be attenuated and differentiation between units may be impossible. Where possible, the interpreted sedimentary characteristics can be verified directly with cores to determine where local unconformities are thought to exist. In many cases within Sachs Harbour these were found at the interface between sand and mud, or where distinctive unconformities are found.

### 5.3 Key processes in sill evolution

The interaction of multiple processes shapes the sills and leads to their evolution to produce their present morphology and depth. The evolution of the coastline and sills is largely a function of environmental forcing (Manson and Solomon 2007) such as wind, waves and currents, ice action, thermal processes, and sea level trends, leading to thermokarst, coastal erosion, spits, and barrier islands (Campeau *et al* 2000).

Apart from the melting of ground ice, wave action and currents are likely the most effective way of removing or remobilizing sediment in the nearshore zone (Héquette and Barnes 1990) including the removal of previously slumped sediment. Likewise, waves and longshore currents aid in the removal of sediment and the mobilization of larger grains where they can be deposited along spits and barriers (Clark *et al* 1984). The likelihood that sediment is still being deposited along sill tops that are presently along the drift path is shown by the prograding Sachs Spit and hook (see Figure 4.1). However, it was not entirely clear from cores, seismic interpretation, or previous studies, whether this was occurring along all the sills within the estuary or simply along the Inner/Outer Basin sill (sill II) and part of the Inner Basin sill (sill III) where an obvious mobile sand sheet can be seen in the core tops.

Additionally, the Outer Basin sill (sill I) likely would have taken the brunt of the force from sea ice disturbances by acting as a barrier to thick sea ice. Therefore, the only ice to affect the sills within the harbour would have originated within the basins or from the Sachs River. However, during the fall freeze up, anchor and frazil ice formation may have incorporated sediment into the ice canopy and rafted it into basins or offshore (Kempema *et al* 1989). In addition, landfast or grounded ice likely would have increased

the hydraulic flow under ice keels and within channels leading to a winnowing of the fine sediment, even erosion of coarse sand (Héquette and Barnes 1990). Sediment entrainment by under-ice currents (caused by surges and/or tides) was likely an important process in the further removal of sediment within channels located below sea level, where sea ice was frozen to all but the deepest channel sections, leaving only the deep sections open to flow. This is likely still the case during freeze-up and break-up where landfast ice above the Mirabilite Basin sills thickens or melts sufficiently to allow a thin layer of water to pass underneath with each tide cycle.

Channels cross cutting the sills were likely in place long before the entire length of the sills were submerged completely (Figure 5.1). It is probable that significant incision into the sills took place prior to submergence due to preferential erosion and thermokarst caused by warmer lake water flowing over an outlet creating a small channel. This incision may have prematurely lowered the lake level speeding up the inundation process. This is seen from the perched stream inlets leading into the basins today. Furthermore, incision into the sills may have rapidly taken place through melting of ice wedges and ground ice, and thus rapidly depressing the lake level (Marsh 2001). Minor erosion and incision of the channel would likely continue to take place following inundation due to the marine water flowing within the channel. Sills would then be subject to overtopping, and sedimentation within the channel and along the sill tops. The channel incisions prior to submergence of the entire sills is illustrated in aerial photographs (Figure 4.1) where many of the deeper channels, especially sill VI, seem to incise deeply while retaining relatively steep walls, likely due at least in part to permafrost. However, a second scenario exists where the deep incision representing the

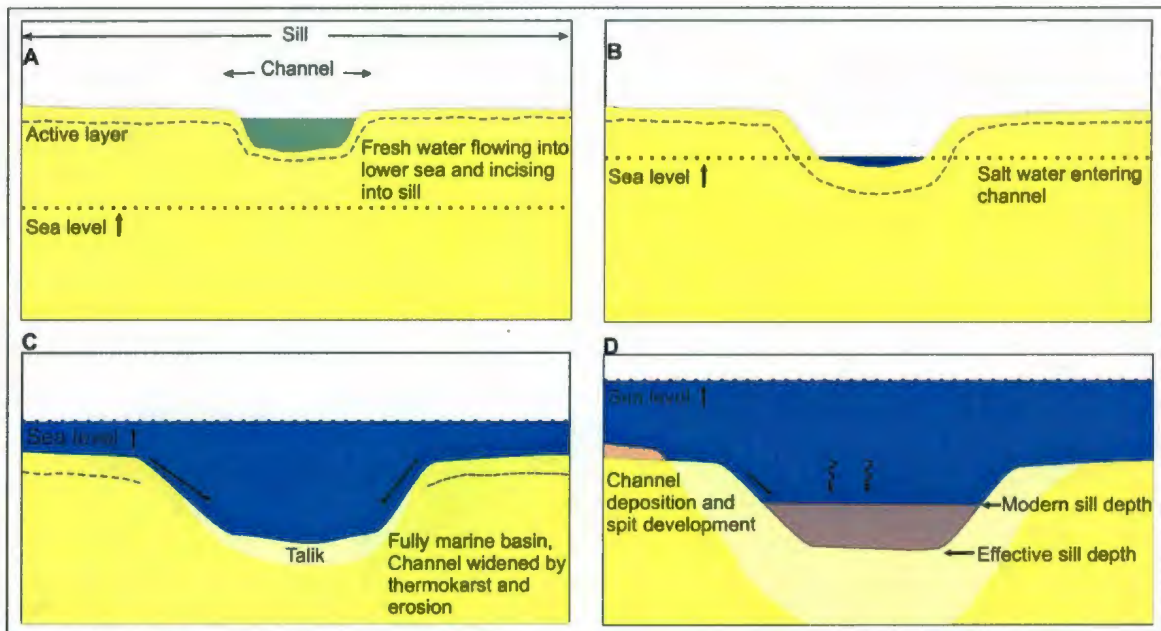


Figure 5.1. Diagram representing typical sill evolution with rising sea level. A: lake water drains over sill and begins downcutting small channel. B: Erosion of channel continues and sea level rises until marine water enters channel causing brackish conditions in the basin. This is the effective sill depth corresponding to brackish diatoms in the basin sediments. C: Residual downcutting from ebb and flow of tides, current winnowing and erosion over fully inundated sill. This is the effective sill depth corresponding to appearance of a complete marine diatom assemblage in the basin sediments. D: Subsequent burial of channel from suspension settling (lithofacies 5) and encroaching spit (lithofacies 4). Modern sill depth is shown at the sediment surface while the effective sill depth is at the base of deposited sediment. Coring into the base of this channel should represent lithofacies 1 and 2 capped by lithofacies 5.

deepest section of the sill may also represent a rapid deepening of the outlet following inundation (Figure 5.1 and 5.2). This would suggest that the broad flat area on either side of the outlet is the erosional signal that accompanies the inundation phase and that the true inundation point lies somewhere between the broad section and the deep outlet. This can be demonstrated by the channel within sill VI that shows a bi-directional flow indicating that erosion and sediment transport likely occurs as bedload during ebb and flow of the tide. However, much of the sediment eroded following the initial inundation has likely occurred in the process of rendering the basin fully marine, while additional sediment is further added by the channel widening. Therefore the channel depth following post-inundation erosion corresponds to the complete marine diatom assemblage in basin sediments. If erosion is considered to have continued since inundation, index points must be interpreted as maximum sea level rise since inundation.

As seen in the cores taken below 2 m water depth (below the base of sea ice), the uppermost sediment was ice free while sediment in less than 2 m water depths near the base of sea ice was ice-bonded (no penetration or frozen sediment was encountered with ice auger). As a result, sill armouring has likely been aided by permafrost as the ice-bonded sediment is more resistant and less likely to erode than non ice-bonded sediment (Dallimore *et al* 1996). Therefore, although subject to a high energy environment, sills are less prone to erosion in the initial stages of inundation than would be expected. However, in some areas near-surface sediment has been shown to melt annually to form subaqueous active layers, refreezing on contact with winter landfast ice (Hill and Solomon 1999). Kobayashi *et al* (1999) have shown that thawing of the ground ice can occur rather rapidly; however thawing was largely dependent on the removal of surface

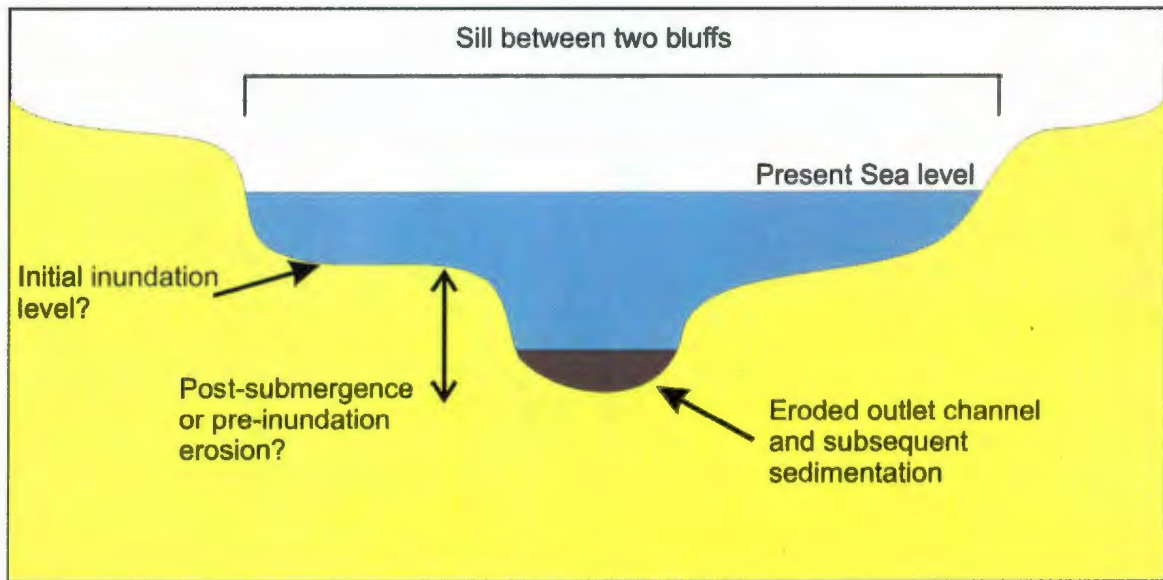


Figure 5.2. Image depicting channel erosion. Whether outlet channel was eroded prior to, or following inundation is unknown. Therefore the sea level index point likely lies somewhere between the channel base and the wide, flatter area on either side.

sediment and heat transfer. Furthermore, Solomon et al (2008), have shown that heat is rapidly removed from sediment once ice becomes bottom-fast. Therefore permafrost may remain in the sediment below the subaqueous active layer until sea ice is no longer in contact with the sea floor (Dyke 1991). However, permafrost may degrade rapidly when ice no longer becomes bottom-fast (Solomon et al 2008).

In addition, the presence of excess pore ice or segregated ice lenses would play a role in the sill subsidence. Calculations have shown that the simple volume reduction of 10% due to thawing of pore ice in sediments of 50% porosity leads to 0.0175 m settlement per metre of thawed sediment if no excess ice is involved (Hill and Solomon 1999). However, due to the large basins surrounding the sills, a talik may have formed beneath the basins extending under the edges, as seen within thaw lakes on Richards Island (Burn 2002). Considering the relative size of the basins in comparison to the width of the sills separating them, it is reasonable to suggest that much of the ice-rich permafrost below the surface of the sill may have melted prior to inundation as the two taliks combine beneath the sill. Much of the settling that would have accompanied the melt of pore ice would therefore have occurred prior to complete inundation and may have led to the initial channel incision. This would indicate that the ice-bonded sediment encountered was indeed a frozen active layer or a thin surface layer of permafrost. Knowledge of the porosity and ice content of the sill sediment prior to its melting, therefore is needed to accurately estimate the amount of subsidence that may have occurred since submergence, if any at all. Ice content and depth could be estimated using nearby drill cores or from adjacent bluffs with similar stratigraphy.

#### **5.4 Sill sediment and basin inundation**

The correct sedimentary interpretation is crucial to sea level reconstruction as the correct identification of glacial (pre-inundation) sediment will aid in determining the lowest breaching point at the surface of the unconformity (i.e., will give a minimum sea level constraint on the model or maximum sea level rise over the time period). Encountering Holocene (post-inundation) marine sediment would simply indicate that sediment had been accumulating in those areas and that the local unconformity was deeper. As shown in Héquette and Hill (1995), it can be difficult to distinguish modern nearshore reworked sands from their Pleistocene precursors that form the nearby bluffs. Misinterpreting Holocene-age sediments as pre-Holocene in age would have important ramifications for a sea level curve.

Sediment from lithofacies 2 can be interpreted as pre-inundation sediment (French and Harry 1982) or as post-inundation sediment such as those from spits and barriers along the Mackenzie Delta (Hill and Solomon 1999). The resemblance is due to the similar marine depositional setting, however the finer sediment found in flaser bedding is not as readily available at Sachs Harbour in comparison with the Mackenzie Delta indicating a pre-inundation origin. Conversely, lithofacies 3, which has been interpreted as cut and fill sediment, was unlikely to have been deposited following basin inundation as the Sachs River was likely estuarine prior to the initial incursion of the Inner Basin. Similarly, if lithofacies 3 is interpreted as submarine channel scour shortly after deglaciation, its deposition would also have been prior to inundation. The presence of lithofacies 3 along the sill therefore attests that the adjacent and underlying sediment must have been deposited prior to inundation. Furthermore, the presence of deep channels

cutting perpendicular to the sill in the location of core 07-001 which has since accumulated fine marine sediment attests to a non-spit like structure. If the early stages of a spit were occurring, sand moving along the sill would have infilled the channel. Similarly, if alongshore currents were moving sand along the Inner Basin sill, core 07-004 would not likely be topped with mud but with sand.

Although difficult to determine between glacial sediment and a post-glacial sediment depicting flaser bedding, it is within reason to believe that the majority of sill sediments (i.e. those not interpreted as mud, channel fill, or sand sheet) are pre-inundation in nature. Cores taken from the centre of the basins are thought to have less than 1 m of marine sediment deposited over probable lacustrine sediment (Smith *et al* 2006). Therefore it is highly unlikely that large bars or considerable sediment would be accumulating above the sills while large sediment sinks (basins) accumulate minimal sediment. Further diatom studies will clarify sedimentation rates.

Within many of the cores taken along the sills, unconformities were thought to occur between 5 and 90 cm from the core tops, while in some cases, cores are thought to be composed entirely of post-inundation marine sediment, most notably those composed of mud. Unconformities found within the deepest sections of the sills are thought to represent the lowest erosional surface where marine water initially flooded into the basins. Their particular depths will be discussed within Section 5.7.

### **5.5 Inundation model**

As previously noted, the marine influence in a basin will start when the saline oceanic water begins to cross the sill of the basin. The highest marine water level is therefore of

utmost importance as it controls when marine waters can enter the basin (Sparenbom *et al* 2006). The southwest of Banks Island is considered to be microtidal with a tidal range between 0.2 and 0.4 m (Canadian Hydrographic Services 2008); however, storm surges have been shown to be as high as 2.4 m in the Beaufort Sea (Harper *et al* 1988) and at least on one occasion resulted in almost total inundation of the Sachs Harbour spit (Harry *et al* 1983) (approximately 0.7 m – Belliveau 2007). Storm waves as high as 1.5 m have been observed in the harbour (Harry 1982) and exceeding 2 m west of Sachs Harbour (Harry *et al* 1983). Analysis of the wind records for the years previous to these observations indicated a probable return rate on the interval of 1-2 years (Harry *et al* 1983). Therefore, within the cores taken from the basin, the initial change from freshwater to brackish water represents the initial overtopping of the sill during storm events. This will influence the timing of incursion as marine diatoms could begin appearing when sea level was on the order of 1 m or more below the level of the channel mouth.

### **5.6 Implications of the model for sea level reconstruction**

In theory, basins that have been inundated at an earlier period should have sills that are lower than those basins that have been inundated more recently, unless sedimentary characteristics suggest differential rates of erosion. Inundation elevations must be judged with caution as the exposure of channels to the open sea may result in higher rates of erosion. In essence, the older the date of the marine incursion, the deeper the index point is to be expected.

The proposed order of inundation and the evolution of the study area are shown in Figure 5.3. As illustrated in Figure 5.3 and aerial photographs of the study area (Figure 1.4), both the Inner and Outer Basins are disproportionately large in comparison to other basins in the study area. These two basins show evidence of small depressions along their margins suggesting that they are made up of multiple smaller basins that have amalgamated into larger basins over time through thaw subsidence and erosion. An amalgamation of basins make interpretation of flooding history more complicated if sub-basins were inundated at different periods. Attempting to associate the proper sill and basin within such a setting could introduce a large source of error into the inundation model. The erosion and settling of sediment may in fact be so great as to obscure any stratigraphic relationships between former sills and actual basins.

Similarly, as suggested by French and Harry (1983), thaw subsidence is feasible within areas noted as having high ice content. However, it is unknown whether much of the subsidence occurs prior to submergence or following the initial incursions. Accurately quantifying subsidence is thought to be quite difficult (Hill and Solomon 1999). Fortunately, storm surges and post inundation erosion and subsidence work in opposition and therefore in combination, may counteract each other to a certain extent.

The ideal conditions for using inundated basins for sea level reconstruction thus occur on relatively newly inundated basins, situated in somewhat sheltered areas so that erosional processes are less intense and alongshore deposition may be minimized. Ideally, basins with sills that are still ice bonded would be used so as to minimize the error from subsidence and the erosional potential. Unfortunately this is not always possible in areas that have been inundated for long periods of time therefore, where

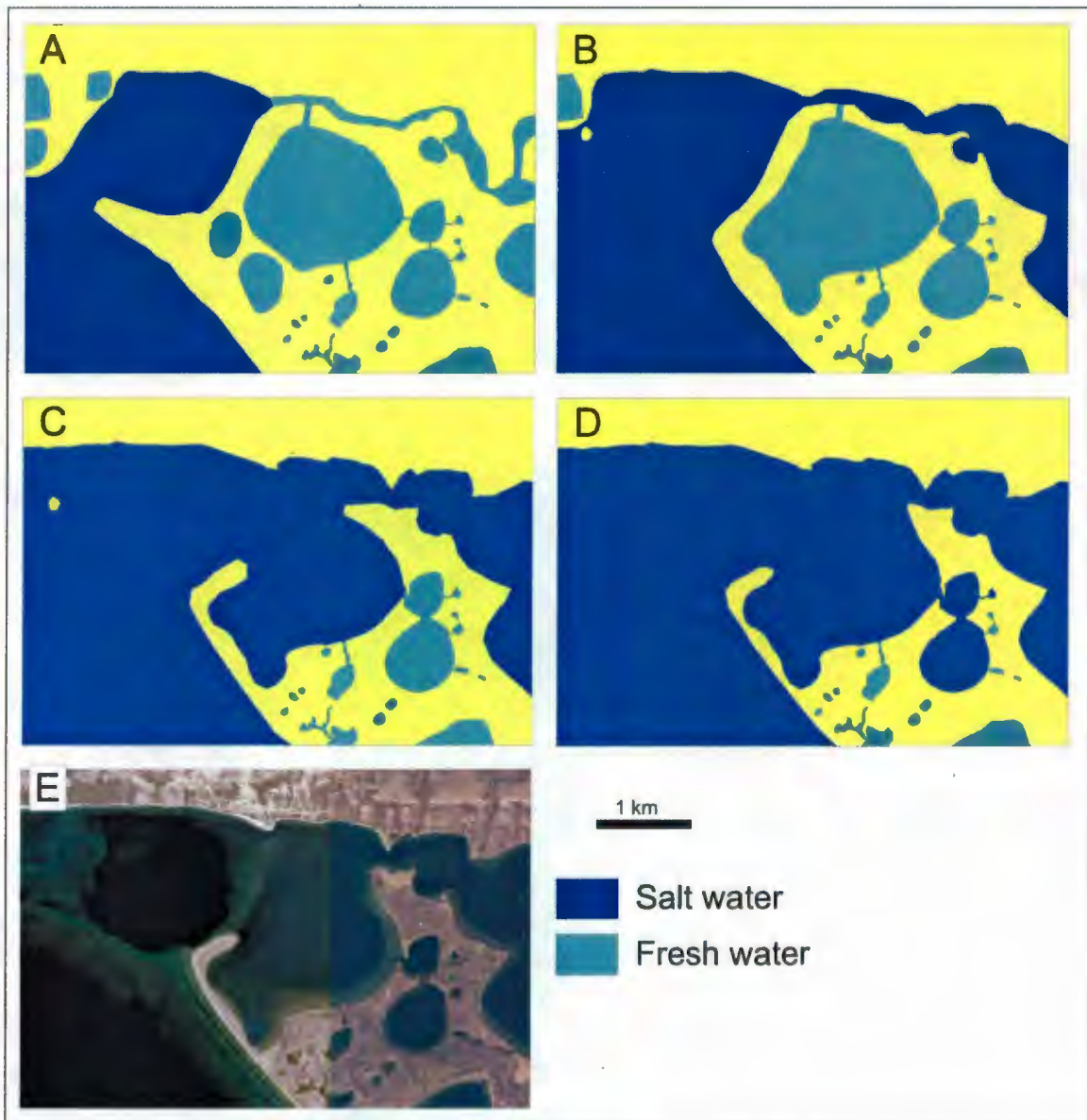


Figure. 5.3. Schematic diagram of possible Sachs Harbour evolution. Images represent inundation events and are not evenly spaced time intervals. A: Following initial inundation of Outer Basin. B: Basin expansion and capture of small lakes in Outer and Inner basins, with inundation of Sachs River and Shore Basin. Inner Basin sill still above sea level. C: Inundation of Inner Basin and erosion of shoreline. D: Inundation of Mirabilite Basins, E: Present-day morphology.

possible, multiple index points within a small area should be used to reduce the chance of error.

### **5.7 Sill breaching points – Index points**

The location of breaching points for each respective basin during sea level rise plays an important role in the reconstruction of palaeo sea levels. A summary of the interpreted depths at which the respective sills were inundated (corrected to low tide) is presented in Table 5.1.

Along the Outer Basin (sill I), there is presently inadequate information to detect the location of the breaching point. The location of the sill, being directly exposed to the Beaufort Sea and therefore susceptible to storm events and offshore sea ice, as well as being a known alongshore sediment transport route (Clark *et al* 1984), suggests that much of the uppermost sediment has likely been reworked, planed off, and redeposited. Similarly, any palaeo channels would have been planed off or infilled with sediment creating difficulties in locating any possible breaching points without additional seismic data.

For the Inner Basin, there are three potential inundation routes; from the Outer Basin over sill II, over sill III from the palaeo Sachs River, or along Thesiger Bay where the spit now lies. From the seismic data and core retrieval, inundation over sill II seems improbable due to water depths shallower than other possible inundation points and the lack of evidence of a former outlet channel.

Within sill III, between the Palaeo Sachs River and the Inner Basin, there are two plausible breaching points: (1) along the deepest and widest section on the eastern portion

Table 5.1. Table representing sill depth and effective sill depth for each of the sills. Uncertainty values are presented corresponding to the appearance of a complete marine diatom assemblage in the basin sediments.

	<b>Present day depth (m)</b>	<b>Interpreted effective sill depth (m)</b>	<b>Uncertainty values – fully marine (m)</b>
<b>Inner Basin - sill III</b>	4.05	4.9	±0.2
<b>Shore Basin - Sill IV</b>	4.6	>5.3	n/a
<b>Mirabilite Basin 2 - Sill V</b>	1.15	1.15	> + 1.35
<b>Mirabilite Basin 1 - Sill VI</b>	2.5	2.5	- 0.4

where water depths are consistently deep (4 to 5 m depth), and (2) through the small channel on the western portion cross cutting the sill. The small channel on the western section of the sill, due to its small size, may have initially acted as an outflow into the Sachs River. Although the depth of the channel is 4.05 m, a local unconformity below estuarine mud is found within core 07-001 at 87 cm depth, indicating that the base of the channel is at 4.9 m. Similarly, where core 07-004 was taken in 4.8 m of water, a hypothesized unconformity is found at 22 cm, indicating a depth of 5.0 m. However, it is unlikely that the outlet channel along the western part of the sill would have formed following inundation if a large channel previously existed on the eastern part of the sill. In addition, depth measurements by lead line method over muddy sediment may present a small error.

Inundation may also have occurred along Thesiger Bay where the Sachs Spit now lies, especially where there appears to be a relatively deep channel near the hook of the spit. However this scenario returns to the problem of basin expansion and capture of small lakes questioning if inundation occurred simultaneously.

Conversely, the Shore Basin breaching point (sill IV) appears to be relatively straight forward, having occurred through the channel in the location of core 07-014. Unfortunately, as only estuarine sediment was penetrated, the depth and characteristics of the underlying sediment are presently unknown, and therefore the depth of a ravinement surface is unknown. However, its depth is in excess of 5.3 m below the surface of the water, therefore the Shore Basin was likely inundated prior to the inundation of the Inner Basin through the Palaeo Sachs River as illustrated in Figure 5.3.

The breaching locations for the two Mirabilite Basins are relatively obvious. Along sill V, the maximum depth encountered was 1.15 m above ice-bonded gravel. The proximity of the encroaching adjacent spit suggests that the small channel has been partially infilled following inundation and that the effective sill depth lies at some position below 1.15 m. The uncertainty for the sill depth is therefore linked to, and was likely deeper than the depth of sill VI prior to the encroachment of the spit. A sediment core or seismic profile would be needed for confirmation.

Sill VI, between the two Mirabilite Basins was also assumed to be ice bonded as the sill surface was solid and had a depth of 2.5 m. However, it is unlikely for sill VI to have been inundated prior to sill V as marine water had to initially enter over sill V prior to sill VI. Possible explanations include that the outlet between the two lakes (sill VI) was deeper than sill V prior to inundation and therefore both lakes were inundated simultaneously or that subsequent deposition has occurred over sill V and refroze to the sill surface. Without proper radiocarbon dating of the timing of inundation or further seismic and core evidence, it is difficult to confirm the depth discrepancy between the two sills. From the morphology of the channel, an uncertainty value of 40 cm has been assigned to sill V as a shallow ledge exists near the deepest section of the channel in 2.2 m water depth and may represent the depth of pre-erosional inundation.

The sediment stratigraphy within the cores provided potential index points, thus at 2.5, 4.9, and over 5.3 m below present sea level. Existing sea level models for the Beaufort Sea would suggest maximum probable transgression ages of 700, 2000, and over 2200 years for these depths (Hill *et al* 1993). Radiocarbon dating of basin sediments will

confirm whether rates of relative sea level rise for Sachs Harbour are similar to those of other areas within the Beaufort Sea.

### **5.8 Summary of findings and conclusions**

There are presently uncertainties with the interpreted ages of sediments within the harbour as dating is yet to be done, however the cores and sub-bottom profiles have proved to be an excellent step towards reconstructing palaeo sea levels in Sachs Harbour.

Within the Shore Basin, the base of the channel was not penetrated, and therefore an index point cannot accurately be determined. However, from this basin, it was noted that large quantities (> 1 m) of mud had accumulated in the channel following inundation further documenting that the lowest portion of the present sea floor cannot be assumed as the breaching point. The Shore Basin, although susceptible to subsidence, with its channel entrance facing away from the Beaufort Sea, is likely less affected by erosion during storm events and may prove to be a better index point in comparison to other more exposed sills. A deeper core or seismic profile penetrating to a ravinement surface is recommended.

The Inner Basin sill, although extensively sampled, may not be an ideal candidate for sea level index points due to multiple possible inundation points and the possibility of basin amalgamation. Similarly, the Outer Basin, due to its exposure to Thesiger Bay, sedimentation, and the possibility of basin amalgamation, may not be an ideal candidate for index points.

Sediment cores have shown that the basin nearest the mouth of the river was not the first to have been inundated as would be expected, but the shore basin with its lower

sill was likely flooded prior to the incursion of the Inner Basin. This is only plausible due to the proximity of the palaeo Sachs River channel. Radiocarbon dating of basin sediments and the timing of each particular inundation will help test this hypothesis.

In conclusion, the oldest and most exposed basins, such as the Inner and Outer Basins, may prove to be poor candidates for the inundation model due to amalgamated basins, erosion, and subsidence. These large basins with multiple possible breaching locations may provide too many error sources, however if local unconformities are found at similar depths and prove to be of similar age, index points may be valid. The Mirabilite basins and Shore Basin are likely the best candidates for sea level reconstruction. In conclusion, the inundation basin model can be considered for sea level reconstruction using basins having sills composed of unconsolidated sediment in areas where breaching points can be determined and erosion and subsidence are likely to introduce the least error. These characteristics were generally found within sheltered basins which have preserved outlet channels.

### **5.9 Considerations for future research**

This thesis has shown the utmost importance of using an approach with a variety of techniques for the inundated basin model using aerial photographs, sub-bottom profiling, and sediment coring. To further the research, an extremely valuable tool in the inundated basin approach would be the use of multibeam bathymetry where water depth permits, and thus facilitating the detection of palaeo channels cross cutting the sills. It should be noted that multibeam was scheduled as part of this investigation but was not available due to technical difficulties.

In addition, a more complete seismic record with a higher resolution would be advisable to further interpret the sill sediment on a larger scale. When taken over inundation points seismic records may reduce the need for time consuming sediment cores if ravinement surfaces can be accurately determined.

Additionally, a more complete record of the surrounding sedimentary structures, both in terms of stratigraphy and ice content, would be useful to further interpret the sill sediments as well as indicate the amount of subsidence that may have occurred. This would help determine the effects of permafrost melt on a small scale. Structures could be mapped from nearby bluffs, or with the help of a CRREL-type sediment corer in shallow ice bonded sills. Similarly, dating of sediment, such as the fine laminated sand or the underlying sediment, would provide additional information on both the age and timing of the sediment deposition and could prove or disprove a glacial origin to the underlying sill sediments.

Further studies on storm surges in Sachs Harbour should be done to reduce the error of index point height as initial flooding of the basins likely occurs during storms where large waves and surges inundated channels and low-lying barriers. Unfortunately much of the work on storm surges has been done in the southern Beaufort Sea and thus may not be directly applicable.

Eventually, the timing of inundation from the fresh/marine interface will be needed from the basin cores to determine a timeline for the palaeo sea levels. Additional cores of greater lengths may be needed depending on the sedimentation rate within each basin and the elapsed time since the initial incursion. Moreover, for a reliable sea level curve, more index points would be needed, and thus coring of other basins further up

estuary would be recommended. Cores could also be analyzed for depth indicative diatoms to provide further index points and reduce the potential for error, such as argued by Campeau *et al* (2000).

## References

- Belliveau, K. 2007. Coastal geomorphology of Southwest Banks Island, NWT: Historical and recent shoreline changes and implications for the future. M.Sc. Thesis, Environmental Science Program, Memorial University of Newfoundland. St John's, NL.
- Benn, D., Evans, D. 1998. *Glaciers and Glaciation*. Arnold, London.
- Boggs, S. 2006. *Principles of sedimentology and stratigraphy*, 4<sup>th</sup> ed. Pearson Prentice Hall, NJ.
- Brown, T., 2007. Benthic biology of two near-shore Arctic locations and potential impacts of sea level change, coastal erosion, and climate change. M.Sc Thesis, Department of Biology, Memorial University of Newfoundland. St John's, NL.
- Burn, C. 2002. Tundra lakes and permafrost, Richards Island, western Arctic coast, Canada. *Canadian Journal of Earth Science*, 39 (8) : 1291-1298.
- Campeau, S., Héquette, A., and Pienitz, R. 2000. Late Holocene diatom biostratigraphy and sea-level changes in the southeastern Beaufort Sea. *Canadian Journal of Earth Sciences*, 37 (1): 63-80.
- Canadell, J., Jackson, R., Ehleringer, J, Mooney, H, Sala, O., and Schulze, E-D. 1996. Maximum Rooting Depth of Vegetation Types at the Global Scale. *Oecologia*, 108 (4): 555-595.
- Canadian Hydrographic Services. 2008. *Tides, Currents, and Water Levels*. Government of Canada, Fisheries and Oceans. (last accessed June 9, 2008) URL: <http://www.waterlevels.gc.ca/cgi-bin/tide-shc.cgi?queryType=showZone&language=english&region=2&zone=36>
- Canadian Ice Services. 2003. *Sea Ice Climate Atlas, Northern Canadian Waters*. Government of Canada, Environment Canada. (Last accessed June 9, 2008) URL: <http://ice-glaces.ec.gc.ca/WsvPageDsp.cfm?ID=1&Lang=eng>
- Church, J., White, N., Coleman, R., Lambeck, K., and Mitrovica, J. 2004. Estimates of the Regional Distribution of Sea Level Rise over the 1950-2000 Period. *Journal of Climate*, 17 (13): 2609-2625.
- Clark, M., French, H., and Harry, D. 1984. Reconnaissance techniques for the estimation of arctic coastal sediment budget and process. *In Coastal Research: UK perspectives*. Edited by M. Clark. Geo Books, University Press, Cambridge. pp 1-15.

- Cowan, E., and Powell, R. 1990. Suspended sediment transport and deposition of cyclically interlaminated sediment in a temperate glacial fjord, Alaska, USA. *In* *Glacimarine Environments: Processes and Sediments*. Edited by J. Dowdeswell, and J. Scourse, Geological Society Special Publication No. 53. pp. 75-89.
- Craig, B., and Fyles, J. 1960. Pleistocene Geology of Arctic Canada. Geological Survey of Canada. Paper 60-10.
- Dallimore, S., Wolfe, S., and Solomon, S. 1996. Influence of ground ice and permafrost on coastal evolution, Richards Island, Beaufort Sea coast, NWT. *Canadian Journal of Earth Sciences*, 33 (5): 664-675.
- Dean, W. 1974. Determination of carbonate and organic matter in calcareous sediments and sedimentary rocks by loss on ignition: comparison with other methods. *Journal of Sedimentary Petrology*, 44 (1): 242-248.
- Dyke, A. 1987. A reinterpretation of glacial and marine limits around the northwestern Laurentide Ice Sheet. *Canadian Journal of Earth Sciences*, 24 (4): 591-601.
- Dyke, A. 1998. Holocene delevelling of Devon Island, Arctic Canada: implications for ice sheet geometry and crustal response. *Canadian Journal of Earth Science*, 35 (8): 885-904.
- Dyke, A. 2004. An outline of North American deglaciation with emphasis on central and northern Canada. *In* *Quaternary Glaciations – Extent and Chronology, Part II*. Edited by J. Ehlers and P.L. Gibbard. Elsevier B.V. pp. 373-424
- Dyke, A., and Prest, V. 1987. Late Wisconsinan and Holocene History of the Laurentide Ice Sheet. *Géographie Physique et Quaternaire*, XLI no. 2: 237-263.
- Dyke, A., Andrews, J., Clark, P., England, J., Miller, G., Shaw, J., and Veillette, J. 2002. The Laurentide and Innuitian ice sheets during the last glacial maximum. *Quaternary Science Reviews*, 21 (1-3): 9-31.
- Dyke, A., Dredge, L., and Hodgson, D. 2005. North American Deglacial Marine- and Lake-Limit Surfaces. *Géographie Physique et Quaternaire*, 59 (2-3): 155-185
- Dyke, L. 1991 Temperature changes and thaw of permafrost adjacent to Richards Island, Mackenzie Delta, N.W.T. *Canadian Journal of Earth Sciences*, 28 (11): 1834-1842
- Environment Canada. 2004. Canadian Climate Normals 1971-2000: Sachs Harbour A, Northwest Territories. Government of Canada. (Last accessed June 9, 2008) URL: [http://www.climate.weatheroffice.ec.gc.ca/climate\\_normals/results\\_e.html](http://www.climate.weatheroffice.ec.gc.ca/climate_normals/results_e.html)

- Forbes, D.L. 2005. Coastal Erosion. *In* Encyclopedia of the Arctic. Edited by M. Nuttall, Routledge, pp. 391-393
- Forbes, D.L., Craymer, M., Solomon, S., and Manson, G. 2004a. Defining Submergence and Erosion Hazards in the Canadian Arctic. Arctic Coastal Dynamics: Report of the 4<sup>th</sup> International Workshop, St. Petersburg, Russia, November 2003. *Berichte zur Polar und Meeresforschung*, 482: 196-202.
- Forbes, D.L., Bell, T., Craymer, M., and Manson, G. 2004b. Coastal submergence and emergence across the Canadian Arctic. ArcticNet ASM program with abstracts, poster session.
- French, H. 2007. *The Periglacial Environment*, third ed. John Wiley and Sons, 458 pp.
- French, H. 1974. Mass-wasting at Sachs Harbour, Banks Island, NWT, Canada. *Arctic and Alpine Research*, 6(1): 71-78
- French, H., Harry, D., and Clark, M. 1982. Ground-Ice Stratigraphy and Late Quaternary Events, South-west Banks Island, Canadian Arctic. *In* Proceedings of Fourth Canadian Permafrost Conference, National Research Council of Canada. Edited by H. French. pp.81-90.
- French, H., and Harry, D., 1983. Ground Ice Conditions and Thaw Lakes, Sachs River Lowlands, Banks Island, Canada. *Abhandlungen der Akademid der Wissenschaften in Goettingen, Mathematisch – Physikalische Klasse*, 35: 70-81.
- French, H., and Harry, D. 1988. Nature and origin of ground ice, Sandhills Moraine, southwest Banks Island, Western Canadian Arctic, *Journal of Quaternary Science*, 3 (1):19-30.
- Furgal, C., and Prowse, T. 2008. Northern Canada; *in* From Impacts to Adaptations: Canada in a Changing Climate 2007, edited by D Lemmen, F. Warren, J. Lacroix, and E. Bush. Government of Canada, Ottawa, ON, pp 57-118
- Glew, J., Smol, J., and Last, W. 2001. Sediment core collection and extrusion. *In* Tracking environmental change using lake sediments, Vol. 1. Edited by W. Last and J. Smol. Kluwer Academic Publishers, pp. 73-105.
- Good, T., and Bryant, I. 1985. Fluvio-aeolian sedimentation – an example from Banks Island, NWT, Canada. *Geografiska Annaler*, 67A (1-2): 33-46.
- Gurney, S. and Worseley, P. 1997. Genetically complex and morphologically diverse pingos in the Fish Lake area of southwest Banks Island, NWT., Canada. *Geografiska Annaler*, 79A (1-2): 41-56.

- Harper, J., Henry, R.F., and Stewart, G. 1988. Maximum storm surge elevations in the Tuktoyaktuk region of the Canadian Beaufort Sea. *Arctic*. 41 (1): 48-52.
- Harry, D. 1982. Aspects of the permafrost geomorphology of southwest Banks Island, Western Canadian Arctic. Unpublished P.h.D. thesis, Department of Geography, University of Ottawa, Ottawa, ON, 230 p.
- Harry, D., French, H., and Clark, M. 1983. Coastal conditions and processes, Sachs Harbour, Banks Island, Western Canadian Arctic. *Zeitschrift für Geomorphologie (Annals of Geomorphology)*, Supplementband 47: Coastal and Inland Periglacial Processes, Canadian Arctic, pp. 1-26.
- Heiri, O., Lotter, A., and Lemcke, G. 2001. Loss on ignition as a method for estimating organic and carbonate content in sediments: reproducibility and comparability of results. *Journal of Paleolimnology*, 25 (1): 101-110.
- Héquette, A., and Barnes, P., 1990. Coastal Retreat and Shoreface Profile Variation in the Canadian Beaufort Sea. *Marine Geology*, 91 (1-2): 113-132.
- Héquette, A., and Hill, P., 1995. Response of the seabed to storm-generated combined flows on sandy arctic shoreface, Canadian Beaufort Sea. *Journal of Sedimentary Research*, A65 (3):461-471.
- Héquette, A., Ruz, M-H., and Hill, P.R. 1995. The Effects of the Holocene Sea Level Rise on the Evolution of the Southeastern Coast of the Canadian Beaufort Sea. *Journal of Coastal Research*, 11(2): 494-507.
- Herbert, P. 2002. Canada's Polar Environments. CyberNatural Software, University of Guelph. Last Accessed, October 5<sup>th</sup> 2008.  
[http://www.arctic.uoguelph.ca/cpe/environments/maps/map\\_frame.htm](http://www.arctic.uoguelph.ca/cpe/environments/maps/map_frame.htm)
- Hill, P., Héquette, A., and Ruz, M.-H. 1993. Holocene sea-level history of the Canadian Beaufort shelf. *Canadian Journal of Earth Science*, 30 (1): 103-108.
- Hill, P., Mudie, P., Moran, K., and Blasco, S. 1985. A sea-level curve for the Canadian Beaufort Shelf. *Canadian Journal of Earth Science*, 22 (10): 1383-1393.
- Hill, P., and Solomon, S. 1999. Geomorphologic and Sedimentary Evolution of a Transgressive Thermokarst Coast, Mackenzie Delta Region, Canadian Beaufort Sea. *Journal of Coastal Research*, 15 (4): 1011-1029.
- Huntington, H., Weller, G., Bush, E., Callaghan, T., Kattsov, V., and Nuttal, M. 2005. An introduction to the Arctic Climate Impact Assessment. *In Arctic Climate Impact Assessment*, Cambridge University press, pp 1-20.

- INAC (Indian and Northern Affairs Canada). 2005. *Communities – A Guide to Mineral Exploration and Development in the NWT, Sachs Harbour*. Government of Canada. (last accessed June 9, 2008). URL: [http://nwt-tno.inac-ainc.gc.ca/mpf/communit/com\\_e.asp?ID=23](http://nwt-tno.inac-ainc.gc.ca/mpf/communit/com_e.asp?ID=23)
- IPCC. 2007. *Intergovernmental Panel on Climate Change fourth assessment report (AR4)*. Cambridge University Press. URL: <http://www.ipcc.ch/>
- Kaufman, D., Ager, T., Anderson, N., Anderson, P., Andrews, J., Bartlein, P., Brubaker, L., Coats, L., Cwynar, L., Duvall, M., Dyke, A., Edwards, M., Eisner, W., Gajewski, K., Geisdottir, A., Hu, F., Jennings, A., Kaplan, M., Kerwin, M., Lozhkin, A., MacDonald, G., Miller, G., Mock, C., Oswald, W., Otto-Bliesner, B., Porinchu, D., Ruhland, K., Smol, J., Steig, E., and Wolfe, B. 2004. Holocene thermal maximum in the western Arctic (0-180°W). *Quaternary Science Reviews*, 23 (5-6): 529 – 560.
- Kempema, E., Reimnitz, E., and Barnes, P. 1989. Sea ice sediment entrainment and rafting in the Arctic. *Journal of Sedimentary Petrology*, 59 (2): 308-317.
- Kerr, D. 1996. Late Quaternary sea level in the Paulatuk to Bathurst Inlet area, Northwest Territories. *Canadian Journal of Earth Sciences*, 33 (3): 389-403.
- Kobayashi, N., Vidrine, J., Nairn, R., and Solomon, S. 1999. Erosion of Frozen Cliffs Due to Storm Surges on Beaufort Sea Coast. *Journal of Coastal Research*, 15 (2): 332-344
- Lonne, I. 1997. Facies characteristics of a proglacial turbiditic sand-lobe at Svalbard. *Sedimentary Geology*, 109 (1-2): 13-35.
- Lonne, I., 1995. Sedimentary facies and depositional architecture of ice-contact glaciomarine systems. *Sedimentary Geology*, 98 (1-4): 13-43.
- Long, A., Roberts, D., and Wright, M. 1999. Isolation basin stratigraphy and Holocene relative sea-level change on Arveprinsen Ejland, Disko Bugt, West Greenland. *Journal of Quaternary Science*, 14 (4): 323-345.
- Mackiewicz, N., Powell, R., Carlson, P., and Molnia, B., 1984. Interlaminated ice-proximal glaciomarine sediments at Muir Inlet, Alaska. *Marine Geology*, 57 (1-4): 113-147.
- Manson, G., and Solomon, S. 2007. Past and future forcing of Beaufort Sea coastal change. *Atmosphere-Ocean*, 45 (2): 107-122.
- Manson, G.K., Solomon, S.M., Forbes, D.L., Atkinson, D.E., and Craymer, M. 2005. *Spatial Variability of Factors Influencing Coastal Change in the Western*

- Canadian Arctic. *Geo-marine Letters*, 25 (2-3): 138-145.
- Marsh, P., and Neumann, N. 2001. Processes controlling the rapid drainage of two ice-rich permafrost-dammed lakes in NW Canada. *Hydrological Processes*. 15: 34433-3446
- Miall, A. 1979. Mesozoic and Tertiary Geology of Banks Island, Arctic Canada; the History of an Unstable Craton Margin. Geological Survey of Canada, Memoir, no 387, 235pp.
- Miettinen, A., Jansson, H., Alenius, T., and Haggren, G. 2007. Late Holocene sea-level changes along the southern coast of Finland, Baltic Sea. *Marine Geology*, 242 (1-3): 27-38.
- NWT Bureau of statistics. 2007. General Statistics. Government of Northwest Territories. (Last accessed June 9, 2008). URL : <http://www.stats.gov.nt.ca/Stainfo/Generalstats/general.html>
- Pielou, E., 1994. *A Naturalist's Guide to the Arctic*. The University of Chicago Press, 327 pp.
- Pienitz, R., Lortie, G., and Allard, M. 1991. Isolation of lacustrine basins and marine regression in the Kuujuaq area, Northern Quebec, as inferred from diatom analysis. *Géographie Physique et Quaternaire*, 45 (2): 155-174.
- Pissart, A, Vincent, J-S., and Edlund, S. 1977. Dépot et phénomènes éoliens sur l'île de Banks, Territoire du Nord-Ouest, Canada. *Canadian Journal of Earth Science*, 14 (11): 2462-2480.
- Powell, R. 1991. Glacimarine processes at grounding-line fans and their growth to ice-contact deltas. *In* *Glacimarine Environments: Processes and Sediments*. Edited by J. Dowdeswell, and J. Scourse, Geological Society Special Publication No. 53: 53-73.
- Powell, R. 1984. Glacimarine processes and inductive lithofacies modeling of ice shelf and tidewater glacier sediments base on Quaternary examples. *Marine Geology*, 57 (1-4): 1-52.
- Prest, V., Grant, D., and Rampton, V. 1968. Glacial map of Canada, Geological Survey of Canada, map 1253A.
- Proshutinsky, A, Pavlov, V., and Bourke, R. 2001. Sea level rise in the Arctic Ocean. *Geophysical Research Letters*, 28 (11): 2237-2240.

- Rampton, V., 1988. Quaternary geology of the Tuktoyaktuk coastlands, Northwest Territories. Geological Survey of Canada, memoir 423.
- Rampton, V., and Bouchard, M. 1975. Surficial geology of Tuktoyaktuk, District of Mackenzie. Paper. Geological Survey of Canada. No. 74-53, 17 pp.
- Reimnitz, E., and Barnes, P. 1987. Sea-ice influence on arctic coastal retreat. *In Coastal Sediments. Edited by N. Kraus.* American Society of Civil Engineering. New Orleans. Vol. 2 pp. 1578-1591.
- Ritchie, J. 1984. Past and Present Vegetation of the Far Northwest of Canada. University of Toronto Press, 251 pp.
- Saulnier-Talbot, E., and Pienitz, R. 2001. Isolation au Postglaciaire d'un bassin cotier pres de Kuujjuaraapik-Whapmagoostui, en Hudsonie (Quebec): une analyse biostratigraphique diatomifere. *Géographie Physique et Quaternaire*, 55(1): 63-74.
- Siferd, T. 2001. Sachs Harbour marine benthic community survey. Summary of results 1999-2000. Canadian Technical Report of Fisheries and Aquatic Sciences, 2366: VII+47p.
- Shaw, J., Taylor, R., Forbes, D., Ruz, M-H., and Solomon, S. 1998. Sensitivity of the coasts of Canada to sea-level rise. Geological Survey of Canada Bulletin 505. Natural Resources Canada.
- Shaw, J., Taylor, R., Solomon, S., Christian, H., and Forbes, D., 1998 B, Potential impacts of global sea-level rise on Canadian coasts. *Canadian Geographer*, 42 (4): 365-379.
- Smith, D. 1984. Vibracoring fluvial and deltaic sediments: tips on improving penetration and recovery. *Journal of Sedimentary Petrology*, 54 (2): 660-663.
- Smith, I.R., Bell, T., Forbes, D., and Martin, B. 2006. A Hypersaline Coastal Marine Transgressive Basin With Sedimentary Mirabilite Formation, Southern Banks Island, NWT. ArcticNet ASM program with abstracts, poster session.
- Solomon, S., Mudie, P., Cranston, R., Hamilton, T., Thibaudeau, S., and Collins, E. 2000. Characterisation of marine and lacustrine sediments in a drowned thermokarst embayment, Richards Island, Beaufort Sea, Canada. *International Journal of Earth Sciences*, 89 (3): 503-521.
- Solomon, S., Taylor, A., and Stevens, C. 2008. Nearshore Ground Temperatures, Seasonal Ice Bonding, and Permafrost Formation Within the Bottom-Fast Ice Zone, Mackenzie Delta, NWT. Ninth International Conference on Permafrost: 1675-1680.

- Sparrenbom, C., Bennike, O., Bjorck, S., and Lambeck, K. 2006. Relative sea-level changes since 15 000 cal. yr BP in the Nanortalik area, southern Greenland. *Journal of Quaternary Science*, 21(1): 28-48.
- Stewart, T., 1988. Deglacial-marine sediments from Clements Markham Inlet, Ellesmere Island, NWT, Canada. PhD Thesis, Department of Geography, University of Alberta, Edmonton, Alberta.
- Stokes, C., Clark, C., and Winsborrow, C. 2006. Subglacial bedform evidence for a major paleo-ice stream and its retreat phase in Amundsen Gulf, Canadian Arctic Archipelago. *Journal of Quaternary Science*, 21 (4): 399-412.
- Vincent, J-S. 1978. Limits of ice advance, glacial lakes, and marine transgressions on Banks Island, District of Franklin: a preliminary interpretation. *In Current Research, Part C, Geological Survey of Canada, Paper 78-1C*, pp. 53-62.
- Vincent, J-S. 1982. The Quaternary History of Banks Island, N.W.T., Canada *Géographie Physique et Quaternaire*. Vol XXXVI, No 1-2: 209-232.
- Vincent, J-S. 1983. La Géologie du Quaternaire et la Géomorphologie de L'île de Banks, Arctique Canadien. *Geological Survey of Canada, Memoir 405*.
- Vincent, J-S. 1984. Quaternary stratigraphy of the western Canadian Arctic Archipelago. *In Quaternary Stratigraphy of Canada – A Canadian Contribution to IGCP project 24. Edited by R.J. Fulton, Geologic Survey of Canada, Paper 84-10*: 87-100.
- Vincent, J-S. 1990. Late Tertiary and Early Pleistocene Deposits and History of Banks Island, Southwestern Canadian Arctic Archipelago. *Arctic*, 43(4): 339-363.
- Vincent, J-S. 1992. The Sangamonian and early Wisconsinan glacial record in the western Canadian Arctic. *In The Last Interglacial-Glacial Transition in North America: Boulder, Colorado, Geological Society of America. Special Paper 270*. pp. 233-252.
- Walsh, J. 2005. Cryosphere and Hydrology, *in Arctic Climate Impact Assessment. Edited by C. Symon, L. Arris, and B. Heal. Cambridge University Press*. pp. 183-242
- West, R., and Pettit, M., 2000. Plant macroscopic remains from recent sediments of Banks Island, Northwest Territories, and Bathurst Island, Nunavut, Canada, and the interpretation of Quaternary cold stage plant macroscopic assemblages. *Journal of Quaternary Science*, 15 (2): 177-184.

Wheeler, J., Hoffman, P., Card, K., Davidson, A., Sandford, B., Okulitch, A., and Roest, W. 1997. Geological map of Canada, Geological Survey of Canada. Map D 1860A.

## Appendix A – Sediment core section logs

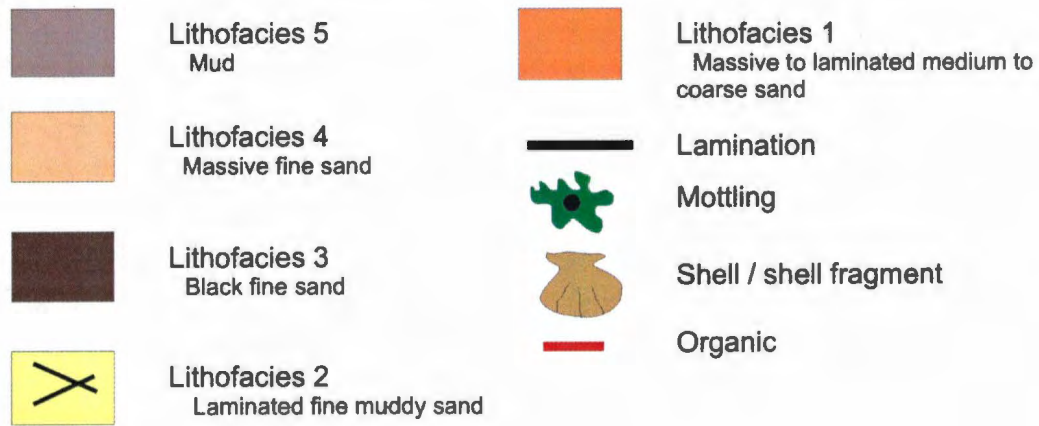


Figure A1. Sediment core legend

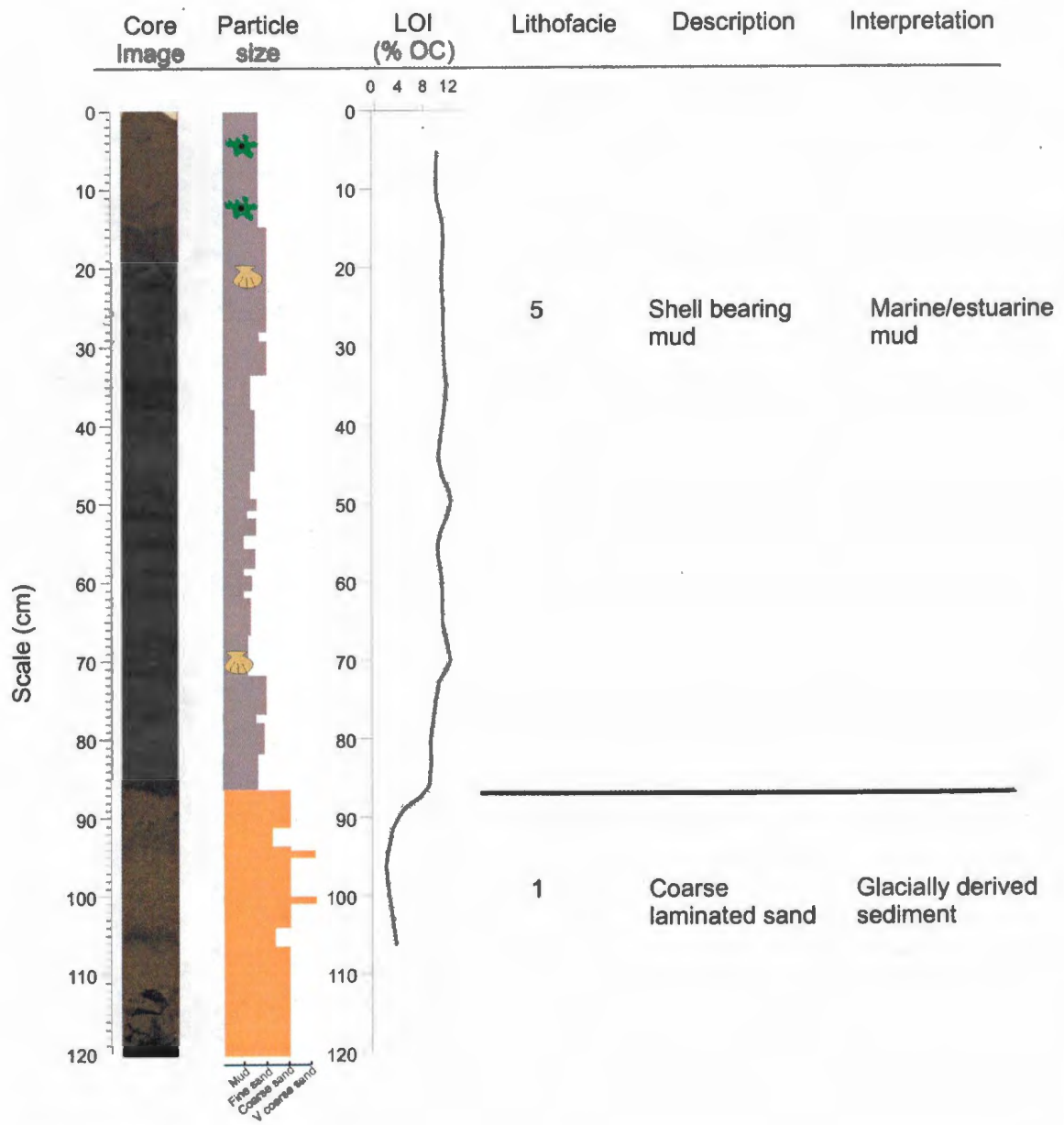


Figure A2. Core 07-001

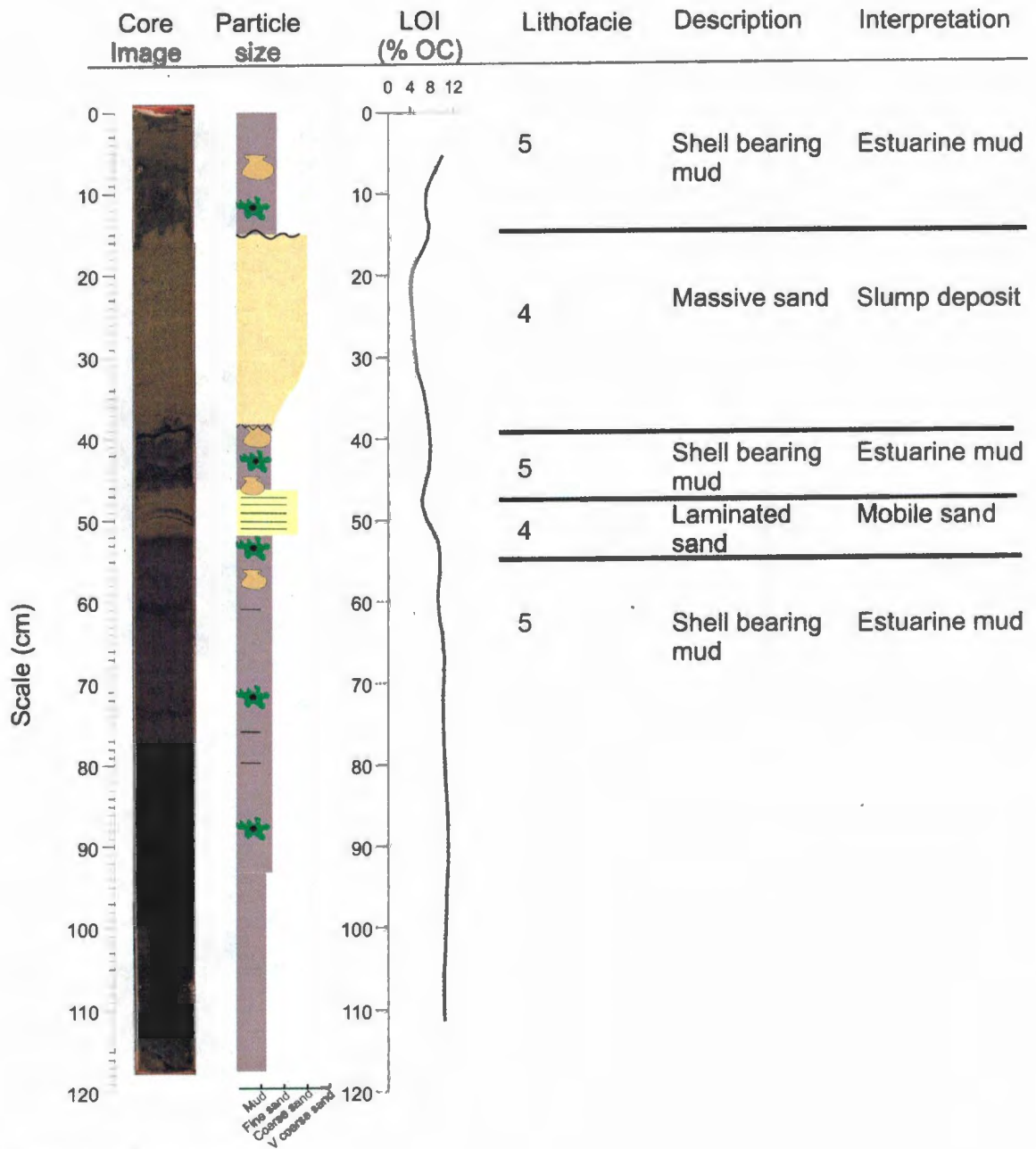


Figure A3. Core 07-002

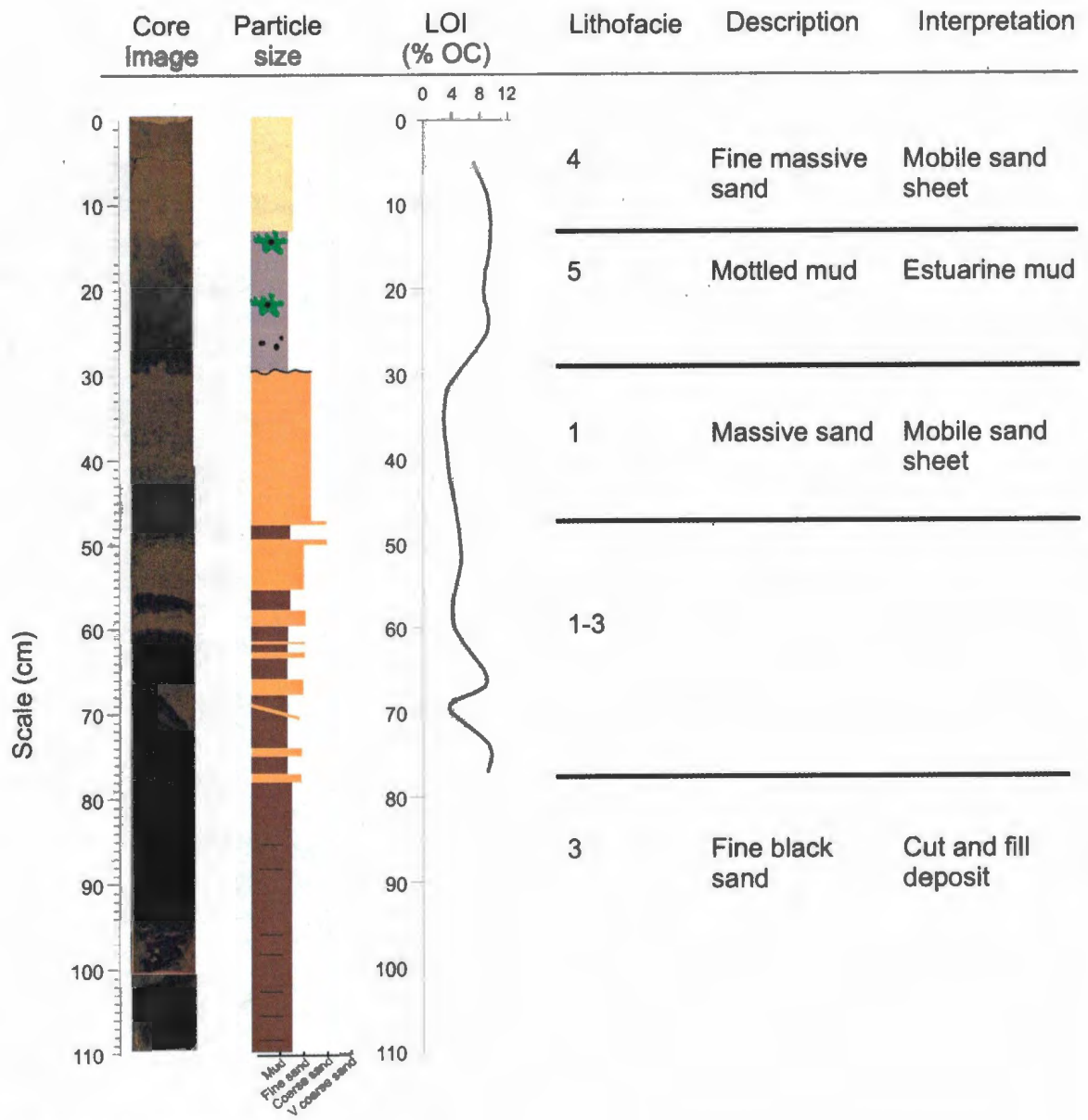


Figure A4. Core 07-003

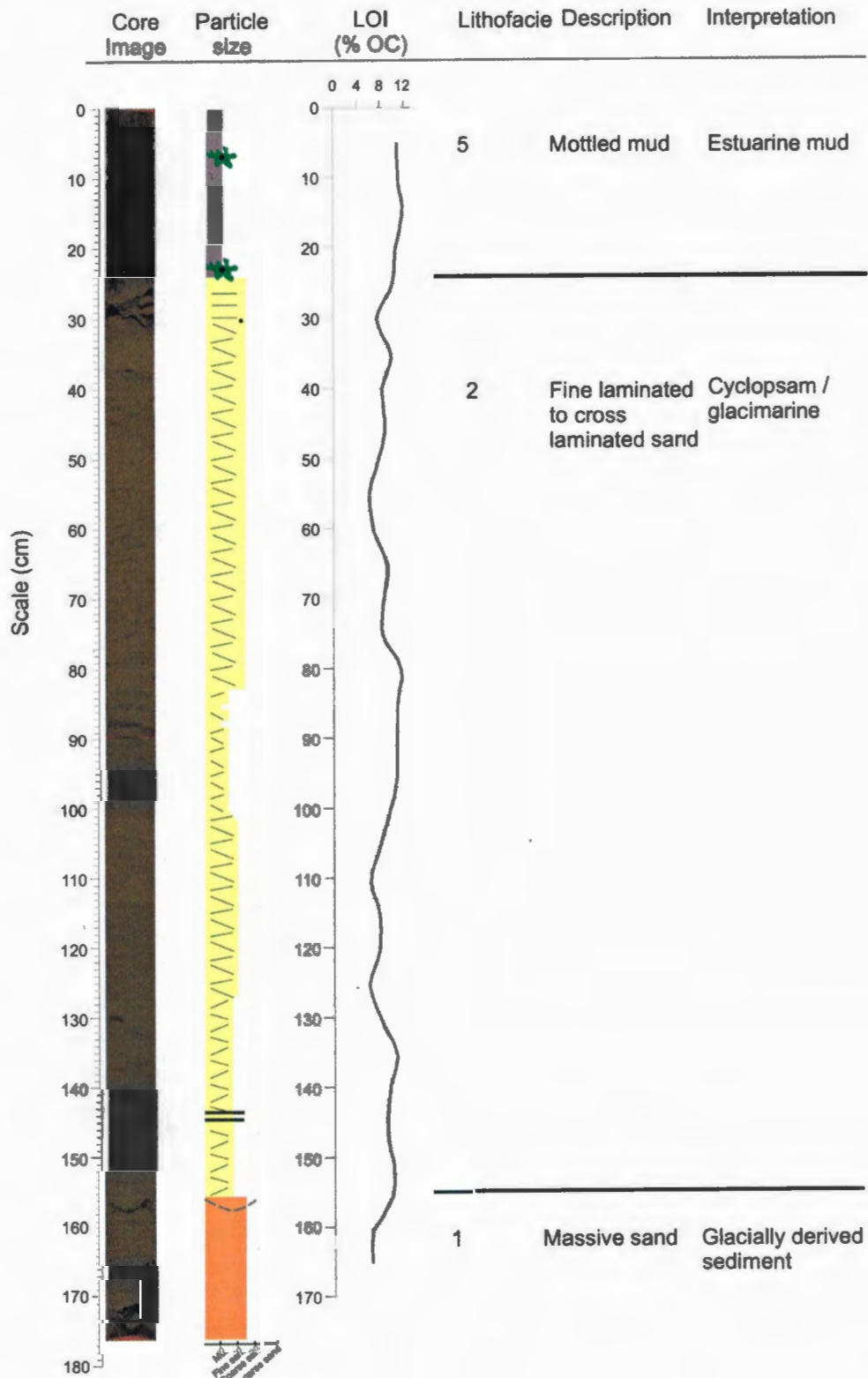


Figure A5. Core 07-004

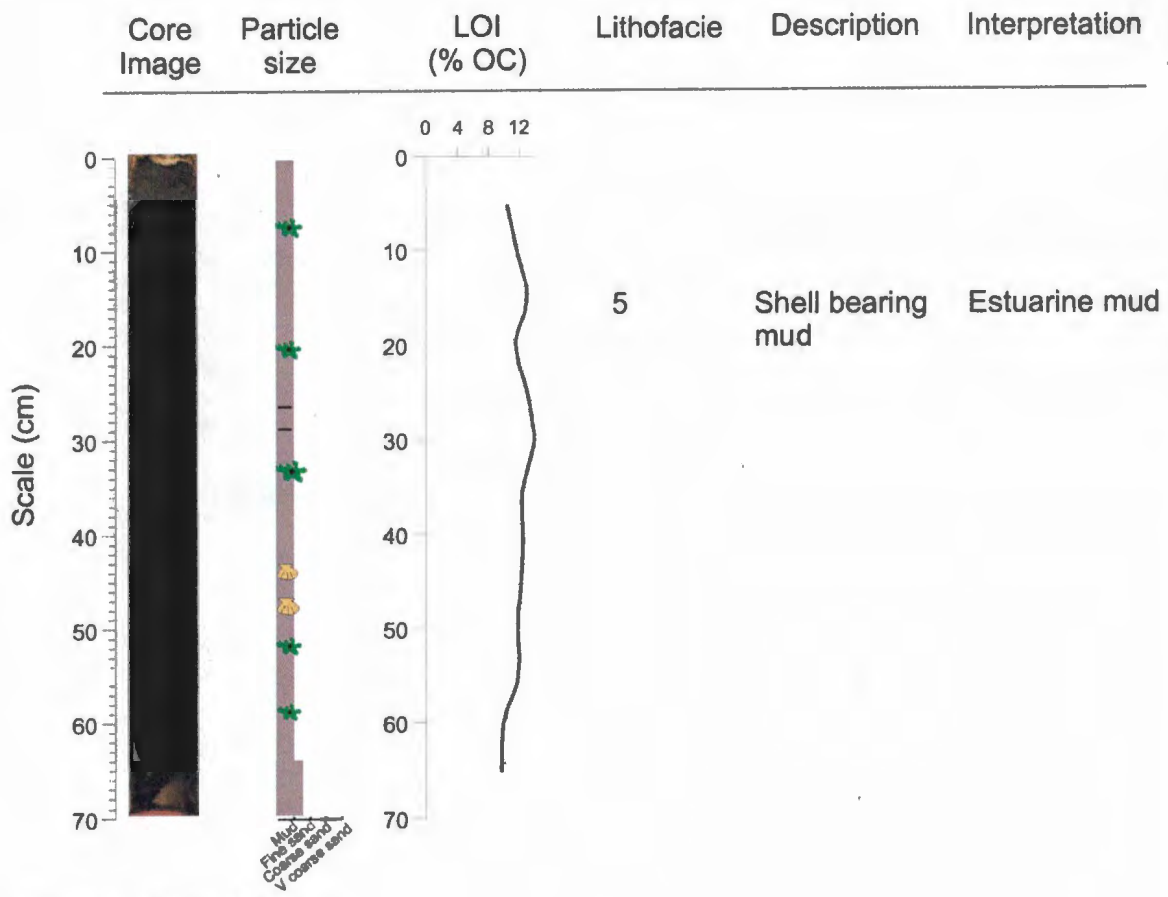


Figure A.6 Core 07-005

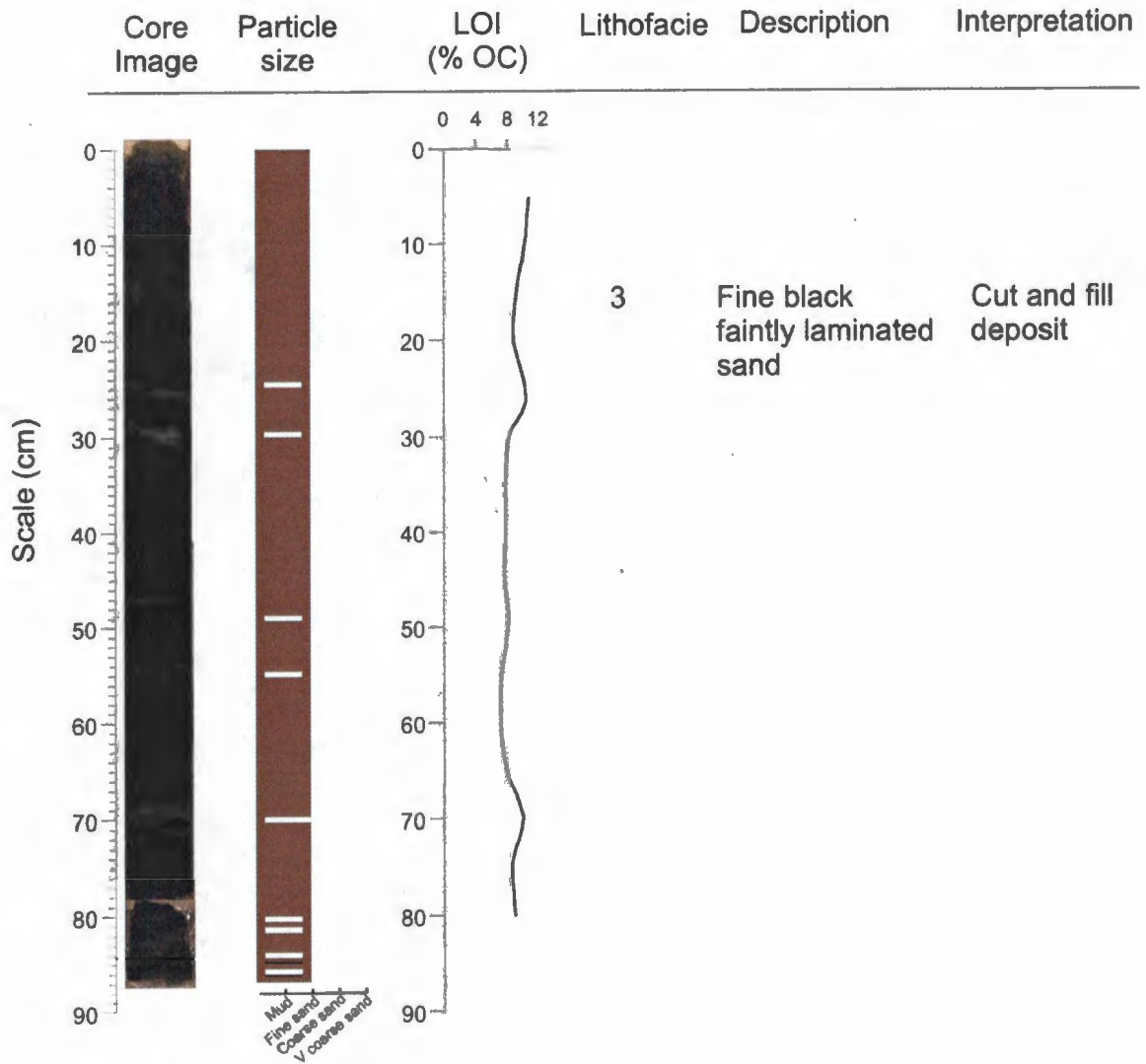


Figure A7. Core 07-006

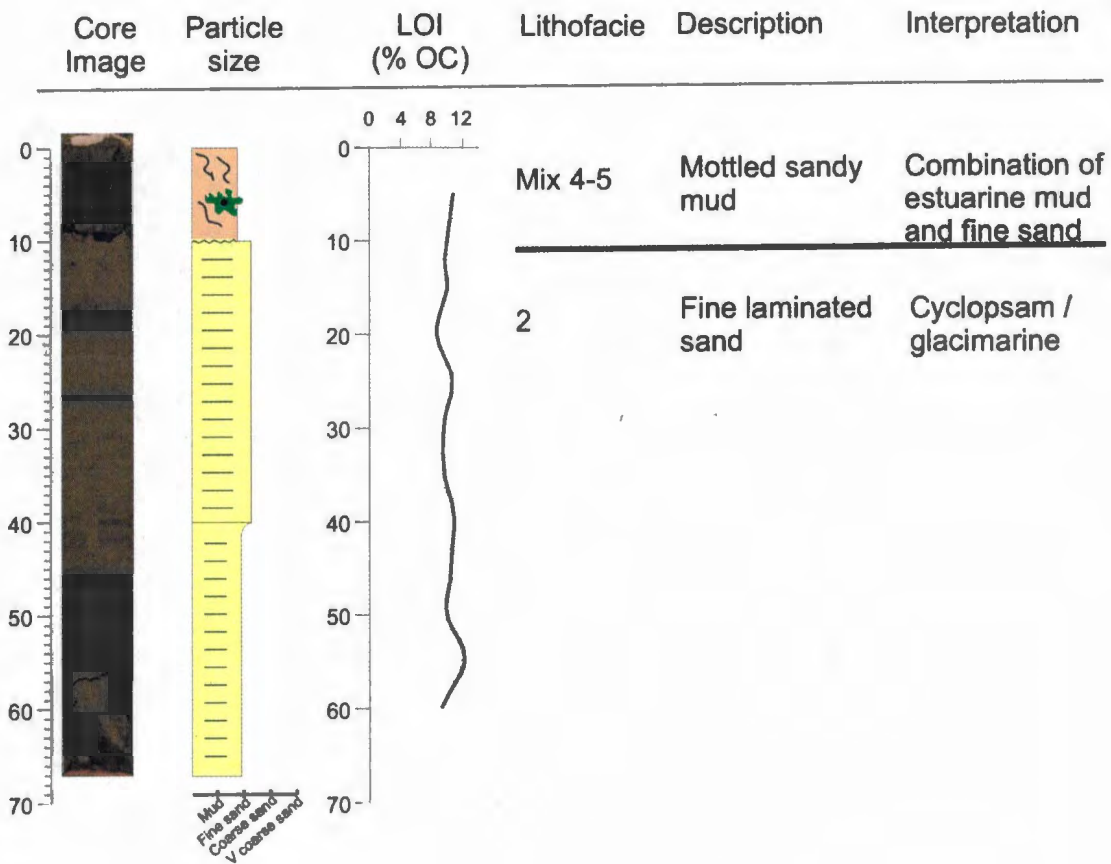


Figure A8. Core 07-007

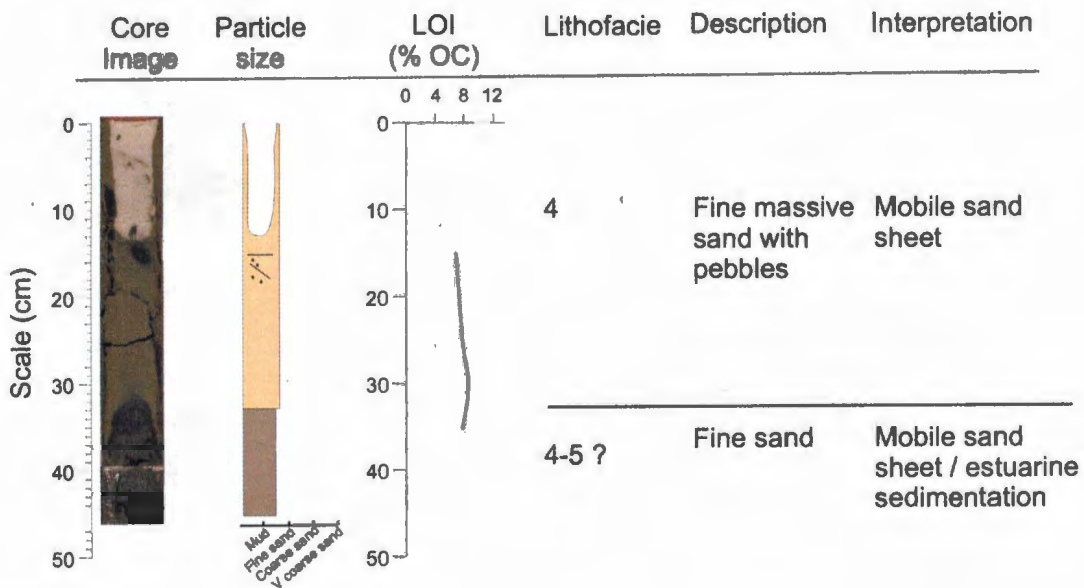


Figure A9. Core 07-009

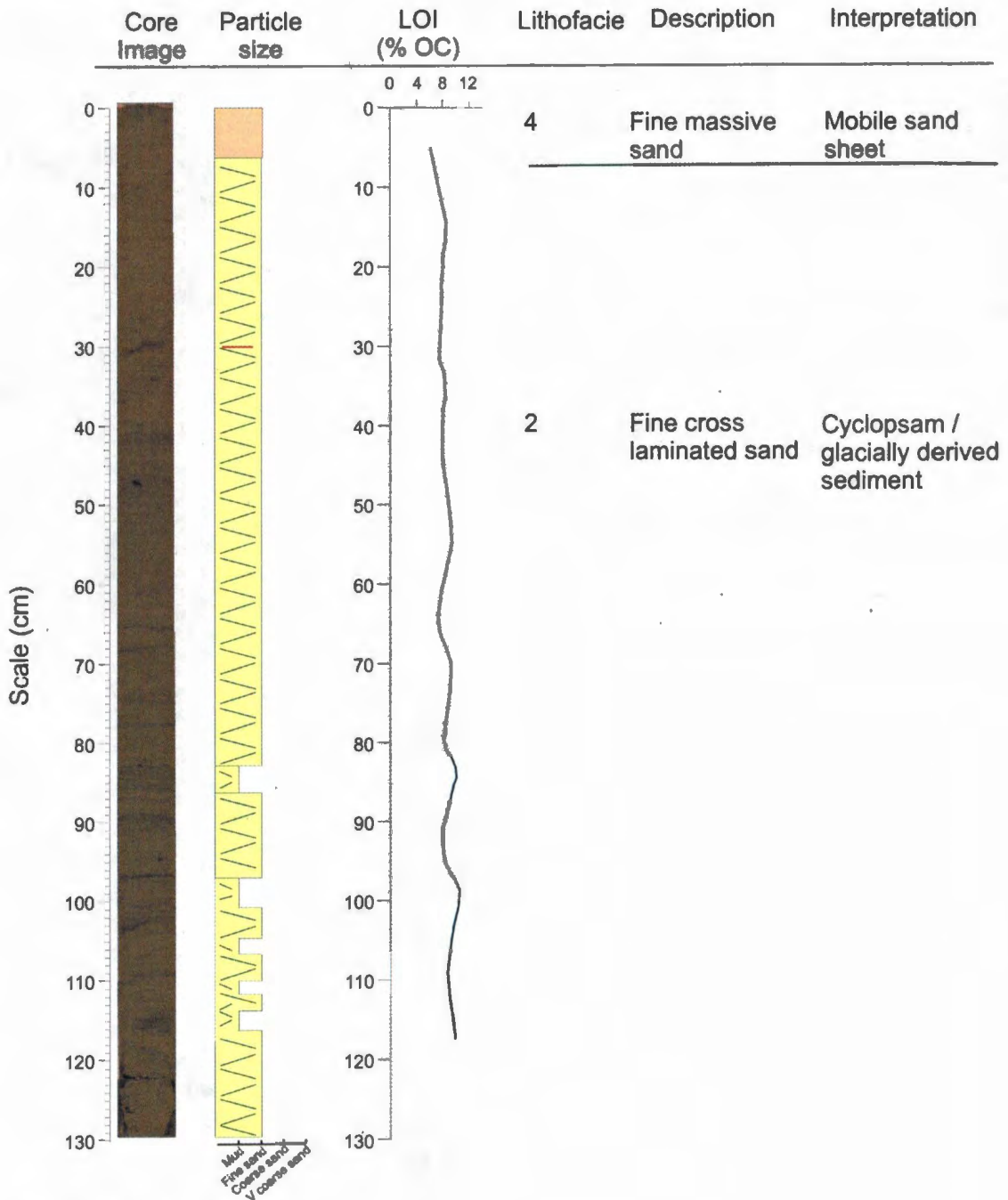


Figure A10. Core 07-013

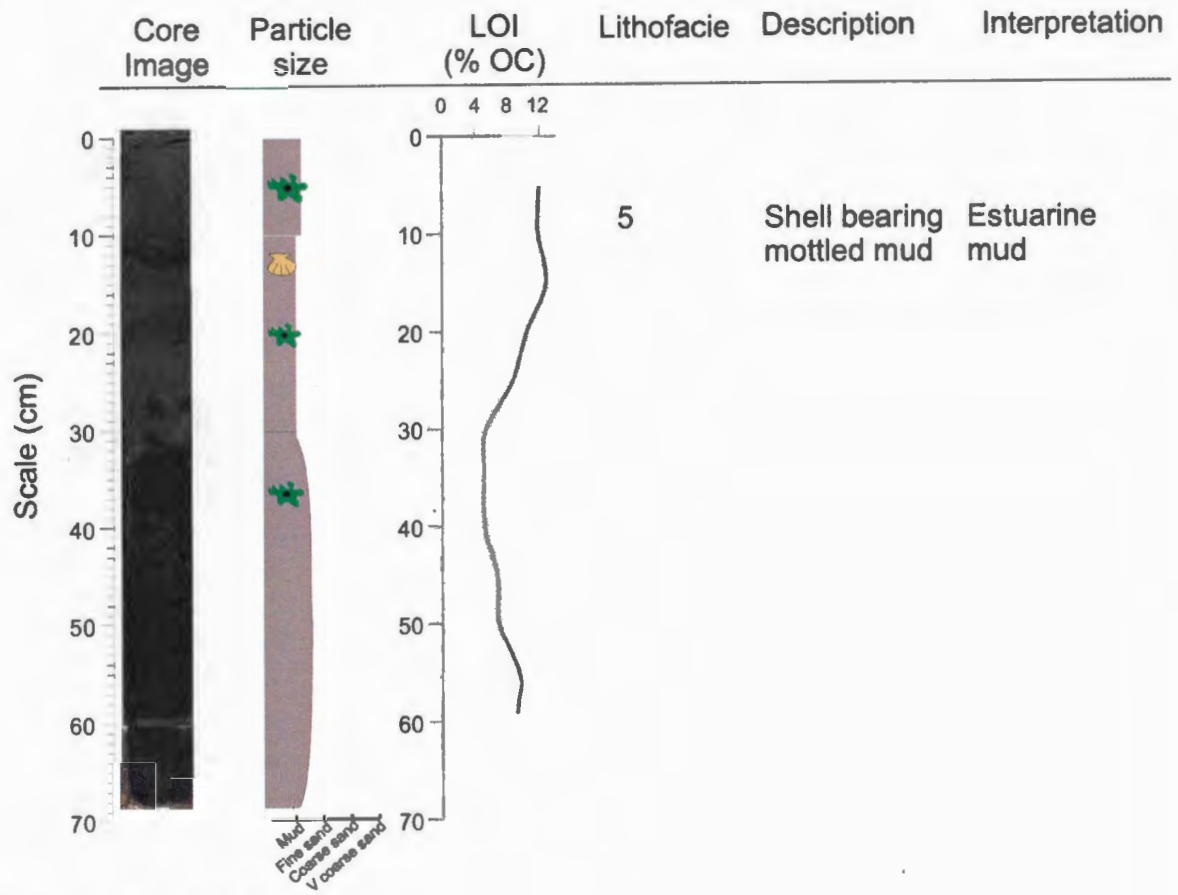
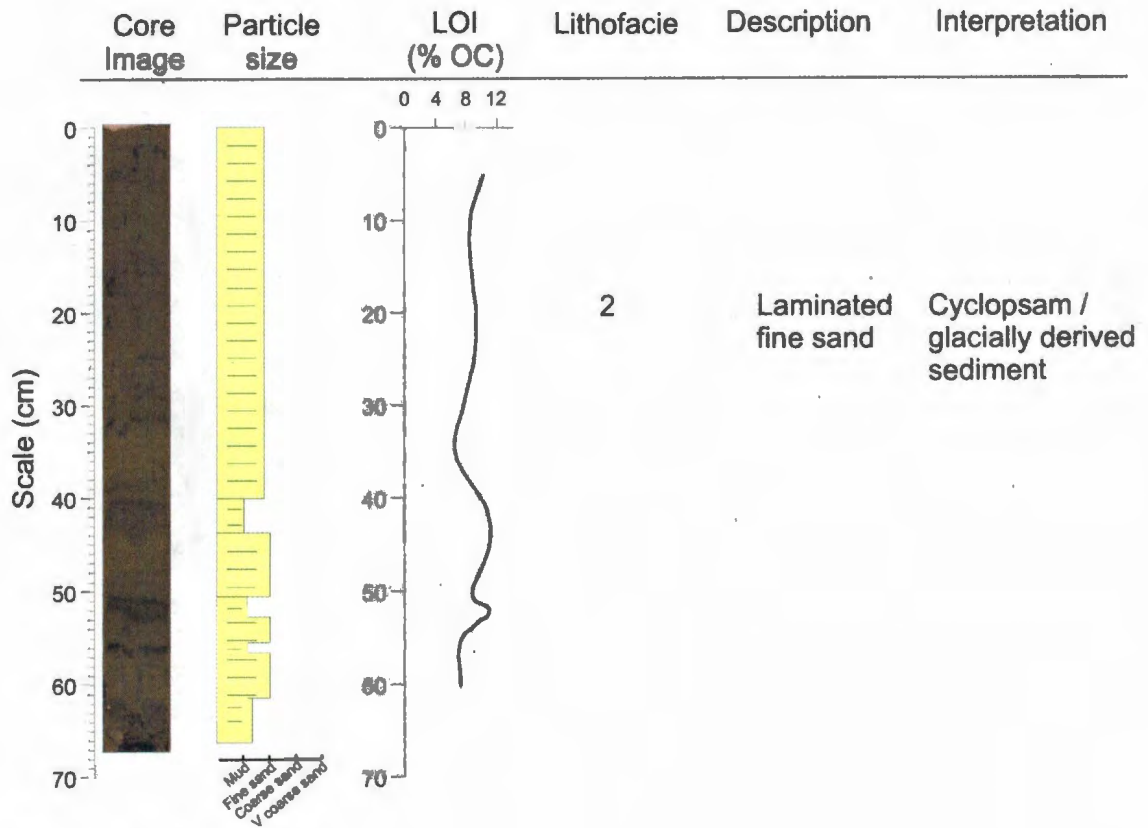


Figure A11. Core 07-014



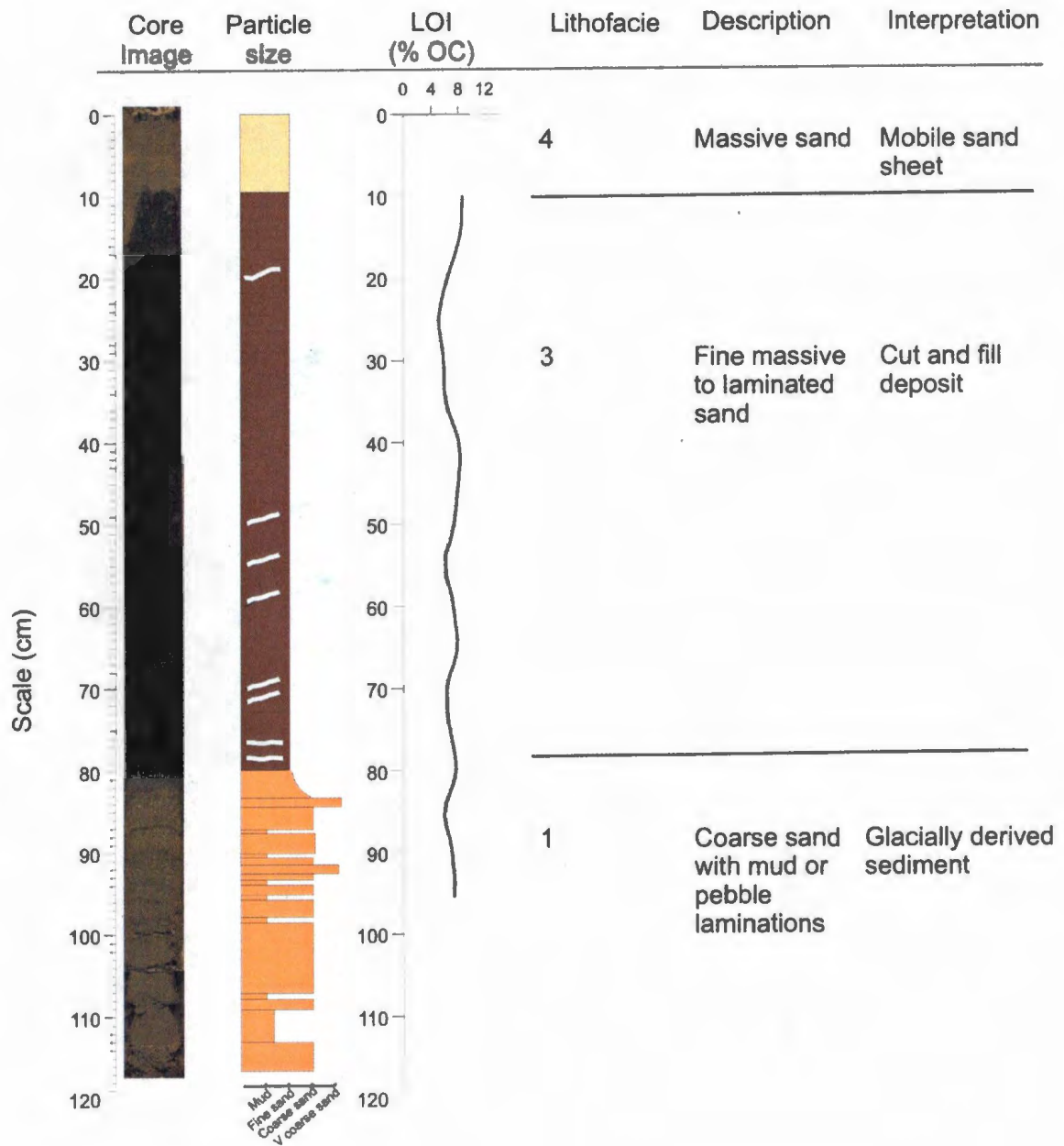
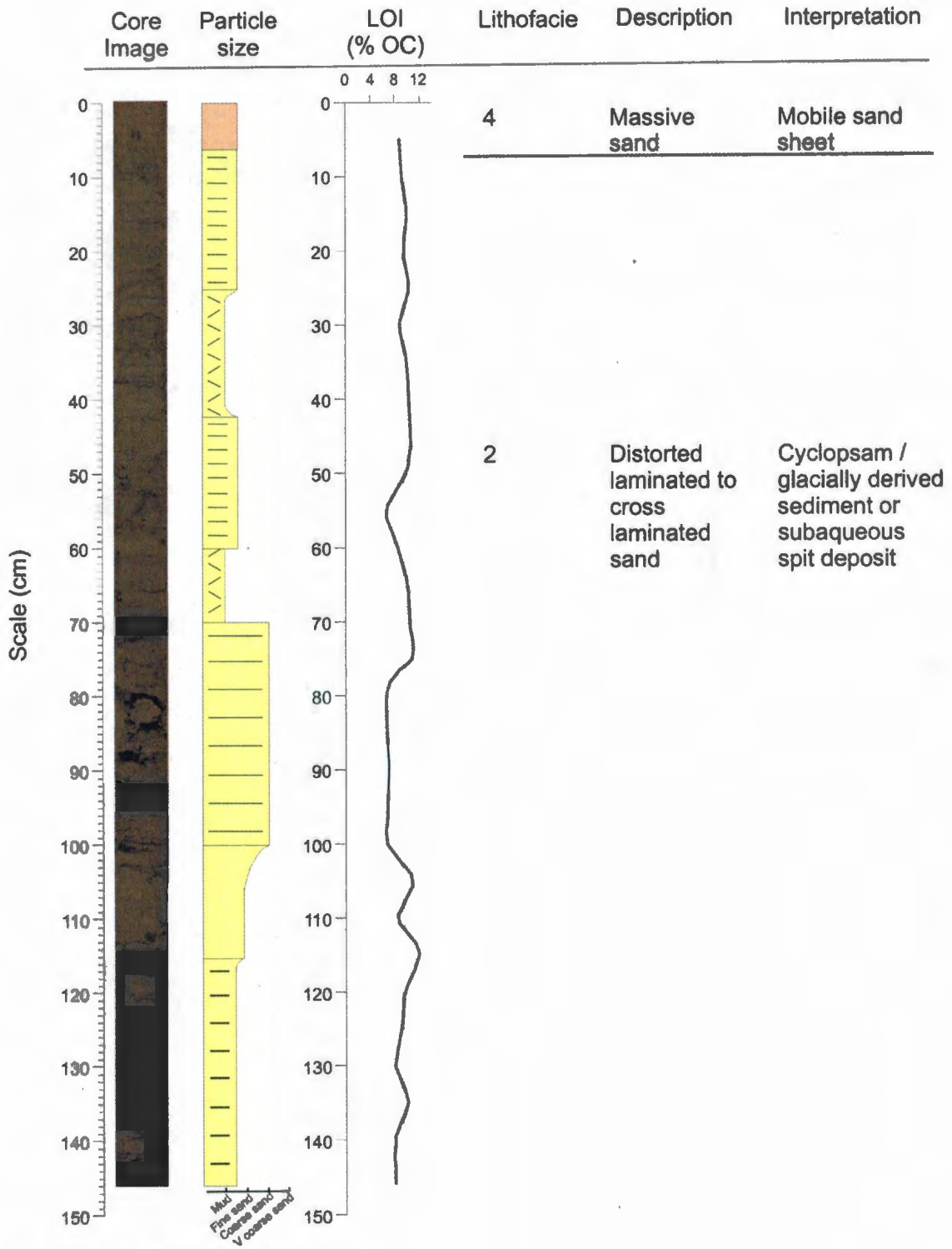


Figure A13. Core 06-003



## **Appendix B – Seismic description**

### **Line 0215**

Seismic line 0215 (Figure B1), taken along a southwest – northeast gradient, was a total of 1.55 km in length and began near the center of the Inner Basin, traversed sill III to the north and ended within the palaeo Sachs channel. The line is situated along a transect of cores 07-005, 07-006, and 07-007, which are each situated approximately 45 m to the northwest of the line. The uppermost section of the seismic line was near acoustically transparent and draped the underlying units within the deep channel and basin. The draped sediment was interpreted as mud. The upper portion of the sill was generally acoustically impenetrable with the exception of a slightly stratified sections interpreted as sandy cut and fill channels. The acoustically impenetrable sections of the sill are interpreted to be fine sand. The sections showing stratification are located adjacent and beneath the palaeo Sachs Channel. The channel, which has a transparent unit overlying the channel fill is interpreted as mud while the upper section of the channel fill lacking the overlying unit is interpreted as sand. Core 07-005, 07-006, and 07-007 were used to ground truth the acoustic interpretations.

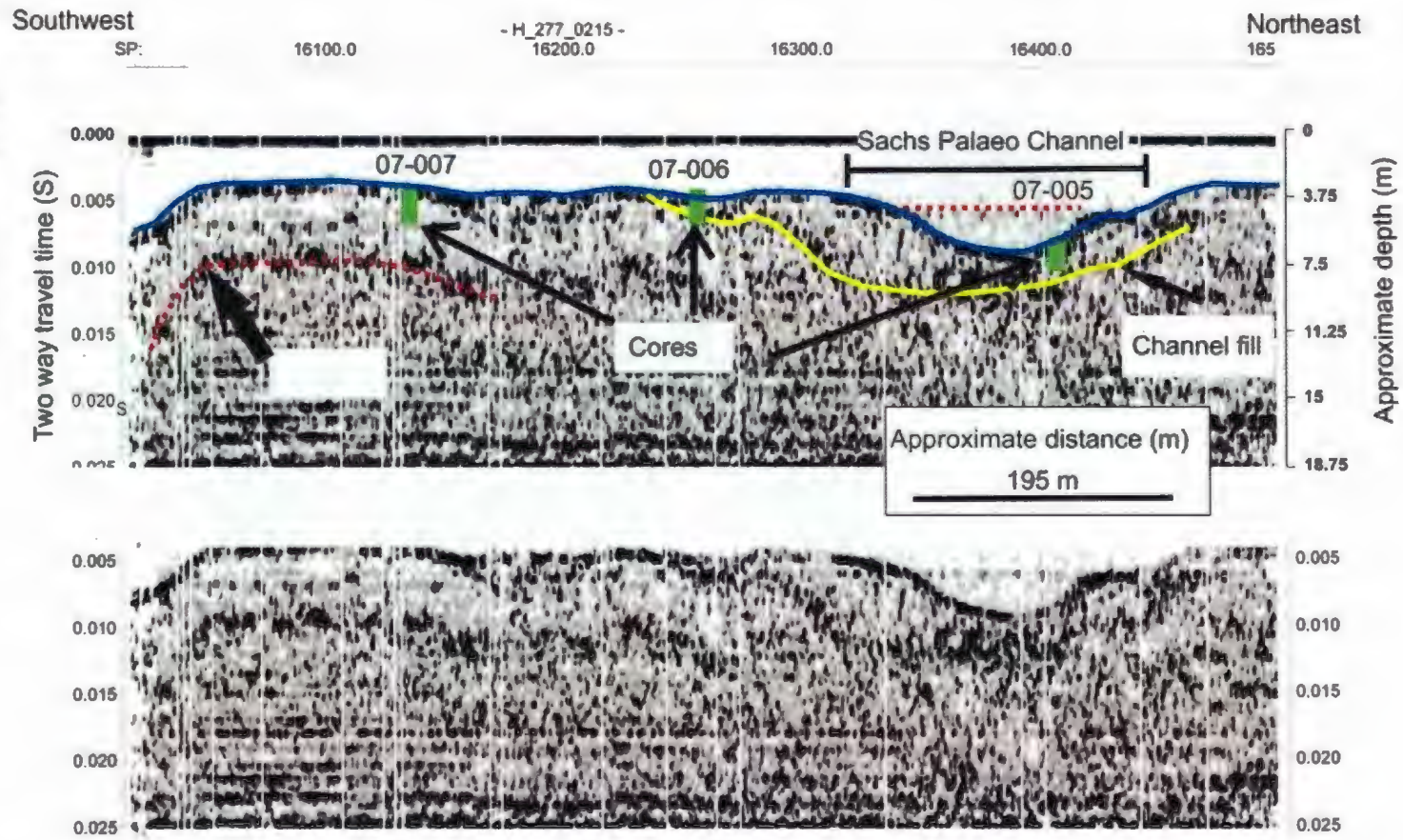
### **Line 0230**

Seismic line 0230 (Figure B2), taken to the west of line 0215 along a southwest – northeast gradient, was a total of 0.7 km in length. It began near the center of the Inner Basin, traversed sill III to the north and ended within the palaeo Sachs channel. The line is situated 24 m from core 06-003 and 103 m from core 07-004. The seismic reflection revealed a thin acoustic unit overlying all but the uppermost section of the line or the steepest portion of the sill on the basin side. The unit is much thicker and acoustically stratified in the deeper troughs, especially within the basin. This unit is interpreted as mud. The lower unit as well as the highest section of the sill appear to be acoustically impenetrable and are interpreted as sand. The depression near shot point 17100 is interpreted as either an erosional scour or a thermokarst depression that has since been inundated. The southwestern end of the line turns sharply to the northwest and joins line 0234.

### **Line 0234**

Seismic line 0234 (Figure B3), taken in a southeast – northwest gradient, was a total of 1.34 km in length and began in the northern portion of the Inner basin at the southern end of line 0230, crossing the Inner/Outer Basin sill (sill II), and ending at the northern shore of the Outer Basin. The seismic reflection of the sill was generally impenetrable with the exception of the troughs appearing within slumps along the steep slope. The upper trough appears to have an accumulation of draped acoustically stratified sediment. Above the slope, two scour and fill channels appear to have been infilled with a slightly acoustically stratified sediment ponding within. The larger of the two structures is approximately 100 m wide and 6 m thick and presently has a small shallow channel cutting into the center. The cut and fill structure lies immediately downslope from the channel from which core 07-001 was taken and may therefore represent a relict of the inlet/outlet channel of the basin. The second channel may

Figure B1. Seismic line 0215



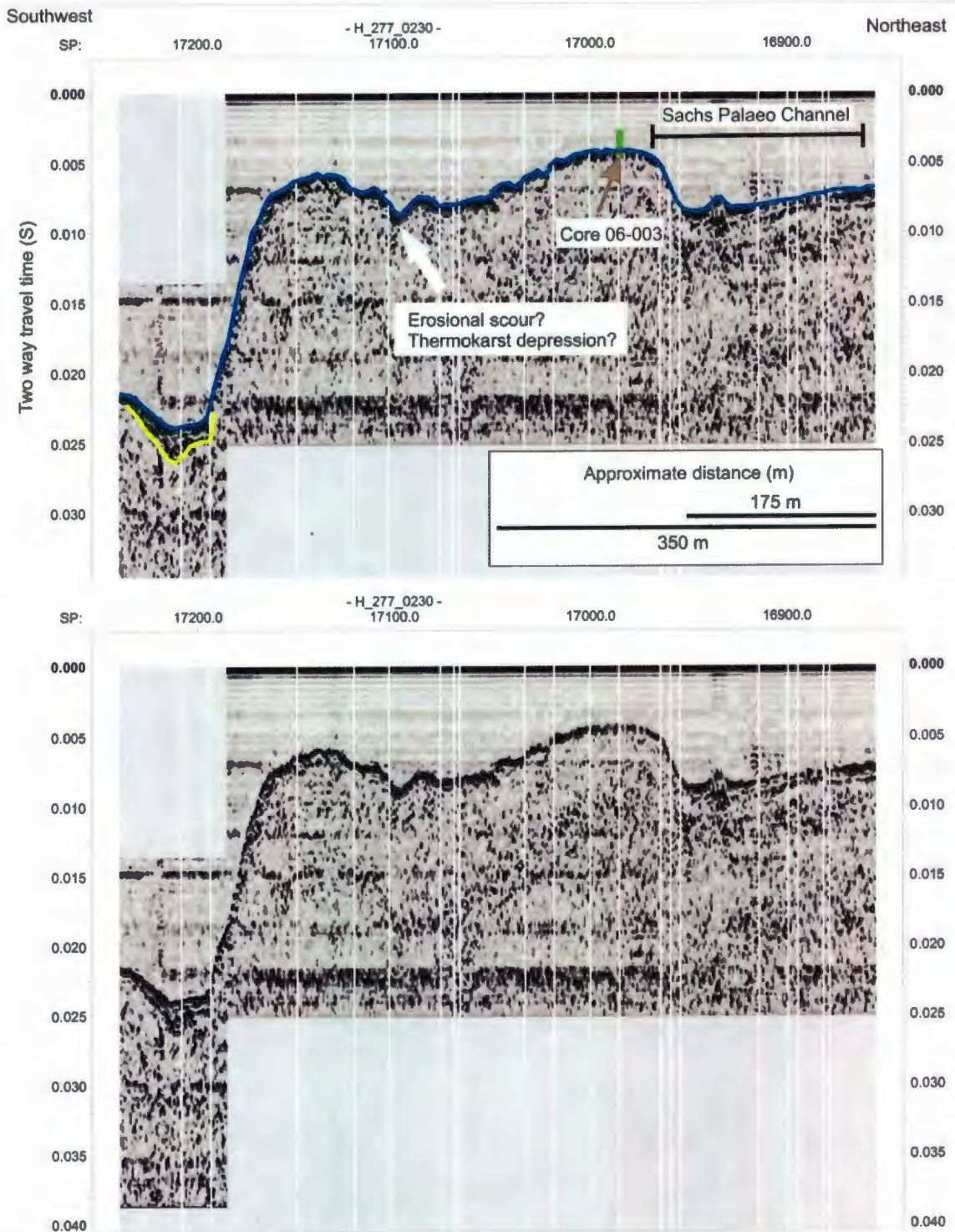
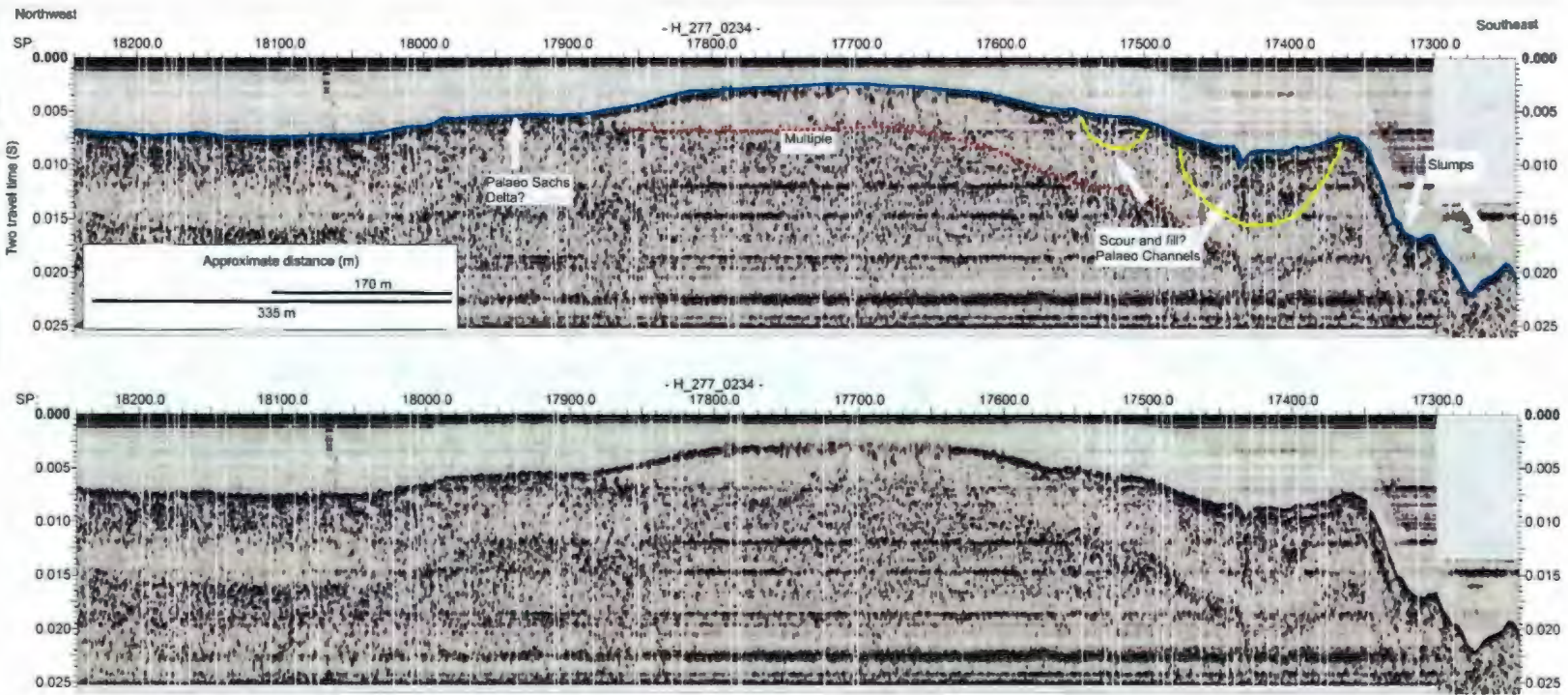


Figure B2. Seismic line 0230

Figure B3. Seismic line 0234



indicate that the original channels were regularly abandoned. Within the larger channel, there appears to be a thin pronounced unit that may be associated with sand found between two mud units within core 07-002. The northwestern section of the line slopes at a shallow angle onto a lower terrace. From its position, this terrace may be related to the outlet of the palaeo Sachs River, however, due to the angle and location of the line this can only be speculated.

#### **Line 0151**

Seismic line 0151 (Figure B4), taken in a southeast – northwest gradient is situated to the south and parallel to line 0234. The line was a total of 3.09 km in length and began near the outlet of the Mirabilite Basin, crossed the Inner Basin and Inner/Outer Basin sill (sill II), and terminated in the center of the Outer basin. The Inner Basin showed a very irregular floor with mounds as high as 15 m above the troughs, which is consistent with kettle holes as the melting of buried ice would cause gradual subsidence leaving an irregular surface (Benn and Evans 1998). The basin then rises abruptly to reach the top of the sill which appears acoustically impenetrable. The upper portion of the sill was interpreted as sand. The floors of the basins showed an acoustically stratified unit draping the basin floors and ponding in the troughs.

#### **Line 0249**

Seismic line 0249 (Figure B5), taken on a northeast – southwest gradient, was a total of 4.89 km in length and began in the eastern side of the Outer Basin, crossed the outer sill near core 07-017, and proceeded seaward towards Thesiger Bay. As noted in the previous line, the Outer Basin floor showed irregularities and slight ponding of an acoustically stratified unit. As the basin floor rose abruptly along the steep sill slope where slumping appears to have occurred, sediment continues to drape the lower troughs with acoustically stratified sediment. Core 07-017, consisting of what appeared to be cyclospam like sediment, does not appear to have been affected by the slumping and is situated over an acoustically impenetrable surface. The sill top had a relatively short, flat section with a poor seismic return followed by a very long gradual slope towards the Thesiger Bay. The sediment appears to show slight acoustic stratification within the deeper water in the southern portion of the line and may indicate draping of sediment originating from the nearby spit.

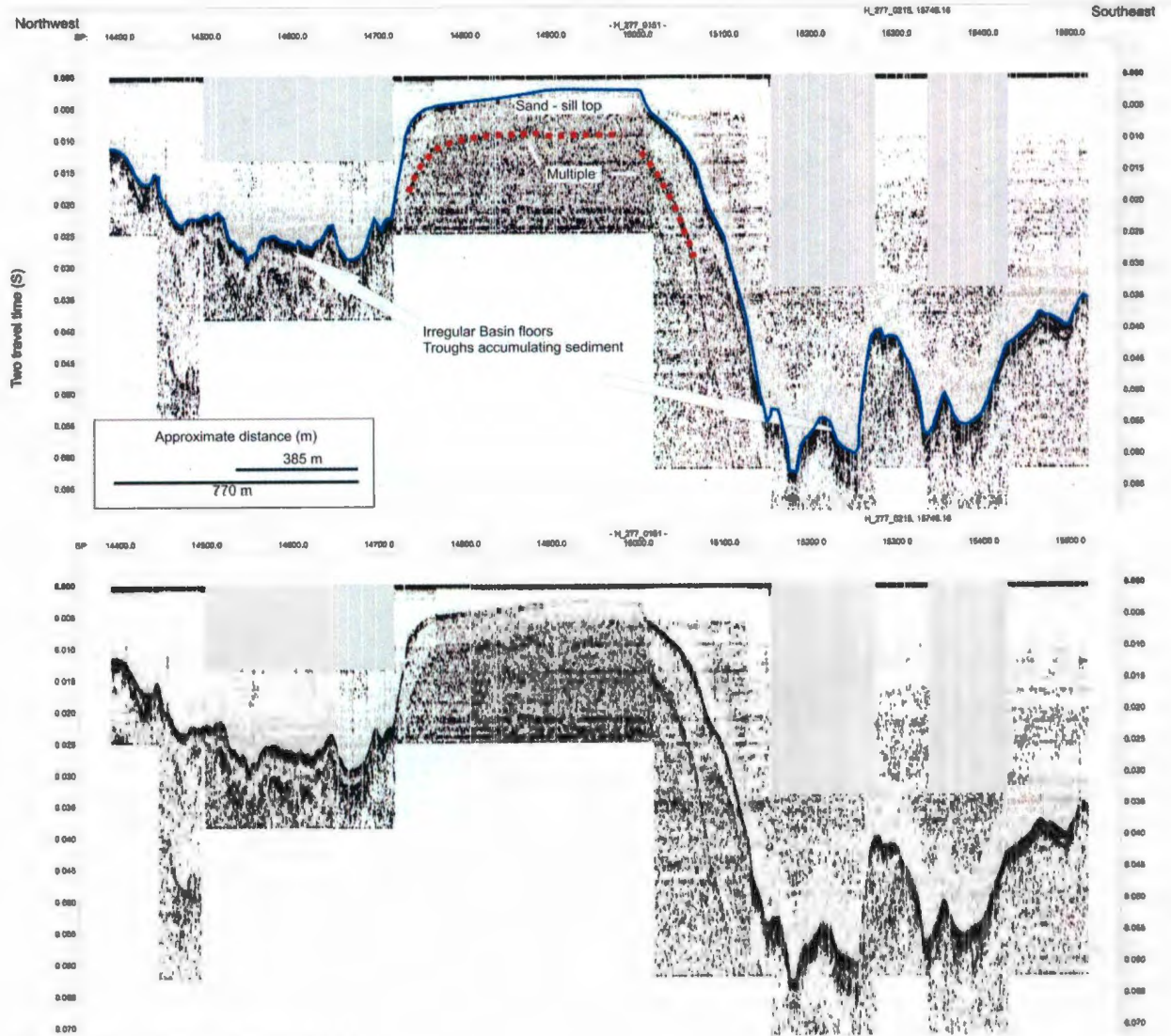


Figure B4. Seismic line 0151

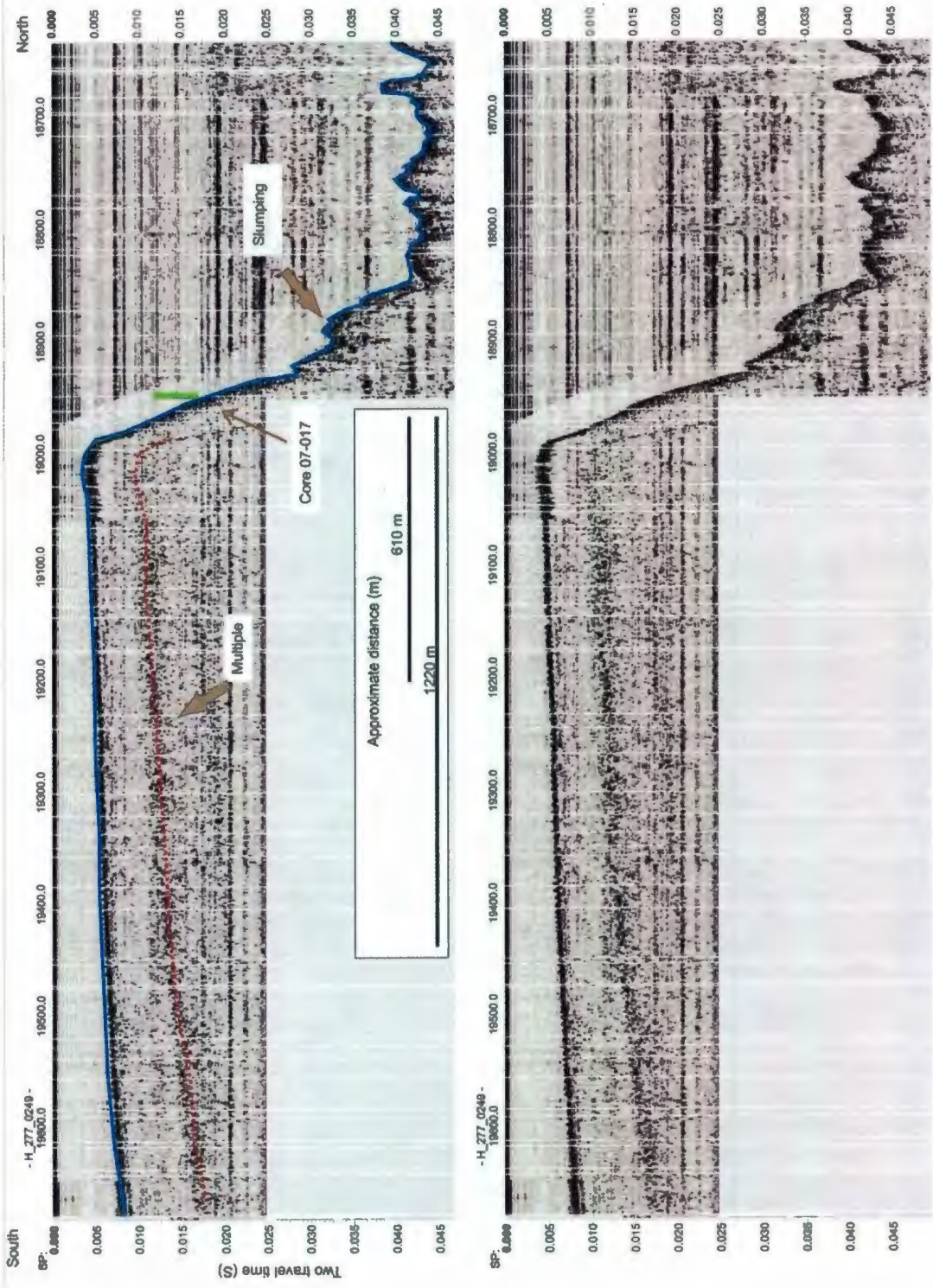


Figure B5. Seismic line 0249

Appendix C – Loss-on-ignition. All values are reported in grams

**core 2007-001**

<u>depth</u>	<u>crucible weight</u>	<u>sample + cru</u>	<u>cru + 550</u>	<u>cru + 950</u>	<u>sample weight</u>	<u>550 W</u>	<u>950 W</u>	<u>LOI 550</u>	<u>LOI 950</u>
5	19.3892	23.3967	22.9997	22.6742	4.0075	3.6105	3.2850	9.9064	8.1223
10	19.4641	23.2205	22.8557	22.5556	3.7564	3.3916	3.0915	9.7114	7.9890
15	19.7004	23.6982	23.2647	23.0515	3.9978	3.5643	3.3511	10.8435	5.3329
20	17.5475	20.3606	20.0603	19.9043	2.8131	2.5128	2.3568	10.6751	5.5455
25	18.0401	21.0505	20.7227	20.5677	3.0104	2.6826	2.5276	10.8889	5.1488
30	19.2684	22.3533	22.0200	21.8552	3.0849	2.7516	2.5868	10.8042	5.3422
35	10.6601	12.2841	12.1025	12.0544	1.6240	1.4424	1.3943	11.1823	2.9618
40	11.4929	14.2509	13.9553	13.8192	2.7580	2.4624	2.3263	10.7179	4.9347
45	12.1389	14.8984	14.6193	14.4405	2.7595	2.4804	2.3016	10.1142	6.4794
50	18.3831	20.9256	20.6272	20.5357	2.5425	2.2441	2.1526	11.7365	3.5988
55	29.5976	32.5872	32.2883	32.1299	2.9896	2.6907	2.5323	9.9980	5.2984
60	28.7408	31.3506	31.0735	30.9390	2.6098	2.3327	2.1982	10.6177	5.1537
65	19.4065	22.6848	22.3323	22.1651	3.2783	2.9258	2.7586	10.7525	5.1002
70	19.4853	22.3085	21.9762	21.8535	2.8232	2.4909	2.3682	11.7703	4.3461
73	19.7220	23.1891	22.8361	22.6352	3.4671	3.1141	2.9132	10.1814	5.7945
80	17.5701	21.3322	20.9977	20.8001	3.7621	3.4276	3.2300	8.8913	5.2524
86	18.0618	21.2976	21.0154	20.8586	3.2358	2.9536	2.7968	8.7212	4.8458
90	19.2921	22.6468	22.5143	22.4242	3.3547	3.2222	3.1321	3.9497	2.6858
95	10.6709	14.3188	14.2374	14.1549	3.6479	3.5665	3.4840	2.2314	2.2616
100	11.5068	15.8400	15.7364	15.6350	4.3332	4.2296	4.1282	2.3908	2.3401
105	12.1550	16.1749	16.0400	15.9373	4.0199	3.8850	3.7823	3.3558	2.5548

**core 2007-002**

<u>depth</u>	<u>crucible weight</u>	<u>sample + cru</u>	<u>cru + 550</u>	<u>cru + 950</u>	<u>sample weight</u>	<u>550 W</u>	<u>950 W</u>	<u>LOI 550</u>	<u>LOI 950</u>
5	12.2206	16.1273	15.7343	15.4704	3.9067	3.5137	3.2498	10.0596	6.7551
10	10.5832	14.8280	14.5342	14.2825	4.2448	3.9510	3.6993	6.9214	5.9296
15	11.9816	15.8029	15.5176	15.2752	3.8213	3.5360	3.2936	7.4660	6.3434
20	19.4216	22.4635	22.3370	22.2189	3.0419	2.9154	2.7973	4.1586	3.8824
25	19.4976	22.8112	22.6586	22.5254	3.3136	3.1610	3.0278	4.6053	4.0198
30	19.7337	23.0118	22.8458	22.7051	3.2781	3.1121	2.9714	5.0639	4.2921
35	17.5809	21.1260	20.8795	20.6765	3.5451	3.2986	3.0956	6.9533	5.7262
42	18.0721	20.3559	20.1758	20.0437	2.2838	2.1037	1.9716	7.8860	5.7842
48	19.3001	22.2765	22.0876	21.9151	2.9764	2.7875	2.6150	6.3466	5.7956
53	10.6748	14.5245	14.1556	13.9100	3.8497	3.4808	3.2352	9.5826	6.3797
60	11.5112	13.8411	13.6248	13.4697	2.3299	2.1136	1.9585	9.2837	6.6569
65	12.2336	15.3091	14.9896	14.7918	3.0755	2.7560	2.5582	10.3886	6.4315
70	10.5948	14.0998	13.7365	13.4851	3.5050	3.1417	2.8903	10.3652	7.1726
75	11.9947	15.1700	14.8406	14.6429	3.1753	2.8459	2.6482	10.3738	6.2262
80	19.4090	22.9584	22.5810	22.3562	3.5494	3.1720	2.9472	10.6328	6.3335
85	19.4884	23.2641	22.8483	22.6218	3.7757	3.3599	3.1334	11.0125	5.9989
90	19.7257	22.5185	22.2024	22.0335	2.7928	2.4767	2.3078	11.3184	6.0477
95	17.5769	21.2084	20.8117	20.5930	3.6315	3.2348	3.0161	10.9239	6.0223
100	18.0662	21.6877	21.2960	21.0614	3.6215	3.2298	2.9952	10.8160	6.4780
105	19.2968	23.3800	22.9524	22.6666	4.0832	3.6556	3.3698	10.4722	6.9994
110	10.6650	13.0246	12.7779	12.6139	2.3596	2.1129	1.9489	10.4552	6.9503

**core 2007-003**

<u>depth</u>	<u>crucible weight</u>	<u>sample + cru</u>	<u>cru + 550</u>	<u>cru + 950</u>	<u>sample weight</u>	<u>550 W</u>	<u>950 W</u>	<u>LOI 550</u>	<u>LOI 950</u>
5	12.1500	15.4342	15.2019	15.0336	3.2842	3.0519	2.8836	7.0733	5.1245
10	12.2240	15.1478	14.8752	14.6820	2.9238	2.6512	2.4580	9.3235	6.6078
15	10.5832	14.2611	13.9179	13.6552	3.6779	3.3347	3.0720	9.3314	7.1427

20	11.9848	16.0555	15.7101	15.4480	4.0707	3.7253	3.4632	8.4850	6.4387
25	19.4041	23.9458	23.5384	23.2833	4.5417	4.1343	3.8792	8.9702	5.6168
32	19.4832	23.1782	23.0563	22.8959	3.6950	3.5731	3.4127	3.2991	4.3410
40	19.7206	23.3809	23.2494	23.1225	3.6603	3.5288	3.4019	3.5926	3.4669
51	17.5712	20.4089	20.2570	20.1942	2.8377	2.6858	2.6230	5.3529	2.2131
59	19.2915	22.4912	22.3586	22.2532	3.1997	3.0671	2.9617	4.1441	3.2941
66	10.6675	14.2843	13.9564	13.7401	3.6168	3.2889	3.0726	9.0660	5.9804
69	11.5043	15.9590	15.7959	15.6632	4.4547	4.2916	4.1589	3.6613	2.9789
74	12.1526	16.0183	15.6460	15.4069	3.8657	3.4934	3.2543	9.6309	6.1852
80	12.2268	15.9871	15.7072	15.5063	3.7603	3.4804	3.2795	7.4436	5.3427
85	10.5871	14.6642	14.2743	13.9921	4.0771	3.6872	3.4050	9.5632	6.9216
90	11.9876	16.1908	15.7903	15.4902	4.2032	3.8027	3.5026	9.5285	7.1398
95	19.4187	22.7517	22.4402	22.1901	3.3330	3.0215	2.7714	9.3459	7.5038
105	19.7320	23.6464	23.2698	22.9923	3.9144	3.5378	3.2603	9.6209	7.0892

core 2007-004

<u>depth</u>	<u>crucible weight</u>	<u>sample + cru</u>	<u>cru + 550</u>	<u>cru + 950</u>	<u>sample weight</u>	<u>550 W</u>	<u>950 W</u>	<u>LOI 550</u>	<u>LOI 950</u>
5	17.5846	20.1713	19.8900	19.7401	2.5867	2.3054	2.1555	10.8749	5.7950
10	19.3037	21.2430	21.0272	20.9295	1.9393	1.7235	1.6258	11.1277	5.0379
15	10.6893	14.1311	13.7276	13.6013	3.4418	3.0383	2.9120	11.7235	3.6696
20	11.5250	14.8040	14.4557	14.3055	3.2790	2.9307	2.7805	10.6221	4.5807
25	12.1748	15.8504	15.4803	15.2455	3.6756	3.3055	3.0707	10.0691	6.3881
30	12.2490	15.6943	15.4327	15.2200	3.4453	3.1837	2.9710	7.5930	6.1736
35	10.6120	12.3951	12.2201	12.0952	1.7831	1.6081	1.4832	9.8144	7.0047
40	19.4344	21.8747	21.6702	21.4700	2.4403	2.2358	2.0356	8.3801	8.2039
45	19.5108	21.6351	21.4443	21.2595	2.1243	1.9335	1.7487	8.9818	8.6993
50	19.7500	22.5732	22.3500	22.1303	2.8232	2.6000	2.3803	7.9059	7.7819
55	18.0887	20.3724	20.2317	20.0731	2.2837	2.1430	1.9844	6.1611	6.9449
60	19.3180	21.1522	21.0258	20.9002	1.8342	1.7078	1.5822	6.8913	6.8477
65	10.6869	12.4603	12.2961	12.1869	1.7734	1.6092	1.5000	9.2591	6.1577

70	11.5220	14.5532	14.2943	14.1146	3.0312	2.7723	2.5926	8.5412	5.9283
75	12.1721	15.8109	15.5046	15.2960	3.6388	3.3325	3.1239	8.4176	5.7327
80	12.2452	13.8405	13.6562	13.5500	1.5953	1.4110	1.3048	11.5527	6.6571
85	12.0058	14.6211	14.3402	14.1501	2.6153	2.3344	2.1443	10.7406	7.2688
95	19.4312	22.5688	22.2314	21.9727	3.1376	2.8002	2.5415	10.7534	8.2452
100	19.5061	24.0168	23.5823	23.2378	4.5107	4.0762	3.7317	9.6327	7.6374
105	19.7445	22.9227	22.6708	22.4380	3.1782	2.9263	2.6935	7.9259	7.3249
110	17.5912	21.0566	20.8400	20.6527	3.4654	3.2488	3.0615	6.2504	5.4049
115	18.0810	21.2505	21.0027	20.7691	3.1695	2.9217	2.6881	7.8183	7.3702
120	19.3109	23.3852	23.0642	22.7585	4.0743	3.7533	3.4476	7.8787	7.5031
125	10.6975	14.5769	14.3441	14.1221	3.8794	3.6466	3.4246	6.0009	5.7225
130	11.5327	15.5032	15.1824	14.8929	3.9705	3.6497	3.3602	8.0796	7.2913
135	12.1828	16.0955	15.6714	15.3121	3.9127	3.4886	3.1293	10.8391	9.1829
140	12.2553	15.3470	15.0565	14.8173	3.0917	2.8012	2.5620	9.3961	7.7368
145	12.0166	15.7520	15.4173	15.1185	3.7354	3.4007	3.1019	8.9602	7.9991
150	19.4369	21.6957	21.4730	21.3036	2.2588	2.0361	1.8667	9.8592	7.4996
155	19.5125	21.9386			2.4261				
160	19.7495	22.0663	21.8367	21.7200	2.3168	2.0872	1.9705	9.9102	5.0371
165	10.7376	11.9000	11.8335	11.7975	1.1624	1.0959	1.0599	5.7209	3.0970
170									
175	11.5753	11.9000	11.8335	11.7975	0.3247				

core 2007-005

<u>depth</u>	<u>crucible weight</u>	<u>sample + cru</u>	<u>cru + 550</u>	<u>cru + 950</u>	<u>sample weight</u>	<u>550 W</u>	<u>950 W</u>	<u>LOI 550</u>	<u>LOI 950</u>
5	10.6980	12.5274	12.3356	12.2305	1.8294	1.6376	1.5325	10.4843	5.7451
10	12.1868	14.8892	14.5745	14.4352	2.7024	2.3877	2.2484	11.6452	5.1547
15	12.2580	14.5890	14.2875	14.2115	2.3310	2.0295	1.9535	12.9344	3.2604
20	10.6186	14.1252	13.7254	13.5814	3.5066	3.1068	2.9628	11.4014	4.1065
25	12.0199	14.4235	14.1135	14.0579	2.4036	2.0936	2.0380	12.8973	2.3132
30	19.4460	21.5300	21.2413	21.2030	2.0840	1.7953	1.7570	13.8532	1.8378

35	19.5207	21.6711	21.4080	21.3328	2.1504	1.8873	1.8121	12.2349	3.4970
40	19.7565	22.1583	21.8627	21.7681	2.4018	2.1062	2.0116	12.3074	3.9387
45	17.6040	20.2461	19.9257	19.8202	2.6421	2.3217	2.2162	12.1267	3.9930
50	18.0922	20.9683	20.6333	20.5024	2.8761	2.5411	2.4102	11.6477	4.5513
55	10.6997	13.8562	13.4857	13.3670	3.1565	2.7860	2.6673	11.7377	3.7605
60	11.5344	16.2448	15.7783	15.5322	4.7104	4.2439	3.9978	9.9036	5.2246
65	12.1860	15.9932	15.6296	15.4360	3.8072	3.4436	3.2500	9.5503	5.0851

core 2007-006

<u>depth</u>	<u>crucible weight</u>	<u>sample + cru</u>	<u>cru + 550</u>	<u>cru + 950</u>	<u>sample weight</u>	<u>550 W</u>	<u>950 W</u>	<u>LOI 550</u>	<u>LOI 950</u>
5	12.2559	15.0245	14.7283	14.5738	2.7686	2.4724	2.3179	10.6985	5.5804
10	10.6150	13.8667	13.5344	13.3413	3.2517	2.9194	2.7263	10.2193	5.9384
15	12.0180	15.8445	15.4968	15.2550	3.8265	3.4788	3.2370	9.0866	6.3191
20	19.4500	23.0156	22.7009	22.5240	3.5656	3.2509	3.0740	8.8260	4.9613
26	19.5274	21.6375	21.4182	21.2806	2.1101	1.8908	1.7532	10.3929	6.5210
30	17.6100	21.4514	21.1360	20.9322	3.8414	3.5260	3.3222	8.2105	5.3054
35	18.0977	21.2694	21.0234	20.8485	3.1717	2.9257	2.7508	7.7561	5.5144
40	18.4265	22.0455	21.7664	21.5723	3.6190	3.3399	3.1458	7.7121	5.3634
45	10.7083	14.2157	13.9485	13.6719	3.5074	3.2402	2.9636	7.6182	7.8862
50	11.5451	14.3028	14.0794	13.8663	2.7577	2.5343	2.3212	8.1010	7.7275
55	12.2677	16.0165	15.7456	15.5066	3.7488	3.4779	3.2389	7.2263	6.3754
60	10.6266	14.7023	14.4152	14.1446	4.0757	3.7886	3.5180	7.0442	6.6394
65	12.0294	14.0786	13.9211	13.7795	2.0492	1.8917	1.7501	7.6859	6.9100
70	19.4622	21.9970	21.7474	21.6006	2.5348	2.2852	2.1384	9.8469	5.7914
75	19.5381	23.5623	23.2194	22.9803	4.0242	3.6813	3.4422	8.5209	5.9416
80	19.7735	22.7686	22.4998	22.3229	2.9951	2.7263	2.5494	8.9747	5.9063

**core 2007-007**

<u>depth</u>	<u>crucible weight</u>	<u>sample + cru</u>	<u>cru + 550</u>	<u>cru + 950</u>	<u>sample weight</u>	<u>550 W</u>	<u>950 W</u>	<u>LOI 550</u>	<u>LOI 950</u>
5	17.6195	21.9043	21.4403	21.1587	4.2848	3.8208	3.5392	10.8290	6.5721
12	18.1091	20.4037	20.1783	19.9958	2.2946	2.0692	1.8867	9.8231	7.9535
15	10.7163	13.7831	13.4743	13.2006	3.0668	2.7580	2.4843	10.0691	8.9246
20	11.5531	15.6853	15.3268	15.0290	4.1322	3.7737	3.4759	8.6758	7.2068
25	12.2065	16.4773	16.0210	15.6478	4.2708	3.8145	3.4413	10.6842	8.7384
30	12.2771	16.1384	15.7664	15.4807	3.8613	3.4893	3.2036	9.6341	7.3991
35	10.6363	14.4934	14.1224	13.8050	3.8571	3.4861	3.1687	9.6186	8.2290
39	12.0376	15.2115	14.8695	14.5713	3.1739	2.8319	2.5337	10.7754	9.3954
45	19.4700	23.6457	23.2060	22.8652	4.1757	3.7360	3.3952	10.5300	8.1615
50	19.5392	23.8004	23.3756	23.0705	4.2612	3.8364	3.5313	9.9690	7.1600
55	17.6313	22.5181	21.9252	21.6356	4.8868	4.2939	4.0043	12.1327	5.9262
60	18.1149	20.3410	20.1317	19.9902	2.2261	2.0168	1.8753	9.4021	6.3564

**core 2007-009**

<u>depth</u>	<u>crucible weight</u>	<u>sample + cru</u>	<u>cru + 550</u>	<u>cru + 950</u>	<u>sample weight</u>	<u>550 W</u>	<u>950 W</u>	<u>LOI 550</u>	<u>LOI 950</u>
15	10.7154	16.2607	15.8726	15.4215	5.5453	5.1572	4.7061	6.9987	8.1348
25	11.5526	16.8746	16.4683	16.0329	5.3220	4.9157	4.4803	7.6343	8.1811
30	12.2067	17.8438	17.3625	16.9037	5.6371	5.1558	4.6970	8.5381	8.1389
35	12.2784	15.7159	15.4456	15.2168	3.4375	3.1672	2.9384	7.8633	6.6560

**core 2007-013**

<u>depth</u>	<u>crucible weight</u>	<u>sample + cru</u>	<u>cru + 550</u>	<u>cru + 950</u>	<u>sample weight</u>	<u>550 W</u>	<u>950 W</u>	<u>LOI 550</u>	<u>LOI 950</u>
5	10.6378	14.9099	14.6503	14.2593	4.2721	4.0125	3.6215	6.0766	9.1524
10	12.0403	15.9025	15.6171	15.2771	3.8622	3.5768	3.2368	7.3896	8.8033
15	19.4735	22.8270	22.5465	22.2775	3.3535	3.0730	2.8040	8.3644	8.0215
20	19.5408	22.8134	22.5589	22.3096	3.2726	3.0181	2.7688	7.7767	7.6178

25	19.7780	21.5722	21.4348	21.3230	1.7942	1.6568	1.5450	7.6580	6.2312
31	18.1136	21.1003	20.8796	20.6695	2.9867	2.7660	2.5559	7.3894	7.0345
35	18.4436	21.8395	21.5560	21.2923	3.3959	3.1124	2.8487	8.3483	7.7652
40	10.7202	13.5203	13.3020	13.0738	2.8001	2.5818	2.3536	7.7962	8.1497
45	11.5563	14.7159	14.4641	14.2076	3.1596	2.9078	2.6513	7.9694	8.1181
50	12.2091	15.3579	15.0789	14.8534	3.1488	2.8698	2.6443	8.8605	7.1615
55	10.6370	13.7897	13.4977	13.1595	3.1527	2.8607	2.5225	9.2619	10.7273
60	12.0407	15.2405	14.9865	14.7220	3.1998	2.9458	2.6813	7.9380	8.2661
65	19.4720	21.1770	21.0539	20.9456	1.7050	1.5819	1.4736	7.2199	6.3519
70	19.7772	23.5371	23.1937	22.9351	3.7599	3.4165	3.1579	9.1332	6.8778
76	17.6334	20.6573	20.3947	20.2007	3.0239	2.7613	2.5673	8.6841	6.4156
80	18.1130	21.1698	20.9208	20.6897	3.0568	2.8078	2.5767	8.1458	7.5602
84	18.4427	21.1041	20.8448	20.6237	2.6614	2.4021	2.1810	9.7430	8.3077
91	10.7225	14.9195	14.5880	14.2328	4.1970	3.8655	3.5103	7.8985	8.4632
95	11.5576	14.8870	14.6194	14.3339	3.3294	3.0618	2.7763	8.0375	8.5751
99	12.2816	14.4239	14.2005	13.9930	2.1423	1.9189	1.7114	10.4280	9.6859
105	10.6379	14.0544	13.7405	13.3367	3.4165	3.1026	2.6988	9.1878	11.8191
110	12.0424	15.3186	15.0336	14.7011	3.2762	2.9912	2.6587	8.6991	10.1490
115	19.4695	22.1379	21.8887	21.6834	2.6684	2.4192	2.2139	9.3389	7.6937
117	19.5371	21.2875	21.1174	20.9565	1.7504	1.5803	1.4194	9.7178	9.1922

core 2007-014

<u>depth</u>	<u>crucible weight</u>	<u>sample + cru</u>	<u>cru + 550</u>	<u>cru + 950</u>	<u>sample weight</u>	<u>550 W</u>	<u>950 W</u>	<u>LOI 550</u>	<u>LOI 950</u>
5	17.6318	20.8245	20.4443	20.2721	3.1927	2.8125	2.6403	11.9084	5.3936
10	18.1115	20.8115	20.4948	20.3550	2.7000	2.3833	2.2435	11.7296	5.1778
15	18.4410	19.8319	19.6548	19.5970	1.3909	1.2138	1.1560	12.7328	4.1556
20	10.7178	12.6355	12.4394	12.3274	1.9177	1.7216	1.6096	10.2258	5.8403
25	11.5529	15.4624	15.1268	14.8873	3.9095	3.5739	3.3344	8.5842	6.1261
30	12.2065	15.9324	15.7319	15.5893	3.7259	3.5254	3.3828	5.3813	3.8273
35	12.2769	15.3079	15.1527	15.0457	3.0310	2.8758	2.7688	5.1204	3.5302

40	10.6336	15.2461	15.0054	14.7997	4.6125	4.3718	4.1661	5.2184	4.4596
45	12.0376	16.3240	16.0375	15.8243	4.2864	3.9999	3.7867	6.6839	4.9739
50	19.4682	24.1969	23.8709	23.6250	4.7287	4.4027	4.1568	6.8941	5.2002
55	19.7760	23.0166	22.7106	22.5163	3.2406	2.9346	2.7403	9.4427	5.9958
59	17.6312	20.4476	20.1925	20.0157	2.8164	2.5613	2.3845	9.0577	6.2775

core 2007-017

<u>depth</u>	<u>crucible weight</u>	<u>sample + cru</u>	<u>cru + 550</u>	<u>cru + 950</u>	<u>sample weight</u>	<u>550 W</u>	<u>950 W</u>	<u>LOI 550</u>	<u>LOI 950</u>
5	18.4392	22.8529	22.4045	22.0691	4.4137	3.9653	3.6299	10.1593	7.5991
10	10.7176	14.4527	14.1356	13.8124	3.7351	3.4180	3.0948	8.4897	8.6530
15	11.5536	14.8853	14.5973	14.3021	3.3317	3.0437	2.7485	8.6442	8.8603
20	12.2068	15.9439	15.5976	15.2979	3.7371	3.3908	3.0911	9.2665	8.0196
25	12.2786	16.2092	15.8533	15.5291	3.9306	3.5747	3.2505	9.0546	8.2481
30	10.6356	14.1514	13.8819	13.6212	3.5158	3.2463	2.9856	7.6654	7.4151
35	12.0398	16.0175	15.7556	15.5036	3.9777	3.7158	3.4638	6.5842	6.3353
41	19.4722	22.7710	22.4223	22.2325	3.2988	2.9501	2.7603	10.5705	5.7536
45	19.5414	21.6394	21.4106	21.3070	2.0980	1.8692	1.7656	10.9056	4.9380
50	18.1145	20.6122	20.3946	20.2443	2.4977	2.2801	2.1298	8.7120	6.0175
52	18.4450	21.3992	21.0763	20.9083	2.9542	2.6313	2.4633	10.9302	5.6868
55	10.7239	14.0490	13.8077	13.5942	3.3251	3.0838	2.8703	7.2569	6.4209
60	11.5593	15.4029	15.1203	14.8792	3.8436	3.5610	3.3199	7.3525	6.2728

core 2006-003

<u>depth</u>	<u>crucible weight</u>	<u>sample + cru</u>	<u>cru + 550</u>	<u>cru + 950</u>	<u>sample weight</u>	<u>550 W</u>	<u>950 W</u>	<u>LOI 550</u>	<u>LOI 950</u>
10	12.2142	14.4809	14.2834	14.1807	2.2667	2.0692	1.9665	8.7131	4.5308
15	12.2851	14.5664	14.3772	14.2711	2.2813	2.0921	1.9860	8.2935	4.6509
20	10.6419	13.7883	13.5845	13.4127	3.1464	2.9426	2.7708	6.4772	5.4602
25	12.0470	15.6603	15.4717	15.3039	3.6133	3.4247	3.2569	5.2196	4.6440
30	19.4764	23.1910	22.9701	22.8174	3.7146	3.4937	3.3410	5.9468	4.1108
35	19.5448	22.9189	22.7114	22.5742	3.3741	3.1666	3.0294	6.1498	4.0663
40	19.7848	22.5709	22.3450	22.2565	2.7861	2.5602	2.4717	8.1081	3.1765
45	17.6407	20.5263	20.2956	20.2155	2.8856	2.6549	2.5748	7.9949	2.7759
50	18.1180	19.7766	19.6532	19.5875	1.6586	1.5352	1.4695	7.4400	3.9612
55	10.7285	13.3197	13.1640	13.0506	2.5912	2.4355	2.3221	6.0088	4.3764
60	12.2169	14.4910	14.3256	14.2291	2.2741	2.1087	2.0122	7.2732	4.2434
65	12.2886	15.1426	14.9177	14.7963	2.8540	2.6291	2.5077	7.8802	4.2537
70	10.6449	13.3825	13.2087	13.0749	2.7376	2.5638	2.4300	6.3486	4.8875
75	12.0501	16.1587	15.8863	15.6759	4.1086	3.8362	3.6258	6.6300	5.1210
80	19.4715	23.0880	22.8087	22.6819	3.6165	3.3372	3.2104	7.7229	3.5062
85	19.5398	22.8693	22.6695	22.5687	3.3295	3.1297	3.0289	6.0009	3.0275
90	19.7809	23.6676	23.3917	23.2690	3.8867	3.6108	3.4881	7.0986	3.1569
95	17.6366	21.6843	21.3812	21.2626	4.0477	3.7446	3.6260	7.4882	2.9301

core 2006-004

<u>depth</u>	<u>crucible weight</u>	<u>sample + cru</u>	<u>cru + 550</u>	<u>cru + 950</u>	<u>sample weight</u>	<u>550 W</u>	<u>950 W</u>	<u>LOI 550</u>	<u>LOI 950</u>
5	18.1142	20.4592	20.2513	20.0789	2.3450	2.1371	1.9647	8.8657	7.3518
10	10.7193	13.7927	13.5119	13.2146	3.0734	2.7926	2.4953	9.1365	9.6733
15	11.5551	14.0521	13.8073	13.5420	2.4970	2.2522	1.9869	9.8038	10.6247
20	12.2079	14.2198	14.0308	13.8570	2.0119	1.8229	1.6491	9.3941	8.6386
25	12.2794	15.2001	14.9059	14.6491	2.9207	2.6265	2.3697	10.0729	8.7924
30	10.6350	13.0366	12.8238	12.5579	2.4016	2.1888	1.9229	8.8608	11.0718

<b>35</b>	12.0414	13.7908	13.6190	13.4491	1.7494	1.5776	1.4077	9.8205	9.7119
<b>40</b>	19.4685	22.0101	21.7530	21.5377	2.5416	2.2845	2.0692	10.1157	8.4710
<b>45</b>	19.5353	23.2776	22.8872	22.5774	3.7423	3.3519	3.0421	10.4321	8.2783
<b>50</b>	19.7767	22.8707	22.5708	22.3476	3.0940	2.7941	2.5709	9.6930	7.2140
<b>55</b>	18.1103	20.6602	20.4902	20.3249	2.5499	2.3799	2.2146	6.6669	6.4826
<b>60</b>	10.7183	14.3868	14.0710	13.6996	3.6685	3.3527	2.9813	8.6084	10.1240
<b>65</b>	11.5547	14.8425	14.5175	14.1838	3.2878	2.9628	2.6291	9.8850	10.1496
<b>70</b>	12.2074	14.2722	14.0600	13.8685	2.0648	1.8526	1.6611	10.2770	9.2745
<b>75</b>	12.2793	15.5486	15.1980	14.9017	3.2693	2.9187	2.6224	10.7240	9.0631
<b>79</b>	10.6343	13.6076	13.4065	13.2385	2.9733	2.7722	2.6042	6.7635	5.6503
<b>90</b>	12.0404	16.5071	16.1959	15.8837	4.4667	4.1555	3.8433	6.9671	6.9895
<b>95</b>	19.4705	22.7490	22.5250	22.3418	3.2785	3.0545	2.8713	6.8324	5.5879
<b>100</b>	19.5385	23.4220	23.1551	22.9430	3.8835	3.6166	3.4045	6.8727	5.4616
<b>105</b>	19.7792	22.2022	21.9394	21.7721	2.4230	2.1602	1.9929	10.8461	6.9047
<b>110</b>	18.1112	20.7546	20.5276	20.3297	2.6434	2.4164	2.2185	8.5874	7.4866
<b>115</b>	18.4404	21.0098	20.7068	20.4875	2.5694	2.2664	2.0471	11.7926	8.5351
<b>120</b>	10.7210	13.8520	13.5556	13.2119	3.1310	2.8346	2.4909	9.4666	10.9773
<b>125</b>	11.5586	14.2828	14.0373	13.7226	2.7242	2.4787	2.1640	9.0118	11.5520
<b>130</b>	12.2105	14.9311	14.7120	14.4923	2.7206	2.5015	2.2818	8.0534	8.0754
<b>135</b>	12.2838	15.0843	14.8075	14.5465	2.8005	2.5237	2.2627	9.8839	9.3198
<b>140</b>	10.6366	12.8353	12.6609	12.4809	2.1987	2.0243	1.8443	7.9320	8.1867
<b>145</b>	12.0433	14.8069	14.5863	14.3574	2.7636	2.5430	2.3141	7.9823	8.2827

Appendix D – Grain size analysis. All values are reported in grams.

**core 2007-001**

sample#	sample weight	4000 um	2000 um	1000 um	500 um	250 um	125 um	63 um	Mud
10	10.3396	0.0786	0	0	0.0518	0.0946	0.7053	4.2098	5.1995
20	8.7587	0	0	0	0.0657	0.1741	0.7092	4.8689	2.9408
30	9.8333	0	0	0	0.0436	0.1887	0.7898	4.268	4.5432
35	6.7985	0	0	0	0.0248	0.1317	0.4826	2.1931	3.9663
50	9.1108	0	0	0	0.0376	0.0848	0.3387	3.0513	5.5984
60	10.0831	0	0	0	0.0182	0.2358	0.7679	3.5617	5.7481
70	10.0563	0	0	0	0.0703	0.1603	0.7401	4.065	5.2778
73	12.7292	0.0852	0	0	0.0876	0.1725	1.117	7.0511	4.6894
86	10.9266	0	0	0	0.8638	1.9084	2.7393	3.4173	2.1705
90	13.0075	0	0.3624	0	5.1858	4.9778	1.1757	0.5436	0.8178
97	16.5681	0	0.2557	0	8.8465	6.3282	0.7737	0.1738	0.1902

**core 07-002**

sample#	sample weight	4000 um	2000 um	1000um	500 um	250 um	125 um	63 um	mud
10	14.2838	0	0	0	0.1835	1.8262	2.1579	4.5095	5.6067
20	14.4075	0	0.673	0	1.1786	8.7214	3.5978	0.1036	0.1331
30	15.7652	0	0	0	0.0423	5.4874	9.6237	0.4498	0.162
39	10.3815	0	0	0	0.1954	0.8003	7.4235	1.6039	0.3584
42	12.3698	0	0	0.006	0.0489	0.7313	5.3919	4.0126	2.1791
48	11.0696	0	0	0.0008	0.0458	1.8154	7.7223	1.1423	0.343
53	9.216	0	0	0.0063	0.0245	0.16	0.5449	4.7199	3.7604
60	11.1096	0	0	0.0094	0.0247	0.1787	2.2384	6.0023	2.6561
70	12.8959	0	0	0	0.009	0.055	0.863	7.5069	4.462
80	11.7285	0	0	0	0.0159	0.1265	0.3763	5.6232	5.5866
90	11.6193	0	0	0	0.0161	0.0579	0.2763	5.5253	5.7437

100	11.3139	0	0	0	0.015	0.0964	0.7824	5.2698	5.1503
110	12.1223	0	0	0	0.0109	0.0793	1.0755	6.1708	4.7858

**Core 07-003**

sample#	sample weight	4000 um	2000 um	1000um	500 um	250 um	125 um	63 um	mud
10	12.3507	0	0	0.0192	0.0244	0.3863	3.9184	6.8559	1.1465
20	13.0233	0	0	0.1046	0.221	1.4466	1.1863	6.0214	4.0434
28	16.7741	0.3319	0.1451	0.3523	0.8813	3.4404	2.8887	4.6036	4.1308
32	16.738	0.2589	1.1135	1.4859	2.3447	6.4115	4.3973	0.5321	0.1941
40	19.2305	1.1969	0.9846	2.1747	2.77	8.0149	3.1196	0.6691	0.3007
48	22.2228	0.0853	1.1609	5.9891	4.9591	3.7598	3.7913	1.6518	0.8255
51	21.2191	0	0.1441	1.2701	2.6459	13.9716	2.3306	0.4013	0.4555
59	16.5892	0	0.0979	0.0828	0.566	11.783	2.3566	0.981	0.7219
66	11.7391	0	0.0326	0.0539	0.1546	0.688	1.0871	3.6022	6.1207
68	13.6722	0	0.1026	0.5495	1.8304	8.1276	2.4572	0.4061	0.1988
74	11.7573	0	0.0147	0.0113	0.0875	1.7815	2.1278	3.0617	4.6728
80	11.791	0	0	0	0.0158	0.2162	2.6313	7.2259	1.7018
90	11.7564	0	0	0	0.0128	0.1265	1.5872	8.6071	1.4228
105	8.1766	0	0	0	0	0.2315	3.7974	3.3273	0.8204

**Core 07-004**

sample#	sample weight	4000 um	2000 um	1000um	500 um	250 um	125 um	63 um	mud
10	3.8967	0	0	0	0.009	0.0643	0.2351	0.7437	2.8446
20	9.9776	0	0	0	0.0548	0.6776	1.595	2.9489	4.7013
30	13.0752	0	0.2532	0.0267	0.1354	2.3858	5.3686	3.66	1.2455
40	12.1021	0	0	0	0.0052	0.0729	6.4334	5.1067	0.4839
50	9.8404	0	0	0	0.0016	0.3463	6.2525	3.0017	0.2383

60	10.1316	0	0	0	0.0024	0.3078	6.2643	2.9886	0.5685
70	11.9774	0	0	0	0.0005	0.3995	7.303	3.7051	0.5693
80	13.0287	0	0	0	0.0003	0.2057	5.1899	6.2548	1.378
90	9.44	0	0	0	0	0.0049	0.1944	5.0003	4.2404
100	8.5359	0	0	0	0	0.0107	0.2007	3.7281	4.5964
105	8.5444	0	0	0	0.0121	1.0586	6.7365	0.4874	0.2498
115	8.737	0	0	0	0.0071	0.7665	6.7935	0.8161	0.3538
130	9.6005	0	0	0	0.0216	1.0478	6.7492	1.147	0.6349
135	8.5967	0	0	0	0	0.0074	0.2144	5.8572	2.5177
145	8.7717	0	0	0.0168	0.0385	0.3327	0.2296	5.6271	2.527
150	9.2134	0	0	0	0.0213	0.7598	1.0625	5.6811	1.6887
155	9.7646	0	0	0	0.0131	0.0647	0.2595	6.0568	3.3705
165	8.872	0	0	0	0.0326	5.4697	2.9142	0.342	0.1135
175	11.4894	0	0	0	0.0495	3.708	6.8816	0.6696	0.1807

Core 07-005

<u>sample#</u>	<u>sample weight</u>	<u>4000 um</u>	<u>2000 um</u>	<u>1000um</u>	<u>500 um</u>	<u>250 um</u>	<u>125 um</u>	<u>63 um</u>	<u>mud</u>
5	7.6045	0	0	0	0.0787	0.2882	0.2911	1.5607	5.3858
15	6.7102	0	0	0	0.0387	0.1602	0.2399	0.9837	5.2877
25	5.8069	0	0	0	0.0212	0.0584	0.1167	0.835	4.7756
30	4.5245	0	0	0	0.0349	0.1054	0.114	0.6283	3.6419
35	8.2484	0	0	0	0.054	0.218	0.2004	1.3119	6.4641
45	8.4546	0	0	0	0.0509	0.2296	0.2432	1.3821	6.5488
55	8.2597	0	0	0	0.0463	0.1284	0.2892	1.6714	6.1244
65	9.7056	0	0	0.0118	0.089	0.865	1.9046	3.0352	3.8

**Core 07-006**

<u>sample#</u>	<u>sample weight</u>	<u>4000 um</u>	<u>2000 um</u>	<u>1000um</u>	<u>500 um</u>	<u>250 um</u>	<u>125 um</u>	<u>63 um</u>	<u>Mud</u>
5	8.6305	0	0	0	0.0356	0.1491	0.6488	3.8442	3.9528
15	8.9449	0	0	0	0.0338	0.3362	2.1173	4.3015	2.1561
20	8.2002	0	0	0	0.0416	0.9857	3.6063	2.4473	1.1193
25	8.5237	0	0	0.0171	0.0337	0.3658	2.171	3.9324	2.0037
30	11.2355	0	0	0	0.0743	1.8489	6.3755	2.1781	0.7587
32	8.8933	0	0	0	0.0503	1.7223	5.4421	1.2662	0.4124
35	10.1484	0	0	0	0.0315	1.4977	5.5108	2.1181	0.9903
40	10.0212	0	0	0	0.0525	2.0162	4.6349	2.1404	1.1772
41	12.9232	0	0	0	0.012	0.9611	6.9082	3.0774	1.9645
50	8.0964	0	0	0	0.0068	0.2281	3.6338	3.4816	0.7461
55	12.698	0	0	0.0059	0.035	2.1187	6.9413	2.6692	0.9279
65	13.4472	0	0	0	0.0174	1.4145	6.9197	3.293	1.8026

**Core 07-007**

<u>sample#</u>	<u>sample weight</u>	<u>4000 um</u>	<u>2000 um</u>	<u>1000 um</u>	<u>500 um</u>	<u>250 um</u>	<u>125 um</u>	<u>63 um</u>	<u>mud</u>
5	12.3812	0	0	0	0.0376	0.4575	3.7607	5.2659	2.8595
15	13.4142	0	0	0	0.0099	0.131	4.5217	7.5516	1.2
25	14.1999	0	0	0	0.007	0.4671	5.2649	6.0596	2.4013
35	14.4112	0	0	0	0.0054	0.1559	4.8521	6.7993	2.5985
45	10.8089	0	0	0	0.0024	0.0155	0.2388	6.5589	3.9933
55	11.6819	0	0	0	0.0025	0.0342	0.3917	3.517	7.7365

**Core 07-009**

<u>sample#</u>	<u>sample weight</u>	<u>4000 um</u>	<u>2000 um</u>	<u>1000um</u>	<u>500 um</u>	<u>250 um</u>	<u>125 um</u>	<u>63 um</u>	<u>mud</u>
15	10.6326	0	0	0.1156	0.1739	1.4904	4.7346	3.6481	0.47
25	11.9632	0	0	0.0344	0.0301	0.5582	4.5509	5.8289	0.9607
30	11.748	0	0	0.0029	0.0513	0.8488	3.3275	6.3302	1.1873
41	8.6981	0	0	0.0143	0.0523	0.8876	1.8466	3.9172	1.9801

**Core 07-013**

<u>sample#</u>	<u>sample weight</u>	<u>4000 um</u>	<u>2000 um</u>	<u>1000 um</u>	<u>500 um</u>	<u>250 um</u>	<u>125 um</u>	<u>63 um</u>	<u>mud</u>
5	11.2815	0	0	0	0.0096	0.756	4.7687	4.5677	1.1795
15	11.2531	0	0	0	0.0139	0.8185	6.2285	3.3509	0.8413
25	11.4562	0	0	0	0.0681	1.1696	7.9474	1.8005	0.4706
35	10.3793	0	0	0	0.0332	0.8658	5.6049	3.0432	0.8322
40	11.1868	0	0	0	0.0051	0.1091	3.0557	5.8238	2.1931
50	11.9216	0	0	0	0.0415	0.7389	3.845	5.402	1.8942
55	11.1989	0	0	0	0	0.0878	2.9703	6.1405	2.0003
60	12.374	0	0	0	0.0122	0.9346	5.68	4.2511	1.4961
70	12.7517	0	0	0	0.0326	0.603	5.0688	5.4051	1.6422
80	11.5159	0	0	0	0.0061	0.1004	6.5893	3.6749	1.1452
85	11.6769	0	0	0	0	0.0083	0.0429	4.2176	7.4081
91	12.6191	0	0	0	0.0691	0.8834	2.8201	5.8076	3.0389
99	10.4176	0	0	0	0	0.0048	0.1503	4.9567	5.3058
105	10.6921	0	0	0	0	0.0044	0.7439	7.1525	2.7913
115	9.8434	0	0	0	0.0218	0.1274	0.14	1.5641	7.9901

**Core 07-014**

<u>sample#</u>	<u>sample weight</u>	<u>4000 um</u>	<u>2000 um</u>	<u>1000um</u>	<u>500 um</u>	<u>250 um</u>	<u>125 um</u>	<u>63 um</u>	<u>mud</u>
5	10.8237	0	0	0	0.0151	0.0369	0.0854	2.8547	7.8316
15	6.8719	0	0	0	0.0551	0.1162	0.141	1.0577	5.5019
25	11.705	0	0	0	0.0322	0.9962	2.6218	2.4588	5.596
35	11.9908	0	0	0.1781	0.7974	4.5137	3.7031	1.2885	1.51
45	11.4714	0	0	0.0269	0.2932	3.0942	4.8354	1.5814	1.6403
55	9.5101	0	0	0.0178	0.0198	0.6356	2.4924	2.9458	3.3987

**Core 07-017**

<u>sample#</u>	<u>sample weight</u>	<u>4000 um</u>	<u>2000 um</u>	<u>1000 um</u>	<u>500 um</u>	<u>250 um</u>	<u>125 um</u>	<u>63 um</u>	<u>mud</u>
5	9.7129	0	0	0	0.0083	0.0245	0.2908	5.2937	4.0956
15	10.2046	0	0	0	0.0111	0.0695	0.9278	4.4998	4.6964
25	10.9164	0	0	0	0.0018	0.0154	1.8985	6.3451	2.6556
35	12.7071	0	0	0	0.0038	0.0677	8.222	3.7476	0.666
45	12.1262	0	0	0	0.0056	0.0422	5.7724	4.7712	1.5348
52	11.188	0	0	0	0.0086	0.0317	0.3667	3.6161	7.1649

**Core 06-003**

<u>sample#</u>	<u>sample weight</u>	<u>4000 um</u>	<u>2000 um</u>	<u>1000um</u>	<u>500 um</u>	<u>250 um</u>	<u>125 um</u>	<u>63 um</u>	<u>mud</u>
10	8.994	0	0	0.0275	0.1713	1.6935	1.8276	2.938	2.3361
20	8.2408	0	0	0	0.0754	2.4031	4.1914	1.0622	0.5087
30	10.1176	0	0	0	0.0957	3.2977	5.3995	0.8666	0.4581
40	10.4699	0	0	0.01	0.1503	2.9812	5.2095	1.6026	0.5163
50	10.6334	0	0	0.0339	0.1905	2.6762	5.1395	1.9783	0.615
60	12.5429	0	0	0	0.2169	3.7796	6.0209	1.8657	0.6598
70	11.9096	0	0	0.0517	0.1811	3.8866	5.8284	1.4233	0.5385
80	13.5956	0	0	0.2566	0.6032	4.9813	5.3938	1.5882	0.7725

90	10.3557	0	0	0.1933	1.0558	4.86	1.333	1.0805	1.8331
----	---------	---	---	--------	--------	------	-------	--------	--------

Core 06-004

<u>sample#</u>	<u>sample weight</u>	<u>4000 um</u>	<u>2000 um</u>	<u>1000um</u>	<u>500 um</u>	<u>250 um</u>	<u>125 um</u>	<u>63 um</u>	<u>mud</u>
5	10.4198	0.1473	0.1174	0.1991	0.2703	2.0538	4.8236	1.6101	1.1982
15	8.3805	0	0	0	0.0045	0.047	0.5557	2.9404	4.8329
25	8.0043	0	0	0	0.001	0.0241	0.9173	2.4767	4.5852
35	8.8994	0	0	0	0.0025	0.0482	0.4684	2.4585	5.9218
45	9.1114	0	0	0	0.0287	0.2206	5.708	2.6694	0.4847
55	9.4256	0	0	0.0117	0.3527	4.9065	2.9332	0.5655	0.656
65	8.1076	0	0	0	0.0025	0.0177	0.0541	3.8808	4.1525
75	7.3451	0	0	0	0.103	0.2408	0.4236	2.8312	3.7465
95	9.2901	0	0	0	0.122	4.3135	2.7231	1.477	0.6545
105	8.9716	0	0	0	0.0273	0.5078	2.7679	4.5898	1.0788
115	6.6242	0	0	0	0.0265	0.2828	0.5917	3.805	1.9182
125	9.3034	0	0	0	0.0829	1.1605	2.7542	3.5458	1.76
135	7.6538	0	0	0	0.0241	0.5376	2.1194	3.9643	1.0084
145	9.2443	0	0	0.0206	0.097	1.8834	2.582	3.4378	1.2235







